Title: Effective Dynamics of CDT in 2+1 Dimensions

Date: Dec 14, 2011 04:00 PM

URL: http://pirsa.org/11120060

Abstract: To study the continuum limit of a microscopic model of gravity we need microscopic observables that have a clear interpretation in terms of continuum geometry. In general the construction of such observables is notoriously difficult. In the model of causal dynamical triangulations (CDT) it is clear what the microscopic observables are, but at present the only known well-behaved observables with a continuum interpretation are spatial volumes. In this talk I will demonstrate what it takes to go beyond these by introducing the moduli as observables for CDT in 2+1 dimensions with spatial topology of the torus. Measurements of these observables using computer simulations provide valuable clues concerning the effective action describing CDT in the continuum. In particular I will present numerical evidence indicating that the effective kinetic term is well described by a modified Wheeler-De Witt metric like the one appearing in Horava-Lifshitz gravity.

Effective dynamics of CDT in 2+1 dimensions

Timothy Budd

Institute for Theoretical Physics, Utrecht University

December 14, 2011
Quantum gravity seminar
Perimeter Institute

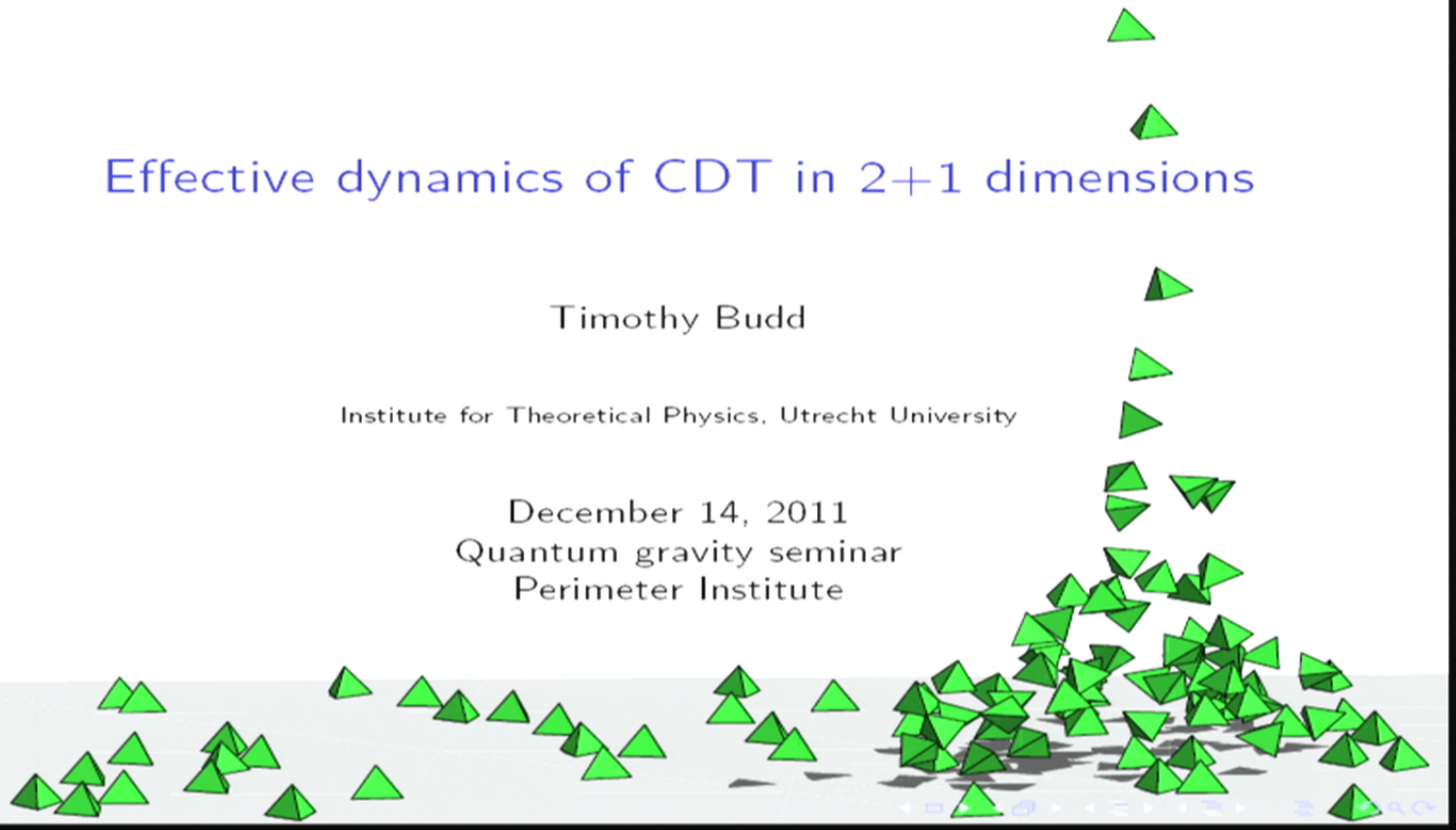

Introduction

- Given some quantum gravity path-integral, how do we determine its effective dynamics?

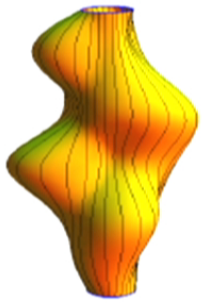

Introduction

- Given some quantum gravity path-integral, how do we determine its effective dynamics?
- Ultimately the only correct way is by studying microscopic observables with a continuum interpretation!
- True for any approach, however in CDT one is constantly reminded of this: measurement $\Leftrightarrow$ algorithm that assigns numbers to CDT configurations $\Leftrightarrow$ observable.

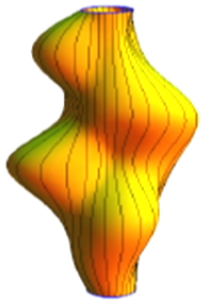

- Succes story in CDT: spatial volumes as observables.

Challenges

- Construct observables that measure macroscopic shape in a meaningful way.
  - This is perhaps the hardest part. In fact: whole journals are dedicated to shape recognition in medical imaging, computer graphics, etc. However the random geometries in CDT are much wilder.

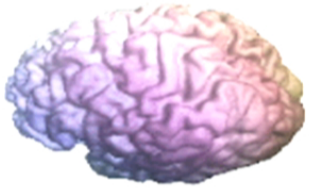

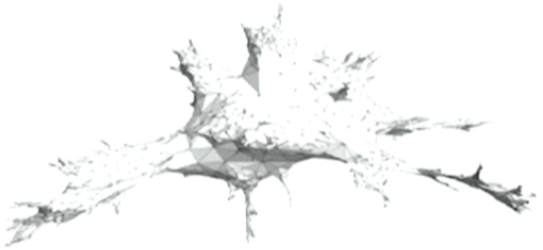

Challenges

- Construct observables that measure macroscopic shape in a meaningful way.
  - This is perhaps the hardest part. In fact: whole journals are dedicated to shape recognition in medical imaging, computer graphics, etc. However the random geometries in CDT are much wilder.

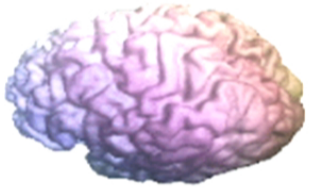

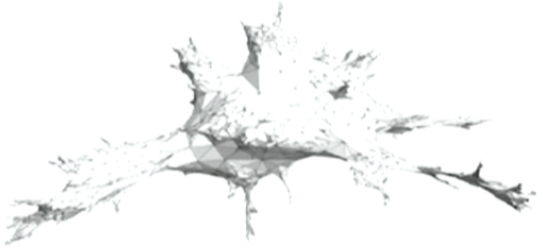

- Construct a class of possible effective actions and work out for each one exactly what correlations in the measurements it predicts.
- Determine the boundary conditions for the path integral that maximize the information contained in the correlations.

Challenges

- Construct observables that measure macroscopic shape in a meaningful way.
  - This is perhaps the hardest part. In fact: whole journals are dedicated to shape recognition in medical imaging, computer graphics, etc. However the random geometries in CDT are much wilder.

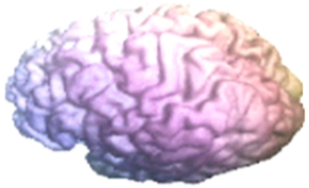

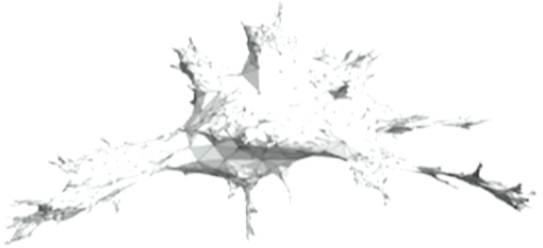

- Construct a class of possible effective actions and work out for each one exactly what correlations in the measurements it predicts.
- Determine the boundary conditions for the path integral that maximize the information contained in the correlations.
- Try to match correlations to the effective actions (analytically or numerically).

Outline

- Introduction to CDT in 2+1 dimensions
  - Previous results for spherical topology
- Effective actions for CDT
  - Conformal mode problem
  - Alternative ansatz a la Hořava–Lifshitz
- Moduli in CDT with torus topology
  - Introduce moduli as observables
  - Boundary conditions
  - Comparison with ansatz
- Summary and outlook

CDT in 2+1 dimensions

- Causal Dynamical Triangulation is a regularization of the Euclidean path integral over geometries

$$Z = \int \frac{\mathcal{D}g}{Diff} e^{-S_{EH}[g]} \quad \rightarrow \quad Z_{CDT} = \sum_{\text{triangulations } T} \frac{1}{C_T} e^{-S_{CDT}[T]}.$$

- Triangulations T are built from equilateral tetrahedra. The sum is over inequivalent ways of putting them together.
- "Causal" in CDT means that we only allow triangulations that are foliated by 2D triangulations with constant topology.

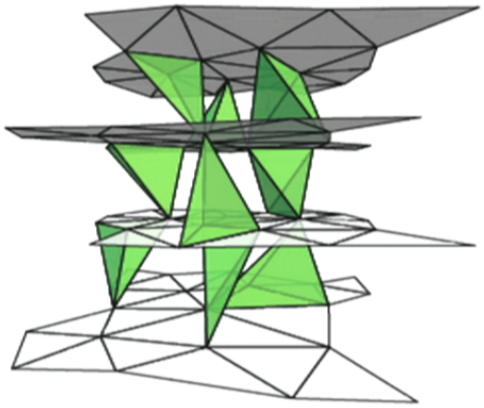

CDT in 2+1 dimensions

- Causal Dynamical Triangulation is a regularization of the Euclidean path integral over geometries

$$Z = \int \frac{\mathcal{D}g}{Diff} e^{-S_{EH}[g]} \quad \rightarrow \quad Z_{CDT} = \sum_{\text{triangulations } T} \frac{1}{C_T} e^{-S_{CDT}[T]}.$$

- Triangulations T are built from equilateral tetrahedra. The sum is over inequivalent ways of putting them together.
- "Causal" in CDT means that we only allow triangulations that are foliated by 2D triangulations with constant topology.
- The Euclidean Einstein–Hilbert action $S[g] = -\kappa \int d^3x \sqrt{g}(R - 2\Lambda)$ evaluated on the piecewise linear geometry leads to

$$S_{CDT}[T] = k_3 N_3 - k_0 N_0.$$

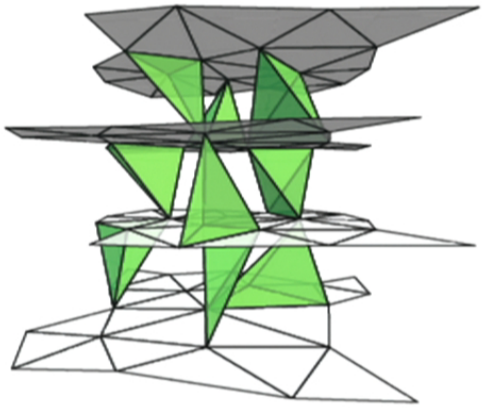

Monte Carlo simulations

- The fixed volume partition function reads

$$Z(N_3) = \sum_T \frac{1}{C_T} e^{-k_0 N_0}.$$

Monte Carlo simulations

- The fixed volume partition function reads

$$Z(N_3) = \sum_T \frac{1}{C_T} e^{-k_0 N_0}.$$

- The expectation value of an observable $\mathcal{O} : T \to \mathcal{O}(T)$ is given by

$$\langle \mathcal{O} \rangle_{N_3} = \frac{1}{Z} \sum_T \frac{\mathcal{O}(T)}{C_T} e^{-k_0 N_0}.$$

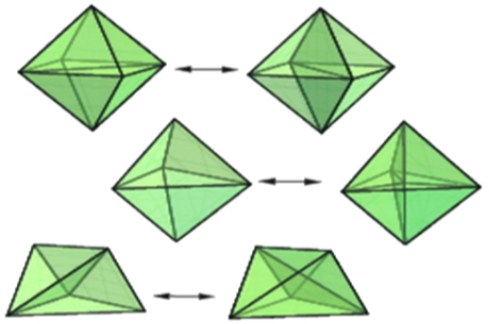

- We use Monte Carlo methods to approximate these:

$$\langle \mathcal{O} \rangle_{N_3} \approx \frac{1}{n} \sum_{i=1}^{n} \mathcal{O}(T_i),$$

where the $\{T_i\}$ is a large set of random triangulations generated by applying a large number of random update moves satisfying a detailed balance condition.

Effective actions for CDT

- Given a set of observables $f_i : \{\text{CDT triangulations}\} \to \mathbb{R}$, $i = 1, \ldots, k$, measuring large scale geometry, we can write

$$Z_{CDT}(N_3) = \sum_T \frac{1}{C_T} e^{-k_0 N_0} = \int df_1 \int df_2 \cdots \int df_k \, e^{-S_{\mathit{eff}}[f_i]}, \qquad (1)$$

where $S_{\mathit{eff}}[f_i] = -\log\left(\sum_T \frac{\delta(f_i - f_i(T))}{C_T} e^{-k_0 N_0}\right)$.

Effective actions for CDT

- Given a set of observables $f_i : \{\text{CDT triangulations}\} \to \mathbb{R}$, $i = 1, \ldots, k$, measuring large scale geometry, we can write

$$Z_{CDT}(N_3) = \sum_T \frac{1}{C_T} e^{-k_0 N_0} = \int df_1 \int df_2 \cdots \int df_k \, e^{-S_{\mathit{eff}}[f_i]}, \quad (1)$$

  where $S_{\mathit{eff}}[f_i] = -\log\left(\sum_T \frac{\delta(f_i - f_i(T))}{C_T} e^{-k_0 N_0}\right)$.
- What does the effective action look like around its minimum as $N_3 \to \infty$?
- Main question: if we could take the observables f_i to be a complete set describing "the continuum geometry", would S_{eff} have anything to do with the Einstein-Hilbert action?

Effective actions for CDT

- Given a set of observables $f_i : \{\text{CDT triangulations}\} \to \mathbb{R}$, $i = 1, \ldots, k$, measuring large scale geometry, we can write

$$Z_{CDT}(N_3) = \sum_T \frac{1}{C_T} e^{-k_0 N_0} = \int df_1 \int df_2 \cdots \int df_k \, e^{-S_{\mathit{eff}}[f_i]}, \quad (1)$$

  where $S_{\mathit{eff}}[f_i] = -\log\left(\sum_T \frac{\delta(f_i - f_i(T))}{C_T} e^{-k_0 N_0}\right)$.
- What does the effective action look like around its minimum as $N_3 \to \infty$?
- Main question: if we could take the observables f_i to be a complete set describing "the continuum geometry", would S_{eff} have anything to do with the Einstein-Hilbert action?
- We can learn about $S_{\mathit{eff}}[f_i]$ by measuring expectation values $\langle f_i \rangle$ and correlations $\langle f_i f_j \rangle$.
- Simplest set of observables in CDT: $\{V(t)\}_t$, spatial volume $V(t)$ at time t.

Effective actions for CDT

- Given a set of observables $f_i : \{\text{CDT triangulations}\} \to \mathbb{R}$, $i = 1, \ldots, k$, measuring large scale geometry, we can write

$$Z_{CDT}(N_3) = \sum_T \frac{1}{C_T} e^{-k_0 N_0} = \int df_1 \int df_2 \cdots \int df_k \, e^{-S_{\mathit{eff}}[f_i]}, \quad (1)$$

  where $S_{\mathit{eff}}[f_i] = -\log\left(\sum_T \frac{\delta(f_i - f_i(T))}{C_T} e^{-k_0 N_0}\right)$.
- What does the effective action look like around its minimum as $N_3 \to \infty$?
- Main question: if we could take the observables f_i to be a complete set describing "the continuum geometry", would S_{eff} have anything to do with the Einstein-Hilbert action?
- We can learn about $S_{\mathit{eff}}[f_i]$ by measuring expectation values $\langle f_i \rangle$ and correlations $\langle f_i f_j \rangle$.
- Simplest set of observables in CDT: $\{V(t)\}_t$, spatial volume $V(t)$ at time t.

Spherical topology

- Take the topology to be $S^1 \times S^2$ (periodic boundary conditions).

Spherical topology

- Take the topology to be $S^1 \times S^2$ (periodic boundary conditions).
- $\langle V(t) \rangle \propto \cos^2(\sqrt{c_1}\, t)$ plus minimal "stalk". [AJL, hep-th/0011276]

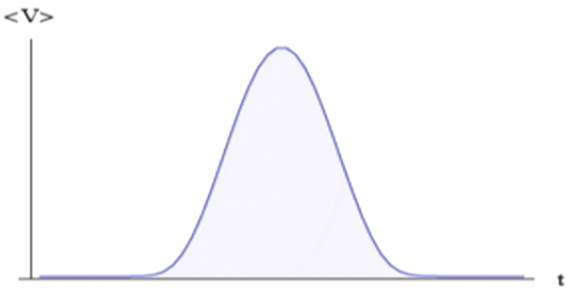

Spherical topology

- Take the topology to be $S^1 \times S^2$ (periodic boundary conditions).
- $\langle V(t) \rangle \propto \cos^2(\sqrt{c_1}\, t)$ plus minimal "stalk". [AJL, hep-th/0011276]
- Classical solution to

$$S_{\mathit{eff}}[V] = c_0 \int dt \left(\frac{\dot{V}^2}{V} - 2c_1 V \right).$$

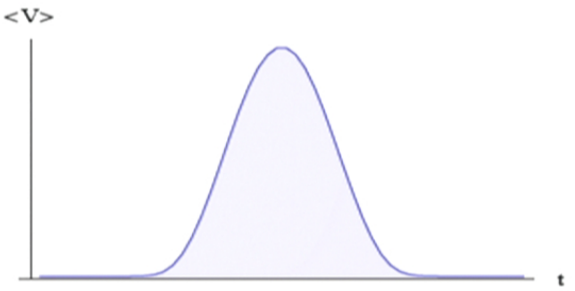

- Also correlations $\langle V(t)V(t') \rangle$ well-described by this action for suitable values $c_0, c_1 > 0$.
- Euclidean Einstein–Hilbert action $\int d^3x\sqrt{g}(-R + 2\Lambda)$ evaluated on spherical cosmology $ds^2 = dt^2 + V(t)d\Omega^2$ gives

$$S_{EH} = -\kappa \int dt \left(\frac{\dot{V}^2}{V} - 2\Lambda V \right) \qquad (2)$$

Conformal mode problem

- Euclidean EH action in 2+1D (and 3+1D) is unbounded from below.

Conformal mode problem

- Euclidean EH action in 2+1D (and 3+1D) is unbounded from below.
- Metric in proper-time form, $ds^2 = dt^2 + g_{ab}(t,x)dx^a dx^b$. Then

$$S_{EH} = \kappa \int dt \int d^2x \sqrt{g} \left(\frac{1}{4} \dot{g}_{ab} \mathcal{G}^{abcd} \dot{g}_{cd} - R + 2\Lambda \right) \qquad (3)$$

where $\mathcal{G}^{abcd}$ is the Wheeler-DeWitt metric,

$$\mathcal{G}^{abcd} = \frac{1}{2} \left(g^{ac} g^{bd} + g^{ad} g^{bc} \right) - g^{ab} g^{cd}. \qquad (4)$$

Conformal mode problem

- Euclidean EH action in 2+1D (and 3+1D) is unbounded from below.
- Metric in proper-time form, $ds^2 = dt^2 + g_{ab}(t,x)dx^a dx^b$. Then

$$S_{EH} = \kappa \int dt \int d^2x \sqrt{g} \left(\frac{1}{4} \dot{g}_{ab} \mathcal{G}^{abcd} \dot{g}_{cd} - R + 2\Lambda \right) \qquad (3)$$

where $\mathcal{G}^{abcd}$ is the Wheeler-DeWitt metric,

$$\mathcal{G}^{abcd} = \frac{1}{2} \left(g^{ac} g^{bd} + g^{ad} g^{bc} \right) - g^{ab} g^{cd}. \qquad (4)$$

- Indefinite metric! Positive definite on traceless directions, negative definite on trace/conformal directions in superspace.

Conformal mode problem

- Euclidean EH action in 2+1D (and 3+1D) is unbounded from below.
- Metric in proper-time form, $ds^2 = dt^2 + g_{ab}(t,x)dx^a dx^b$. Then

$$S_{EH} = \kappa \int dt \int d^2x \sqrt{g} \left(\frac{1}{4} \dot{g}_{ab} \mathcal{G}^{abcd} \dot{g}_{cd} - R + 2\Lambda \right) \qquad (3)$$

where $\mathcal{G}^{abcd}$ is the Wheeler-DeWitt metric,

$$\mathcal{G}^{abcd} = \frac{1}{2} \left(g^{ac} g^{bd} + g^{ad} g^{bc} \right) - g^{ab} g^{cd}. \qquad (4)$$

- Indefinite metric! Positive definite on traceless directions, negative definite on trace/conformal directions in superspace.
- CDT is a (well-defined) statistical system, therefore it better be described by a bounded effective action, e.g. in

$$Z_{CDT}(N_3) = \int dV(1) \int dV(2) \cdots \int dV(T) e^{-S_{\mathit{eff}}[V(t)]}. \qquad (5)$$

- The foliation in CDT has consequences for the effective dynamics in two (related) ways.

- The foliation in CDT has consequences for the effective dynamics in two (related) ways.
- First of all: geometries in CDT have fixed distance between initial and final boundary (unlike GR).

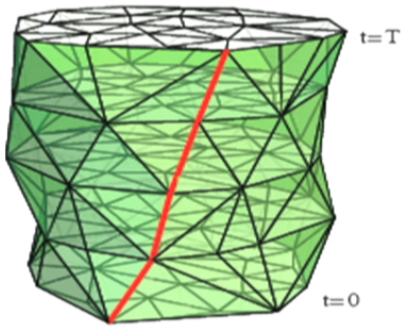

- The foliation in CDT has consequences for the effective dynamics in two (related) ways.

- First of all: geometries in CDT have fixed distance between initial and final boundary (unlike GR).
- We should restrict $S_{eff}[g]$ to an analogous subclass of continuum geometries $\{g\}$. The natural choice is to take those for which the metric can be written in 2+1 split with lapse $N = 1$:

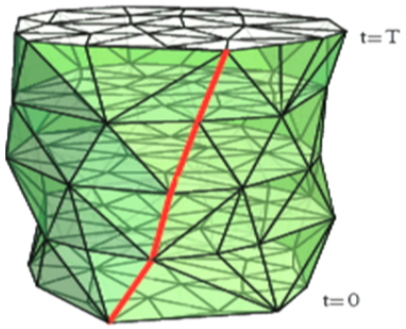

$$ds^2 = dt^2 + (dx^a + N^a dt)(dx^b + N^b dt)g_{ab}(t)$$

- The foliation in CDT has consequences for the effective dynamics in two (related) ways.

- First of all: geometries in CDT have fixed distance between initial and final boundary (unlike GR).
- We should restrict $S_{eff}[g]$ to an analogous subclass of continuum geometries $\{g\}$. The natural choice is to take those for which the metric can be written in 2+1 split with lapse $N = 1$:

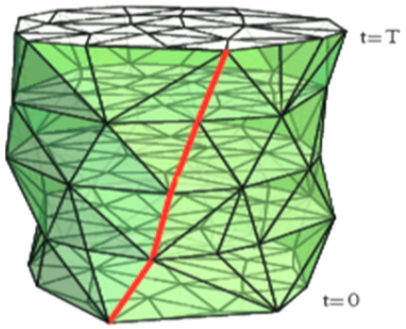

$$ds^2 = dt^2 + (dx^a + N^a dt)(dx^b + N^b dt)g_{ab}(t)$$

- As a consequence we cannot expect a "Hamiltonian constraint" $\delta S/\delta N = 0$ as one of the effective equations of motion.

- The foliation in CDT has consequences for the effective dynamics in two (related) ways.

- First of all: geometries in CDT have fixed distance between initial and final boundary (unlike GR).
- We should restrict $S_{eff}[g]$ to an analogous subclass of continuum geometries $\{g\}$. The natural choice is to take those for which the metric can be written in 2+1 split with lapse $N = 1$:

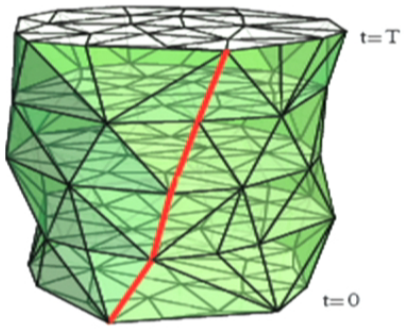

$$ds^2 = dt^2 + (dx^a + N^a dt)(dx^b + N^b dt)g_{ab}(t)$$

- As a consequence we cannot expect a "Hamiltonian constraint" $\delta S/\delta N = 0$ as one of the effective equations of motion.
- The preferred time-slicing leads a priori to a local scalar degree of freedom: the conformal factor.

- The second consequence is that we should restrict the symmetry group of $S_{eff}[g]$ to foliation preserving diffeomorphisms $\subset Diff$.
- The Einstein–Hilbert action (with $N = 1$ and $N^a = 0$)

$$S_{EH} = \kappa \int_0^T dt \int d^2x \sqrt{g} (\dot{g}_{ab} \mathcal{G}^{abcd} \dot{g}_{ab} + R - 2\Lambda)$$

generalizes naturally to

$$S_{ansatz} = \kappa \int_0^T dt \int d^2x \sqrt{g} (\dot{g}_{ab} \mathcal{G}_\lambda^{abcd} \dot{g}_{ab} - U[g]),$$

in which the most general ultralocal supermetric is

$$\mathcal{G}_\lambda^{abcd} = \frac{1}{2} (g^{ac} g^{bd} + g^{ad} g^{bc}) - \lambda g^{ab} g^{cd}.$$

- The second consequence is that we should restrict the symmetry group of $S_{eff}[g]$ to foliation preserving diffeomorphisms $\subset Diff$.
- The Einstein–Hilbert action (with $N = 1$ and $N^a = 0$)

$$S_{EH} = \kappa \int_0^T dt \int d^2x \sqrt{g} (\dot{g}_{ab} \mathcal{G}^{abcd} \dot{g}_{ab} + R - 2\Lambda)$$

generalizes naturally to

$$S_{ansatz} = \kappa \int_0^T dt \int d^2x \sqrt{g} (\dot{g}_{ab} \mathcal{G}_\lambda^{abcd} \dot{g}_{ab} - U[g]),$$

in which the most general ultralocal supermetric is

$$\mathcal{G}_\lambda^{abcd} = \frac{1}{2} (g^{ac} g^{bd} + g^{ad} g^{bc}) - \lambda g^{ab} g^{cd}.$$

- $\mathcal{G}_\lambda$ is positive definite for $\lambda < 1/2$; $\lambda = 1$ in EH.

- The second consequence is that we should restrict the symmetry group of $S_{eff}[g]$ to foliation preserving diffeomorphisms $\subset Diff$.
- The Einstein–Hilbert action (with $N = 1$ and $N^a = 0$)

$$S_{EH} = \kappa \int_0^T dt \int d^2x \sqrt{g} (\dot{g}_{ab} \mathcal{G}^{abcd} \dot{g}_{ab} + R - 2\Lambda)$$

generalizes naturally to

$$S_{ansatz} = \kappa \int_0^T dt \int d^2x \sqrt{g} (\dot{g}_{ab} \mathcal{G}_\lambda^{abcd} \dot{g}_{ab} - U[g]),$$

in which the most general ultralocal supermetric is

$$\mathcal{G}_\lambda^{abcd} = \frac{1}{2} \left(g^{ac} g^{bd} + g^{ad} g^{bc} \right) - \lambda g^{ab} g^{cd}.$$

- $\mathcal{G}_\lambda$ is positive definite for $\lambda < 1/2$; $\lambda = 1$ in EH.
- We have ended up with an ansatz in the realm of Euclidean (projectable) Hořava–Lifshitz gravity.

CDT with spatial topology of the torus

- To test the kinetic term in

$$S_{ansatz} = \kappa \int_0^T dt \int d^2x \sqrt{g} (\dot{g}_{ab} \mathcal{G}^{abcd}_{\lambda} \dot{g}_{ab} - U[g]),$$

we need some observable that measures traceless degrees of freedom in the spatial metric.

- Torus topology! The torus has a two-parameter family of conformal shapes, parametrized by the moduli $\tau = \tau_1 + i\tau_2$.

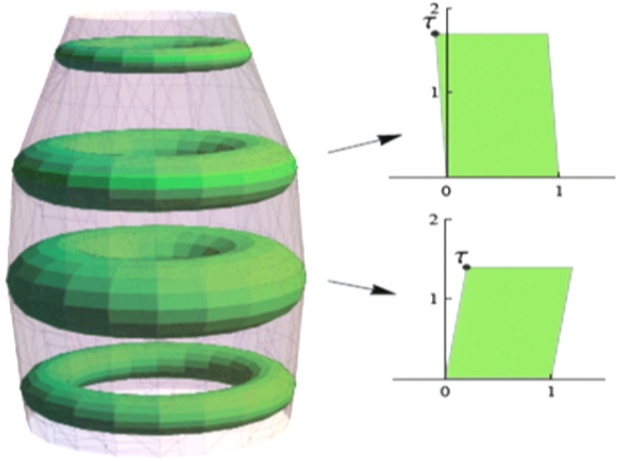

Measurement of τ in the continuum

- Any metric g_{ab} on the torus is conformally flat and up to diffeomorphisms the flat unit-volume metrics are given by

$$\hat{g}_{ab}(\tau, x) = \frac{1}{\tau_2} \begin{pmatrix} 1 & \tau_1 \\ \tau_1 & \tau_1^2 + \tau_2^2 \end{pmatrix}.$$

- How do we find the "periodic" coordinates $x^1, x^2 \in [0, 1)$ such that $ds^2 = \Omega^2(x)\hat{g}_{ab}dx^a dx^b$?

Measurement of τ in the continuum

- Any metric g_{ab} on the torus is conformally flat and up to diffeomorphisms the flat unit-volume metrics are given by

$$\hat{g}_{ab}(\tau, x) = \frac{1}{\tau_2} \begin{pmatrix} 1 & \tau_1 \\ \tau_1 & \tau_1^2 + \tau_2^2 \end{pmatrix}.$$

- How do we find the "periodic" coordinates $x^1, x^2 \in [0, 1)$ such that $ds^2 = \Omega^2(x)\hat{g}_{ab}dx^a dx^b$?
- The 1-forms $\alpha^1 = dx^1$ and $\alpha^2 = dx^2$ are special: they form a basis of the space of harmonic forms, i.e. $d\alpha^i = \delta\alpha^i = 0$ or $\Delta\alpha^i = 0$ with

$$\Delta = d\delta + \delta d \quad \text{(Hodge Laplacian)}$$

d exterior derivative, δ its adjoint w.r.t. standard inner-product $\langle \phi, \psi \rangle = \int \phi \wedge *\psi$.

Measurement of τ in the continuum

- Any metric g_{ab} on the torus is conformally flat and up to diffeomorphisms the flat unit-volume metrics are given by

$$\hat{g}_{ab}(\tau, x) = \frac{1}{\tau_2} \begin{pmatrix} 1 & \tau_1 \\ \tau_1 & \tau_1^2 + \tau_2^2 \end{pmatrix}.$$

- How do we find the "periodic" coordinates $x^1, x^2 \in [0, 1)$ such that $ds^2 = \Omega^2(x)\hat{g}_{ab}dx^a dx^b$?
- The 1-forms $\alpha^1 = dx^1$ and $\alpha^2 = dx^2$ are special: they form a basis of the space of harmonic forms, i.e. $d\alpha^i = \delta\alpha^i = 0$ or $\Delta\alpha^i = 0$ with

$$\Delta = d\delta + \delta d \quad \text{(Hodge Laplacian)}$$

d exterior derivative, δ its adjoint w.r.t. standard inner-product $\langle \phi, \psi \rangle = \int \phi \wedge *\psi$.

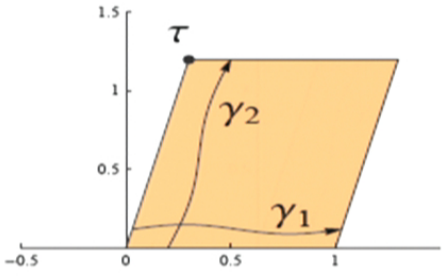

- Given generators γ_j, the α^i are uniquely determined by $\int_{\gamma_j} \alpha^i = \delta^i_j$.

Measurement of τ in the continuum

- Any metric g_{ab} on the torus is conformally flat and up to diffeomorphisms the flat unit-volume metrics are given by

$$\hat{g}_{ab}(\tau, x) = \frac{1}{\tau_2} \begin{pmatrix} 1 & \tau_1 \\ \tau_1 & \tau_1^2 + \tau_2^2 \end{pmatrix}.$$

- How do we find the "periodic" coordinates $x^1, x^2 \in [0, 1)$ such that $ds^2 = \Omega^2(x)\hat{g}_{ab}dx^a dx^b$?
- The 1-forms $\alpha^1 = dx^1$ and $\alpha^2 = dx^2$ are special: they form a basis of the space of harmonic forms, i.e. $d\alpha^i = \delta\alpha^i = 0$ or $\Delta\alpha^i = 0$ with

$$\Delta = d\delta + \delta d \quad \text{(Hodge Laplacian)}$$

d exterior derivative, δ its adjoint w.r.t. standard inner-product $\langle \phi, \psi \rangle = \int \phi \wedge *\psi$.

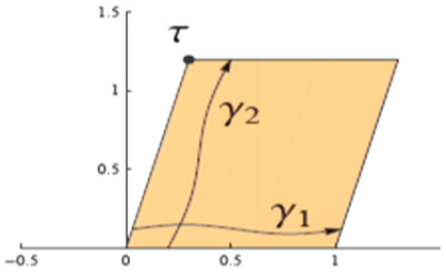

- Given generators γ_j, the α^i are uniquely determined by $\int_{\gamma_j} \alpha^i = \delta^i_j$.
- $\tau = -\frac{\langle \alpha^1, \alpha^2 \rangle}{\langle \alpha^2, \alpha^2 \rangle} + i\sqrt{\frac{\langle \alpha^1, \alpha^1 \rangle}{\langle \alpha^2, \alpha^2 \rangle} - \left(\frac{\langle \alpha^1, \alpha^2 \rangle}{\langle \alpha^2, \alpha^2 \rangle}\right)^2}$.

Measurement of τ for torus triangulations

- Recipe: [Ambjørn, Barkley, TB, arXiv:1110.4649]
  - Determine pair of curves γ_j that generate fundamental group.
  - Find the 2-dimensional kernel of Δ.
  - Determine basis α_j such that $\int_{\gamma_j} \alpha^i = \delta^i_j$.
  - Compute $\tau = -\frac{\langle \alpha^1, \alpha^2 \rangle}{\langle \alpha^2, \alpha^2 \rangle} + i\sqrt{\frac{\langle \alpha^1, \alpha^1 \rangle}{\langle \alpha^2, \alpha^2 \rangle} - \left(\frac{\langle \alpha^1, \alpha^2 \rangle}{\langle \alpha^2, \alpha^2 \rangle}\right)^2}$.
- We need discrete differential forms! We will borrow them from the theory of simplicial complexes.
- Once we have these ingredients we can construct discrete conformal maps:

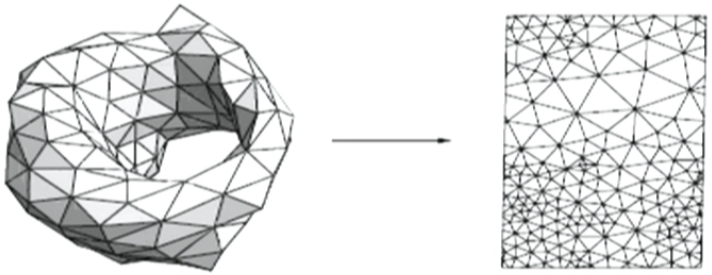

Discrete differential forms

- In 2d triangulations we have
  - Vertices: 0-simplices denoted by i,
  - Edges: 1-simplices denoted by (ij),
  - Triangles: 2-simplices denoted by (ijk).

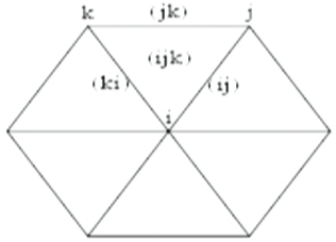

- A discrete p-form ϕ assigns a real number ϕ_σ to each (oriented) p-simplex σ.
- Exterior derivative on 1-forms: $(d\phi)_{(ijk)} = \phi_{(ij)} + \phi_{(jk)} + \phi_{(ki)}$
- Divergence on 1-forms: $(\delta\phi)_j = \sum_{\text{edges } (ij)} \phi_{(ij)}$
- More generally: $(d\psi)(\sigma_{p+1}) = \sum_{\sigma_p \in \sigma_{p+1}} (-1)^{\sigma_p} \psi(\sigma_p)$.
- δ adjoint of d w.r.t. $\langle \phi, \psi \rangle = \sum_\sigma \phi(\sigma)\psi(\sigma)$.

Discrete differential forms

- In 2d triangulations we have
  - Vertices: 0-simplices denoted by i,
  - Edges: 1-simplices denoted by (ij),
  - Triangles: 2-simplices denoted by (ijk).

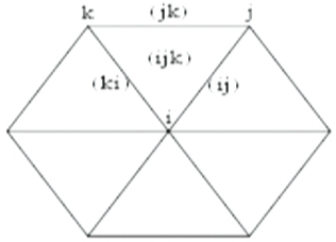

- A discrete p-form ϕ assigns a real number ϕ_σ to each (oriented) p-simplex σ.
- Exterior derivative on 1-forms: $(d\phi)_{(ijk)} = \phi_{(ij)} + \phi_{(jk)} + \phi_{(ki)}$
- Divergence on 1-forms: $(\delta\phi)_j = \sum_{\text{edges } (ij)} \phi_{(ij)}$
- More generally: $(d\psi)(\sigma_{p+1}) = \sum_{\sigma_p \in \sigma_{p+1}} (-1)^{\sigma_p} \psi(\sigma_p)$.
- δ adjoint of d w.r.t. $\langle \phi, \psi \rangle = \sum_\sigma \phi(\sigma)\psi(\sigma)$.

Discrete differential forms

- In 2d triangulations we have
  - Vertices: 0-simplices denoted by i,
  - Edges: 1-simplices denoted by (ij),
  - Triangles: 2-simplices denoted by (ijk).

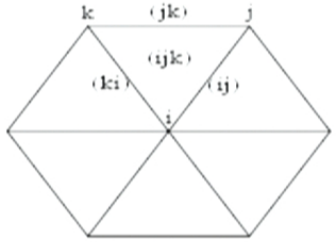

- A discrete p-form ϕ assigns a real number ϕ_σ to each (oriented) p-simplex σ.
- Exterior derivative on 1-forms: $(d\phi)_{(ijk)} = \phi_{(ij)} + \phi_{(jk)} + \phi_{(ki)}$
- Divergence on 1-forms: $(\delta\phi)_j = \sum_{\text{edges } (ij)} \phi_{(ij)}$
- More generally: $(d\psi)(\sigma_{p+1}) = \sum_{\sigma_p \in \sigma_{p+1}} (-1)^{\sigma_p} \psi(\sigma_p)$.
- δ adjoint of d w.r.t. $\langle \phi, \psi \rangle = \sum_\sigma \phi(\sigma)\psi(\sigma)$.
- $\Delta = d\delta + \delta d$ becomes a matrix of which we can determine the nullspace $\Delta\alpha = 0$ ($\Leftrightarrow$ $d\alpha = 0$ and $\delta\alpha = 0$)

Boundary conditions

- Periodic time $T^2 \times S^1$: contrary to the spherical case we do not observe symmetry breaking in time, i.e. no "stalk" appears with minimal spatial volume. Expectation values seem time-independent.
- Several ways to make it non-trivial: insert sources for spatial volume, twisted boundary conditions, ...
- Can also take fixed boundaries. In particular: we can take the tori to degenerate to ring-shaped singularities at the boundaries. What we get is the Hopf foliation of S^3:

Hopf Link

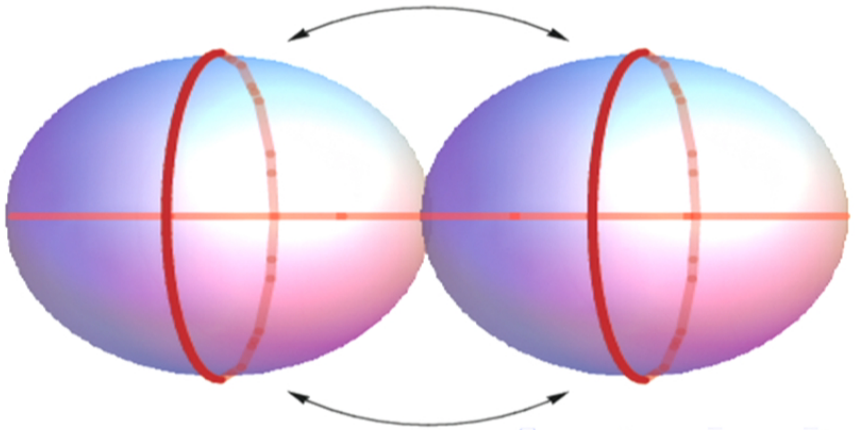

Boundary conditions

- Periodic time $T^2 \times S^1$: contrary to the spherical case we do not observe symmetry breaking in time, i.e. no "stalk" appears with minimal spatial volume. Expectation values seem time-independent.
- Several ways to make it non-trivial: insert sources for spatial volume, twisted boundary conditions, ...
- Can also take fixed boundaries. In particular: we can take the tori to degenerate to ring-shaped singularities at the boundaries. What we get is the Hopf foliation of S^3:

Hopf Link

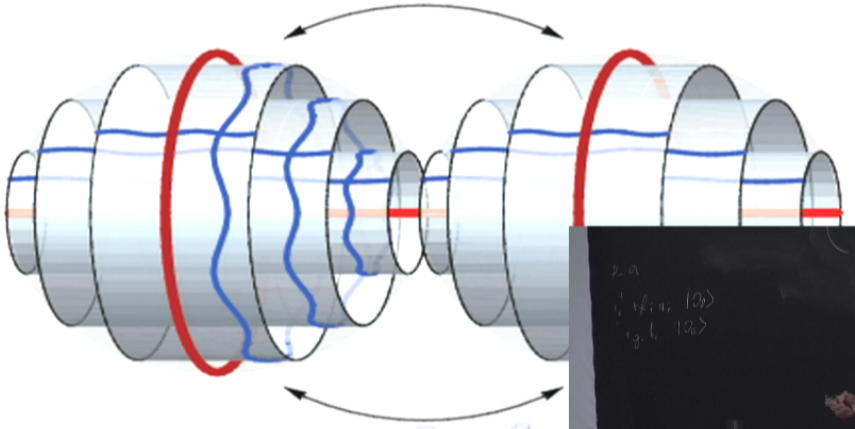

- The initial and final (degenerate) geometry correspond to moduli $\tau = 0$ and $\tau = i\infty$ respectively.
- A CDT configuration determines a sequence of moduli in the upper-half plane. Map to Poincaré disk for convenience:

$$\tilde{\tau} = \frac{\tau - i}{\tau + i}$$

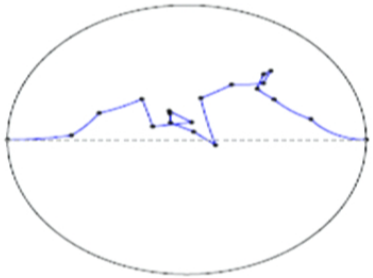

- We can measure expectation values $\langle \tilde{\tau}_i(t) \rangle$ and correlations $\langle \tilde{\tau}_i(t)\tilde{\tau}_j(t') \rangle$ in addition to the spatial volume $\langle V(t) \rangle$ and $\langle V(t)V(t') \rangle$.

Data

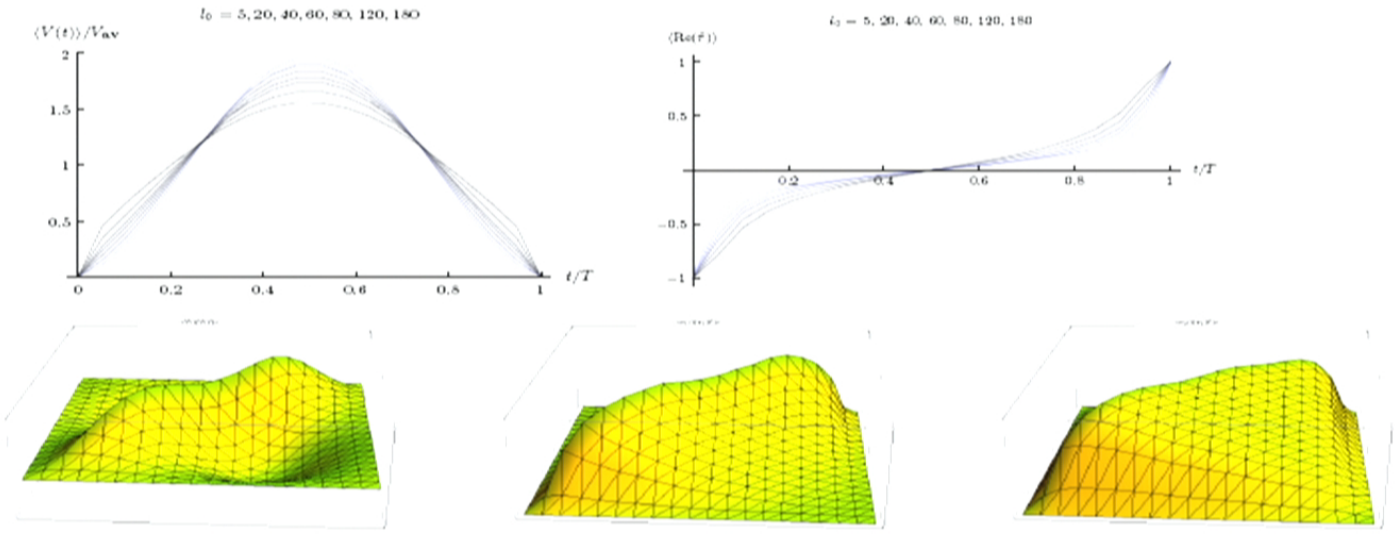

- Plenty of data, but where to start?

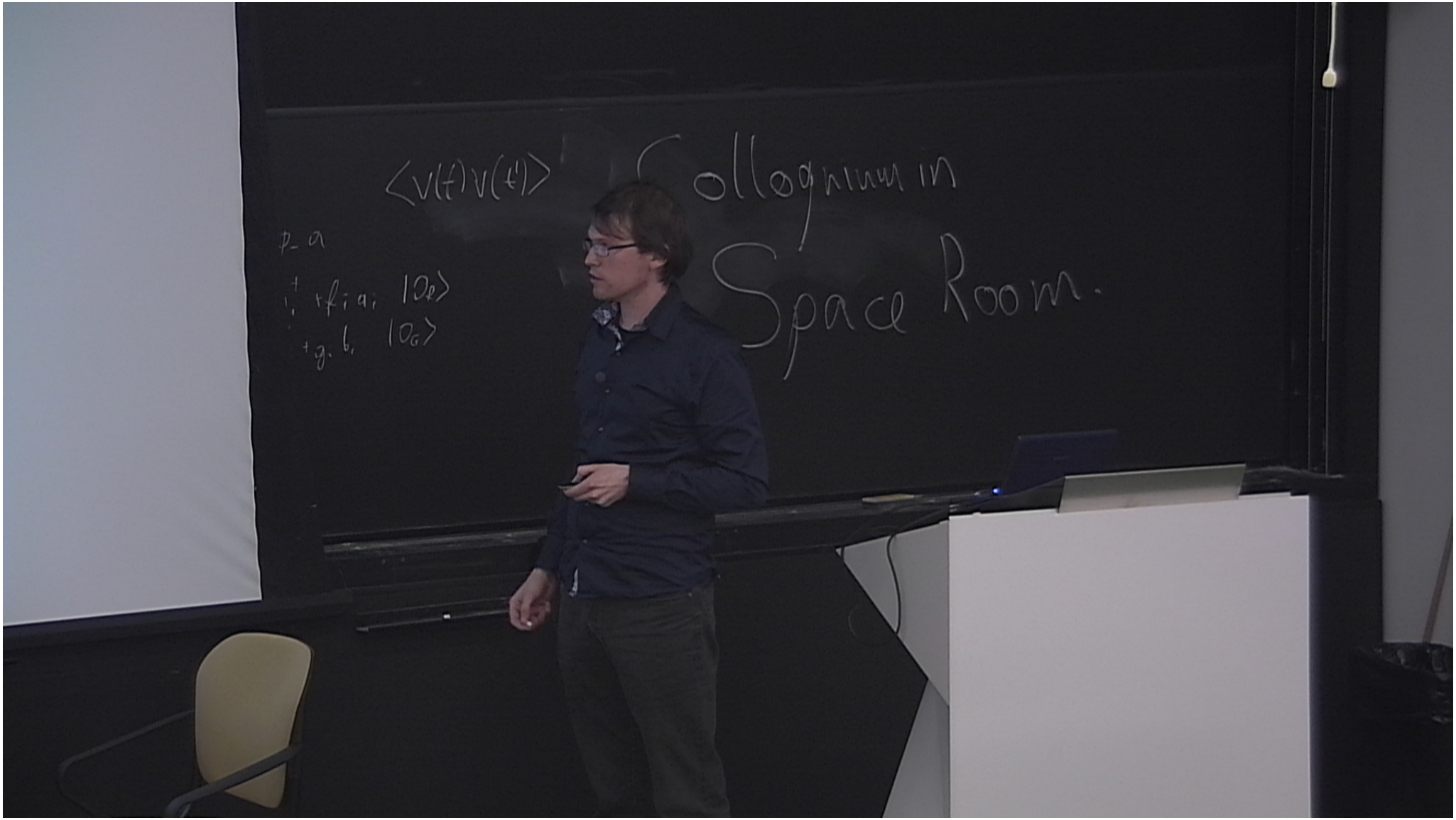
Space Room.

Data

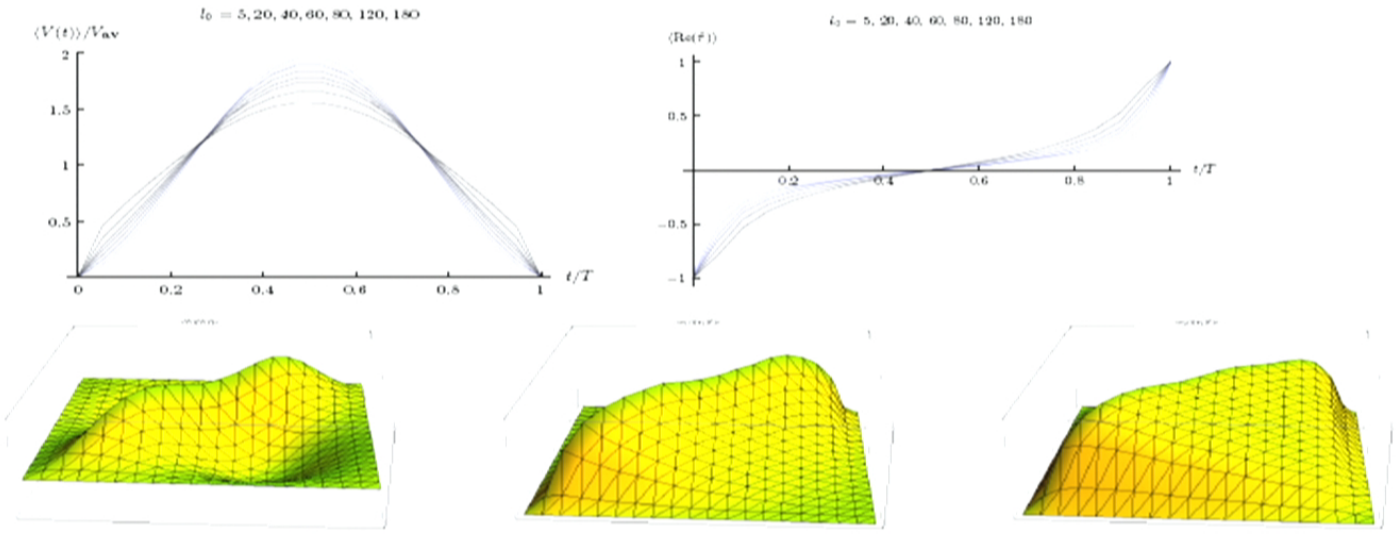

- Plenty of data, but where to start?
- The "cusp" on the diagonal of the correlators tells us about the effective kinetic term!

Comparison to ansatz

- Evaluating

$$S_{ansatz} = \kappa \int_0^T dt \int d^2x \sqrt{g} (\dot{g}_{ab} \mathcal{G}_\lambda^{abcd} \dot{g}_{ab} - U[g]),$$

on homogeneous cosmology $ds^2 = dt^2 + V(t)\hat{g}_{ab}(\tau)dx^a dx^b$ gives

$$S[V,\tau] = \kappa \int dt \Big((\frac{1}{2} - \lambda) \frac{\dot{V}^2}{V} + \frac{V}{2} \frac{\dot{\tau}_1^2 + \dot{\tau}_2^2}{\tau_2^2} - U(V,\tau) \Big).$$

Comparison to ansatz

- Evaluating

$$S_{ansatz} = \kappa \int_0^T dt \int d^2x \sqrt{g} (\dot{g}_{ab} \mathcal{G}_\lambda^{abcd} \dot{g}_{ab} - U[g]),$$

on homogeneous cosmology $ds^2 = dt^2 + V(t)\hat{g}_{ab}(\tau)dx^a dx^b$ gives

$$S[V,\tau] = \kappa \int dt \Big((\frac{1}{2} - \lambda)\frac{\dot{V}^2}{V} + \underbrace{\frac{V}{2}}_{\text{Depends sensitively on the flatness.}} \frac{\dot{\tau}_1^2 + \dot{\tau}_2^2}{\tau_2^2} - U(V,\tau) \Big).$$

- We can do better: this prefactor is related to the change of τ under a normalized metric deformation δg_{ab} w.r.t. $\mathcal{G}_\lambda$.

$$S[V,\tau] = \kappa \int dt \Big((\frac{1}{2} - \lambda)\frac{\dot{V}^2}{V} + \frac{1}{2A[g]} \frac{\dot{\tau}_1^2 + \dot{\tau}_2^2}{\tau_2^2} - U(V,\tau) \Big).$$

with

$$A[g] = \frac{\delta_{ij}}{4\tau_2^2} \int d^2x \sqrt{g} \frac{\delta\tau_i}{\delta g_{ab}} \mathcal{G}^\lambda_{abcd} \frac{\delta\tau_j}{\delta g_{cd}}.$$

- Writing the metric in conformal gauge $ds^2 = \Omega(x)^2 \hat{g}_{ab} dx^a dx^b$ we find

$$\begin{aligned} A[g] &= \frac{\delta_{ij}}{4\tau_2^2} \int d^2x \sqrt{g} \frac{\delta \tau_i}{\delta g_{ab}} \mathcal{G}^{\lambda}_{abcd} \frac{\delta \tau_j}{\delta g_{cd}} \\ &= \int d^2x \sqrt{\hat{g}}\, \Omega(x)^{-2} \\ &= \frac{\int d^2x \sqrt{g}\, \exp(2\Delta^{-1} R)}{\left(\int d^2x \sqrt{g}\, \exp(\Delta^{-1} R)\right)^2} \geq \frac{1}{V} \end{aligned}$$

- A natural discretization of $A[g]$ to triangulations T is $A[T] = \sum_{\sigma \in T} \mathrm{area}(\sigma)^2$, where $\mathrm{area}(\sigma)$ is the area of the triangle σ in the conformal embedding of T in the plane.

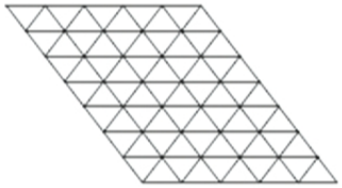

$VA[T] = 1$

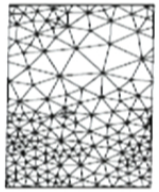

$VA[T] \approx 1.9$

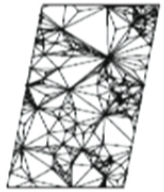

$VA[T] \approx 4.9$

Comparison to ansatz

- Evaluating

$$S_{ansatz} = \kappa \int_0^T dt \int d^2x \sqrt{g} (\dot{g}_{ab} \mathcal{G}_\lambda^{abcd} \dot{g}_{ab} - U[g]),$$

on homogeneous cosmology $ds^2 = dt^2 + V(t)\hat{g}_{ab}(\tau)dx^a dx^b$ gives

$$S[V,\tau] = \kappa \int dt \Big((\frac{1}{2} - \lambda)\frac{\dot{V}^2}{V} + \underbrace{\frac{V}{2}}_{\text{Depends sensitively on the flatness.}} \frac{\dot{\tau}_1^2 + \dot{\tau}_2^2}{\tau_2^2} - U(V,\tau) \Big).$$

- We can do better: this prefactor is related to the change of τ under a normalized metric deformation δg_{ab} w.r.t. $\mathcal{G}_\lambda$.

$$S[V,\tau] = \kappa \int dt \Big((\frac{1}{2} - \lambda)\frac{\dot{V}^2}{V} + \frac{1}{2A[g]} \frac{\dot{\tau}_1^2 + \dot{\tau}_2^2}{\tau_2^2} - U(V,\tau) \Big).$$

with

$$A[g] = \frac{\delta_{ij}}{4\tau_2^2} \int d^2x \sqrt{g} \frac{\delta\tau_i}{\delta g_{ab}} \mathcal{G}^\lambda_{abcd} \frac{\delta\tau_j}{\delta g_{cd}}.$$

- Measure $\langle A[g(t)]\rangle$ in CDT configurations: plots for $k_0 = 2.5$, $V = 60000$ and different singularity lengths l_0.

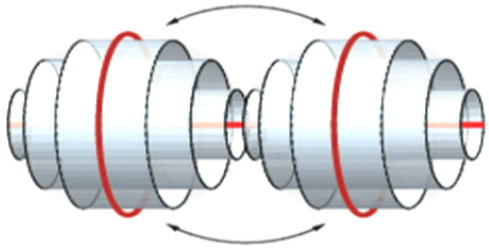

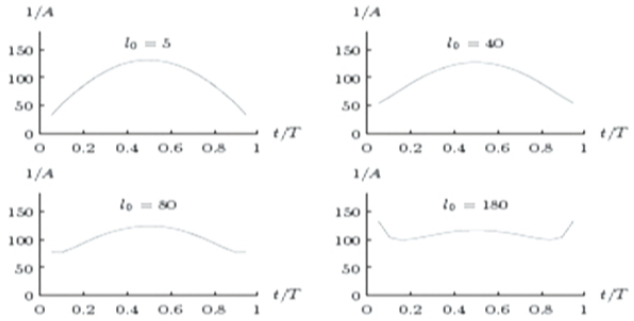

- Now we can start comparing! Semi-classically the correlation matrix $\langle \Delta\tau_i(t)\Delta\tau_j(t')\rangle$ is proportional to the inverse of $\delta^2 S_{\mathit{eff}}/\delta\tau_i(t)\delta\tau_j(t')$.

- Measure $\langle A[g(t)]\rangle$ in CDT configurations: plots for $k_0 = 2.5$, $V = 60000$ and different singularity lengths l_0.

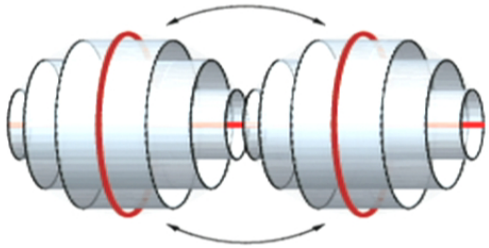

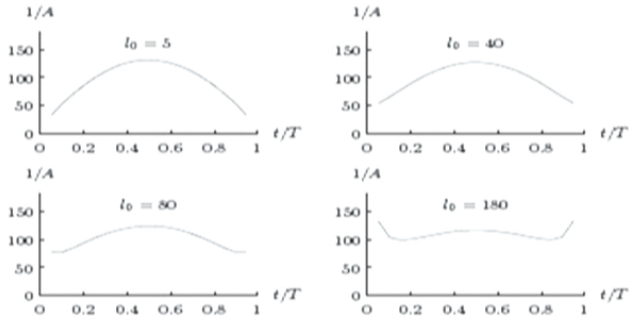

- Now we can start comparing! Semi-classically the correlation matrix $\langle \Delta\tau_i(t)\Delta\tau_j(t')\rangle$ is proportional to the inverse of $\delta^2 S_{\mathit{eff}}/\delta\tau_i(t)\delta\tau_j(t')$.
- Determine the relative prefactor $2(\frac{1}{2} - \lambda)A[g]$ of $\dot{V}^2$ and $\dot{\tau}_i^2$ in

$$S[V,\tau] = \kappa \int dt \Big((\frac{1}{2} - \lambda)\frac{\dot{V}^2}{V} + \frac{1}{2A[g]}\frac{\dot{\tau}_1^2 + \dot{\tau}_2^2}{\tau_2^2} - U(V,\tau) \Big).$$

- Measure $\langle A[g(t)]\rangle$ in CDT configurations: plots for $k_0 = 2.5$, $V = 60000$ and different singularity lengths l_0.

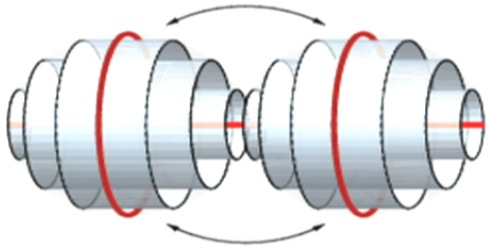

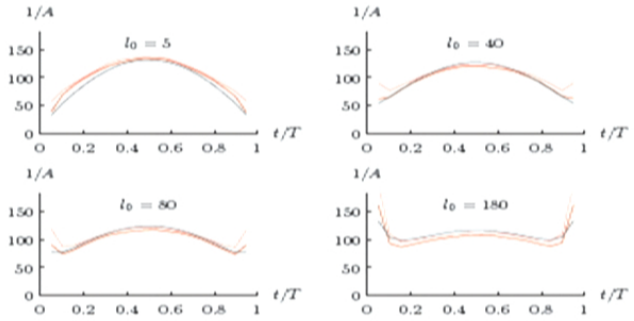

- Now we can start comparing! Semi-classically the correlation matrix $\langle \Delta\tau_i(t)\Delta\tau_j(t')\rangle$ is proportional to the inverse of $\delta^2 S_{\mathit{eff}}/\delta\tau_i(t)\delta\tau_j(t')$.
- Determine the relative prefactor $2(\frac{1}{2} - \lambda)A[g]$ of $\dot{V}^2$ and $\dot{\tau}_i^2$ in

$$S[V,\tau] = \kappa \int dt \Big((\frac{1}{2} - \lambda)\frac{\dot{V}^2}{V} + \frac{1}{2A[g]}\frac{\dot{\tau}_1^2 + \dot{\tau}_2^2}{\tau_2^2} - U(V,\tau) \Big).$$

- Fit to measured $A[g]$ gives $\lambda \approx 0.18$.

- We can perform this analysis for various couplings k_0.

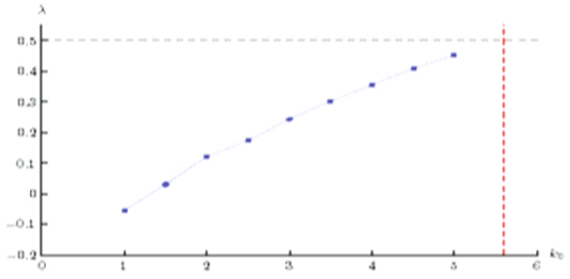

- Measure $\langle A[g(t)]\rangle$ in CDT configurations: plots for $k_0 = 2.5$, $V = 60000$ and different singularity lengths l_0.

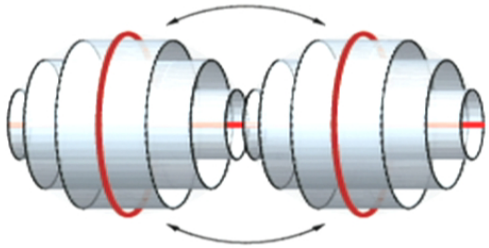

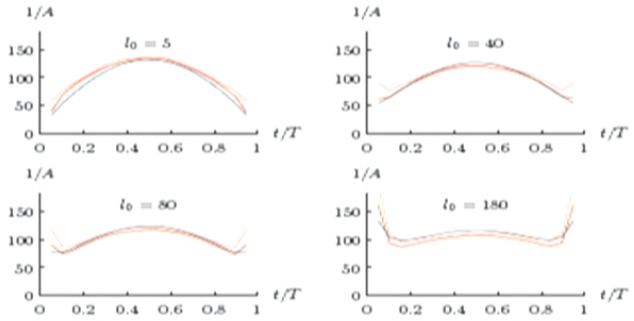

- Now we can start comparing! Semi-classically the correlation matrix $\langle \Delta\tau_i(t)\Delta\tau_j(t')\rangle$ is proportional to the inverse of $\delta^2 S_{\mathit{eff}}/\delta\tau_i(t)\delta\tau_j(t')$.
- Determine the relative prefactor $2(\frac{1}{2} - \lambda)A[g]$ of $\dot{V}^2$ and $\dot{\tau}_i^2$ in

$$S[V,\tau] = \kappa \int dt \Big((\frac{1}{2} - \lambda)\frac{\dot{V}^2}{V} + \frac{1}{2A[g]}\frac{\dot{\tau}_1^2 + \dot{\tau}_2^2}{\tau_2^2} - U(V,\tau) \Big).$$

- Fit to measured $A[g]$ gives $\lambda \approx 0.18$.

- We can perform this analysis for various couplings k_0.

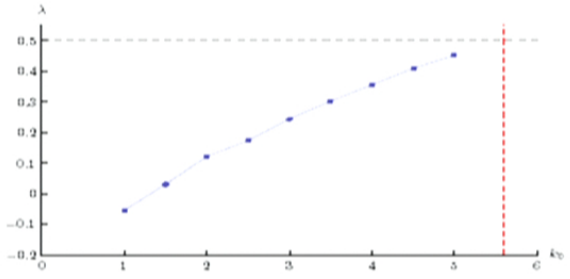

- We can perform this analysis for various couplings k_0.
- As $k_0 \to k_0^*$ the correlation in $V(t)$ of consecutive slices drops to zero compared to correlation in shape τ.

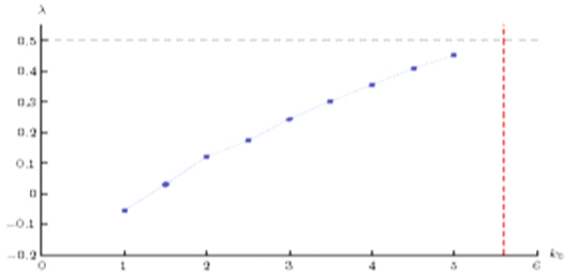

- Similar results have been obtained from studying local metric fluctuations near fixed boundaries in CDT. [TB, arXiv:1110.5158]
- Indication that spatial conformal symmetry is implemented at/near the phase transition. Relation to Shape Dynamics in 2+1 dimensions? [TB, T. Koslowski, arXiv:1107.1287]
  The weak coupling between consecutive spatial geometries may ensure that the conformal properties of 2d gravity are maintained.

Summary

- In general connecting a microscopic model of gravity to its effective dynamics in the continuum limit through observables involves a large number of non-trivial steps.

Summary

- In general connecting a microscopic model of gravity to its effective dynamics in the continuum limit through observables involves a large number of non-trivial steps.
- I have attempted to perform these steps explicitly for the special case of moduli in CDT in 2+1 dimensions on the torus.
- In the presence of a preferred time-foliation direct probes of the effective kinetic term are available. In particular λ in the modified WdW metric can be deduced from measurements.

Summary

- In general connecting a microscopic model of gravity to its effective dynamics in the continuum limit through observables involves a large number of non-trivial steps.
- I have attempted to perform these steps explicitly for the special case of moduli in CDT in 2+1 dimensions on the torus.
- In the presence of a preferred time-foliation direct probes of the effective kinetic term are available. In particular λ in the modified WdW metric can be deduced from measurements.
- CDT and Hořava–Lifshitz gravity seem to be living in the same theory space and indeed our data is well-described by a kinetic term of the type appearing in HL.

Outlook

- Construct full effective action $S[V(t), \tau(t)]$. What is $U[V, \tau]$ and how does $A[g]$ scale with V?
- Conformal invariance at the phase transition. Connection to Shape Dynamics? Analytical tools available (from 2d gravity)?

Outlook

- Construct full effective action $S[V(t), \tau(t)]$. What is $U[V, \tau]$ and how does $A[g]$ scale with V?
- Conformal invariance at the phase transition. Connection to Shape Dynamics? Analytical tools available (from 2d gravity)?
- Discrete differential geometry seems to be the natural toolbox to construct observables in higher dimensional CDT and other discrete approaches, e.g. Quantum Regge, spin foams, colored tensor models.

Outlook

- Construct full effective action $S[V(t), \tau(t)]$. What is $U[V, \tau]$ and how does $A[g]$ scale with V?
- Conformal invariance at the phase transition. Connection to Shape Dynamics? Analytical tools available (from 2d gravity)?
- Discrete differential geometry seems to be the natural toolbox to construct observables in higher dimensional CDT and other discrete approaches, e.g. Quantum Regge, spin foams, colored tensor models.
- Having large scale observables can help with renormalization/coarse graining. Outcome of measurements should be invariant under coarse graining.

Outlook

- Construct full effective action $S[V(t), \tau(t)]$. What is $U[V, \tau]$ and how does $A[g]$ scale with V?
- Conformal invariance at the phase transition. Connection to Shape Dynamics? Analytical tools available (from 2d gravity)?
- Discrete differential geometry seems to be the natural toolbox to construct observables in higher dimensional CDT and other discrete approaches, e.g. Quantum Regge, spin foams, colored tensor models.
- Having large scale observables can help with renormalization/coarse graining. Outcome of measurements should be invariant under coarse graining.

Thanks for your attention!

Price to pay for the high luminosity: larger-than-expected pile-up

Pile-up = number of interactions per crossing
Tails up to ~20 → comparable to design luminosity
(50 ns operation; several machine parameters pushed beyond design)

LHC figures used over the last 20 years:
~ 2 (20) events/crossing at $L=10^{33}$ (10^{34})

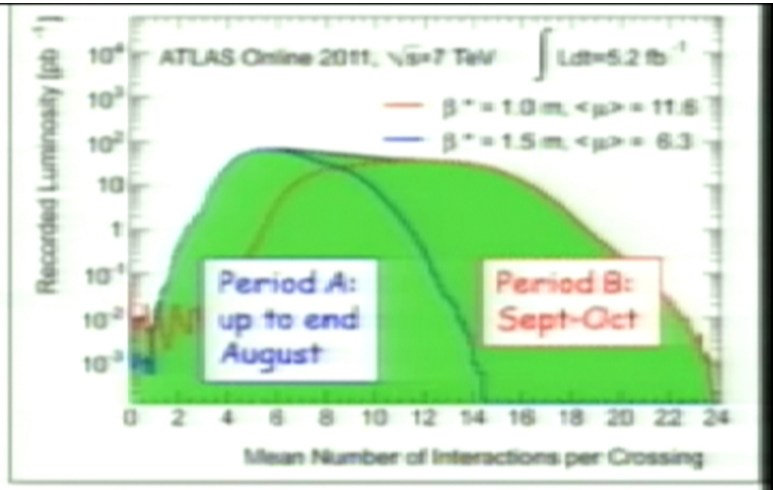

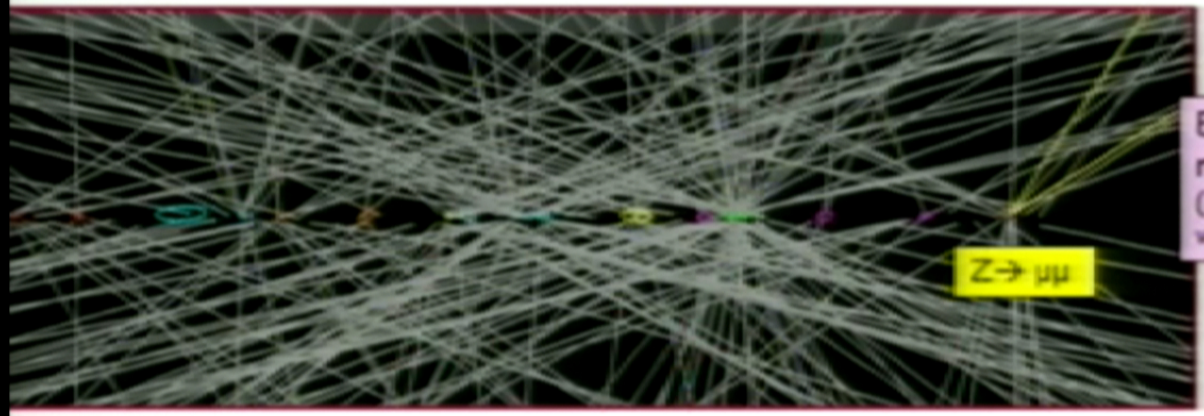

Event with 20 reconstructed vertices
(ellipses have 20 σ size for visibility reasons)

Challenging for trigger, computing resources, reconstruction of physics objects (in particular E_T^{miss}, soft jets, ..)
Precise modeling of both in-time and out-of-time pile-up in simulation is essential

Summary of main electroweak and top cross-section measurements

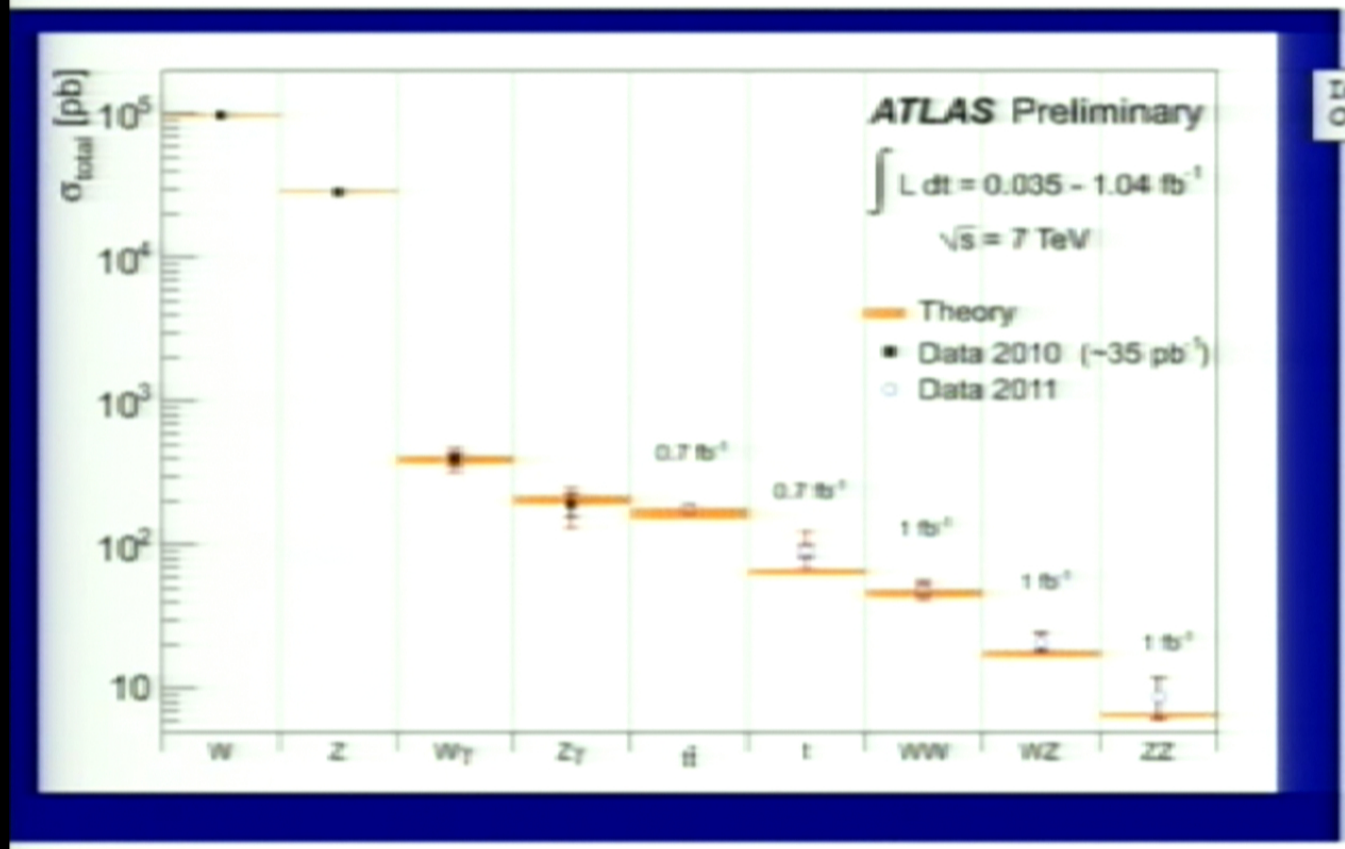

Summary of main electroweak and top cross-section measurements

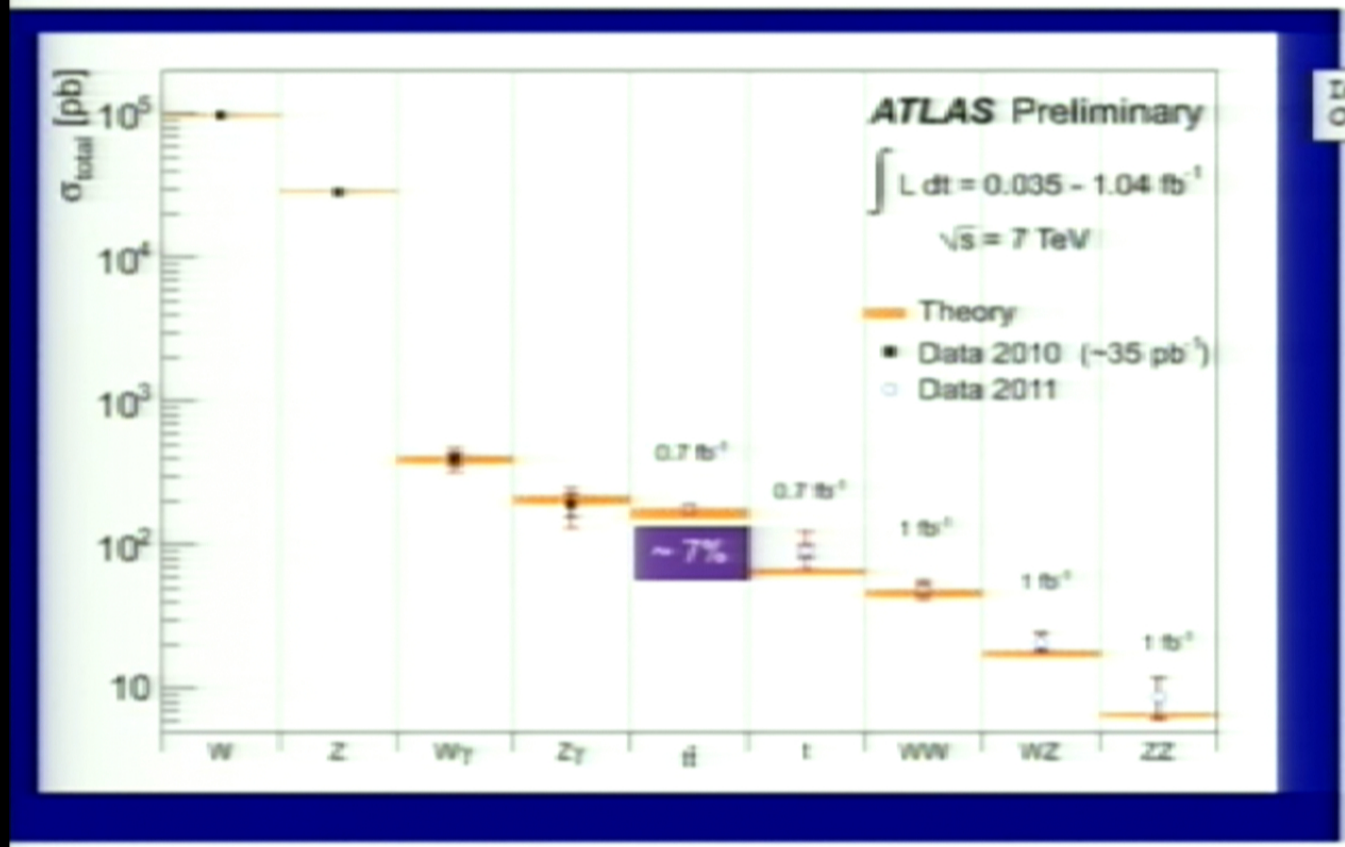

Inner error: statistical
Outer error: total

Good agreement with SM expectations (within present uncertainties)

xperimental precision starts to challenge theory for e.g. tt (background to most H searches)

SM Higgs production cross-section and decay modes

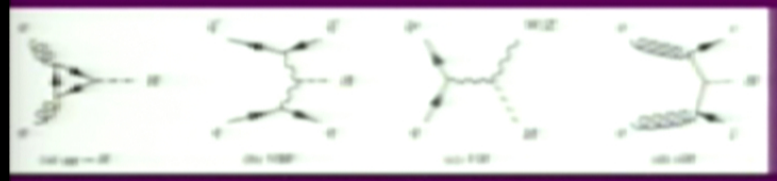

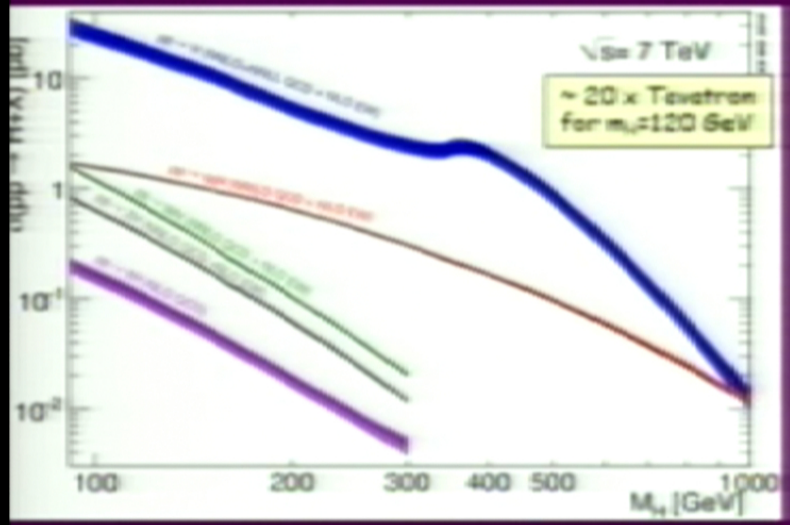

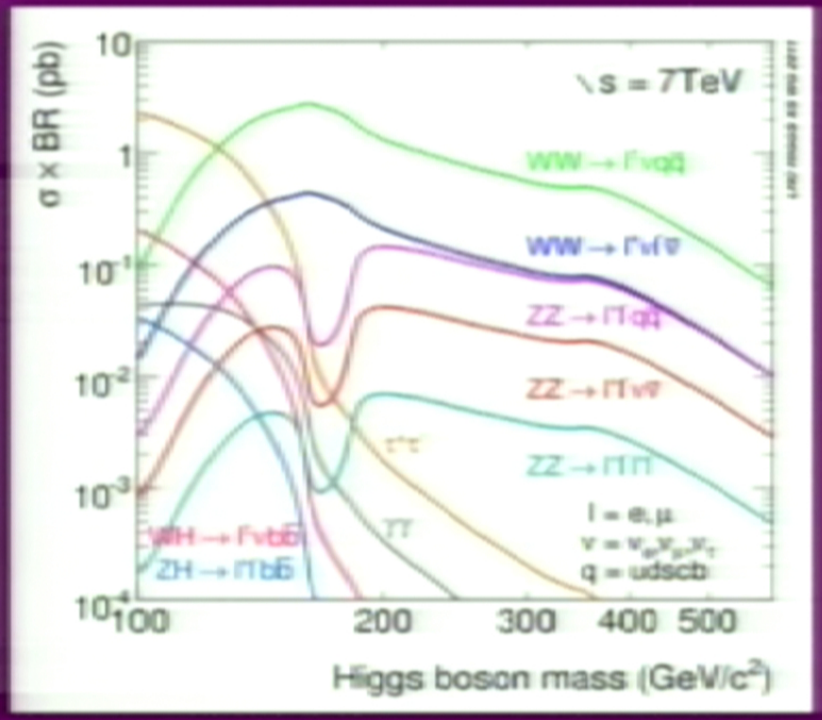

- Cross-sections computed to NNLO in most cases → theory uncertainties reduced to < 20%
- Huge progress also in the theoretical predictions of numerous and complex backgrounds
- Excellent achievements of the theory community; very fruitful discussions with the experiments (e.g. through LHC Higgs Cross Section WG, LPCC, etc.)

SM Higgs production cross-section and decay modes

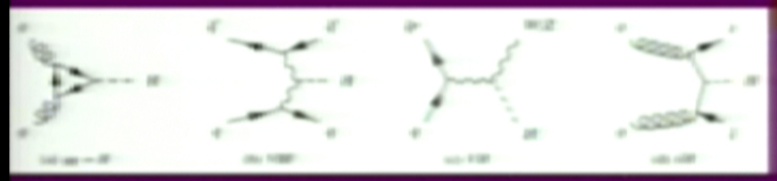

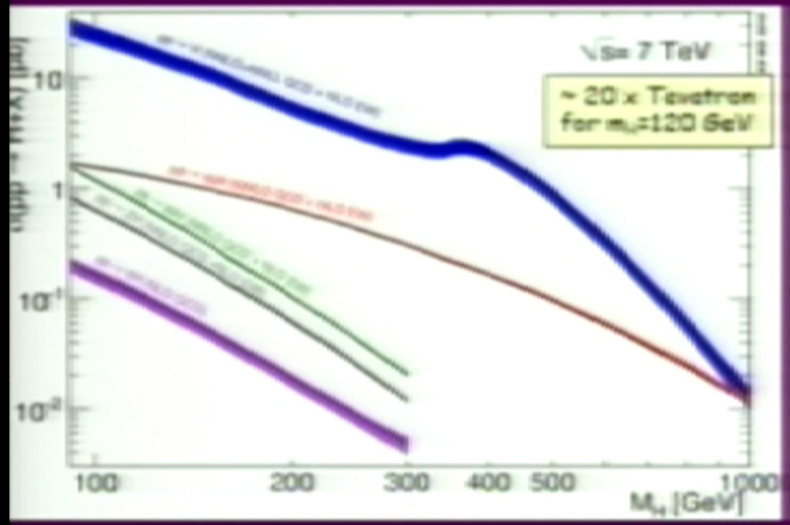

Experimentally most sensitive channels vs m_H

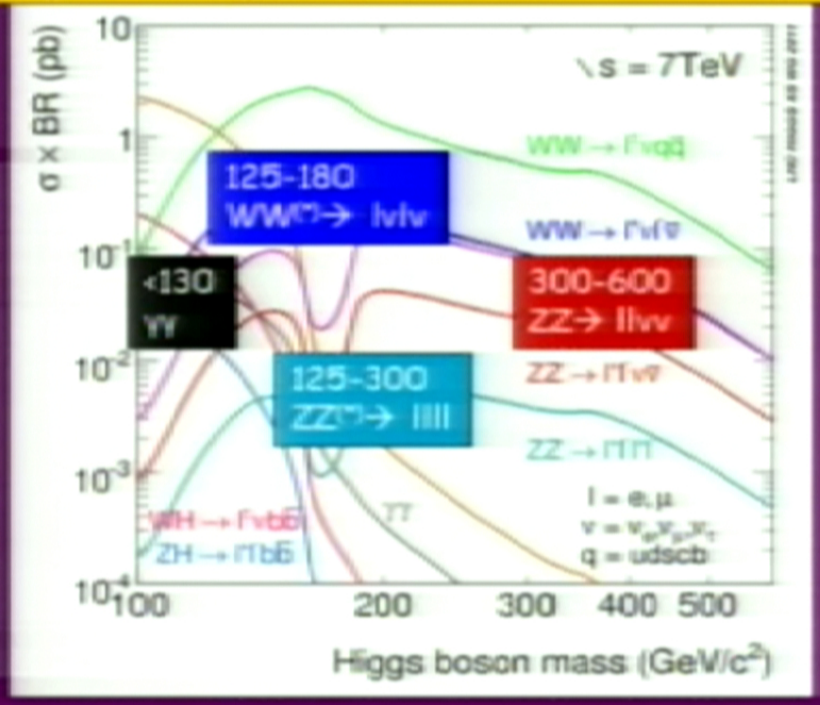

- Cross-sections computed to NNLO in most cases → theory uncertainties reduced to < 20%
- Huge progress also in the theoretical predictions of numerous and complex backgrounds
- Excellent achievements of the theory community: very fruitful discussions with the experiments (e.g. through LHC Higgs Cross Section WG, LPCC, etc.)

Present status (as of this morning …)

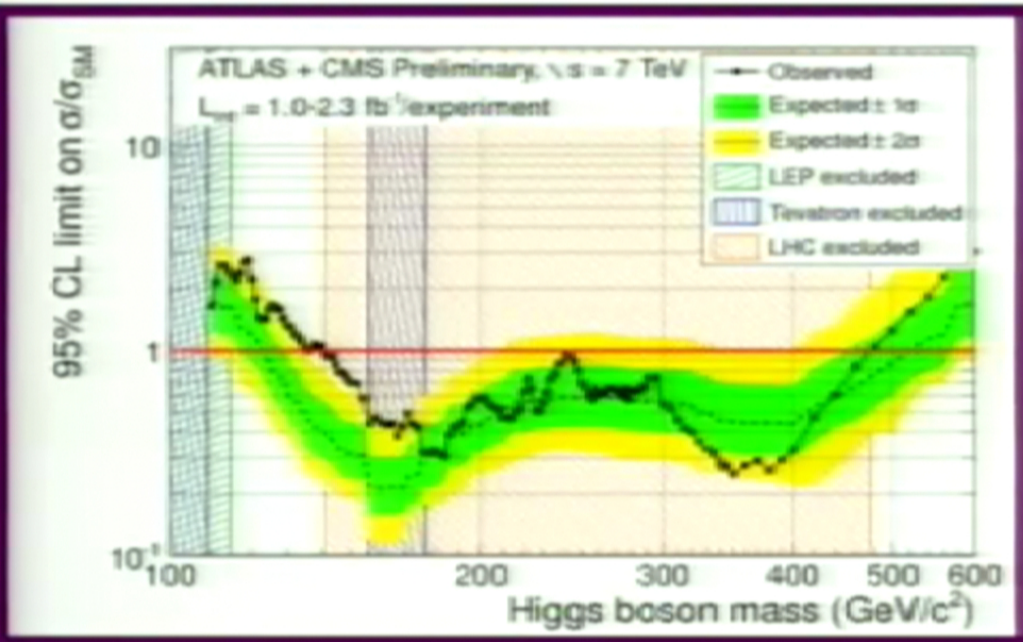

November 2011
CMS PAS HIG-11-023,
ATLAS-CONF-201-157

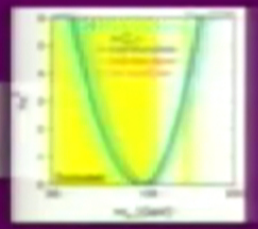

LEP (95%CL)
$m_H > 114.4$ GeV

Tevatron exclusion (95%CL):
$100 < m_H < 109$ GeV
$156 < m_H < 177$ GeV

First ATLAS+CMS combination: based on data recorded until end August 2011:
up to ~2.3 fb^{-1} per experiment

Excluded 95% CL : 141-476 GeV
Excluded 99% CL : 146-443 GeV (except ~222, 238-248, ~295 GeV)
Expected 95% CL : 124-520 GeV → max deviation from background-only: ~ 3σ (m_H~144 GeV)

Present status (as of this morning …)

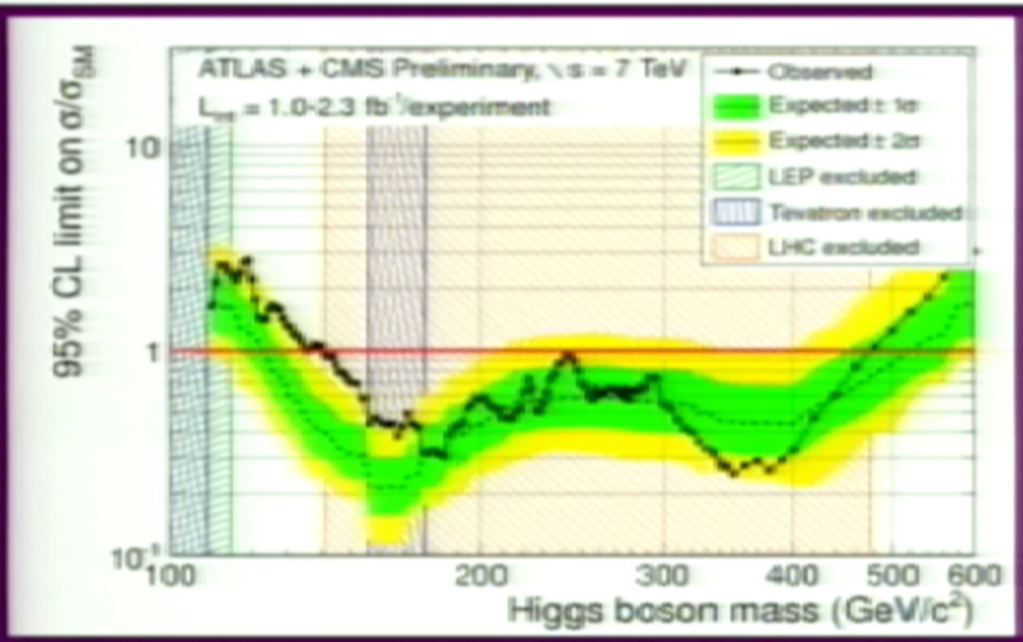

November 2011
CMS PAS HIG-11-023,
ATLAS-CONF-201-157

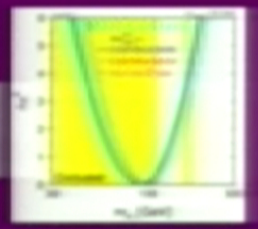

LEP (95%CL)
$m_H > 114.4$ GeV

Tevatron exclusion (95%CL):
$100 < m_H < 109$ GeV
$156 < m_H < 177$ GeV

First ATLAS+CMS combination: based on data recorded until end August 2011:
up to ~2.3 fb^{-1} per experiment

Excluded 95% CL : 141-476 GeV
Excluded 99% CL : 146-443 GeV (except ~222, 238-248, ~295 GeV)
Expected 95% CL : 124-520 GeV → max deviation from background-only: ~ 3σ (m_H~144 GeV)

Present status (as of this morning …)

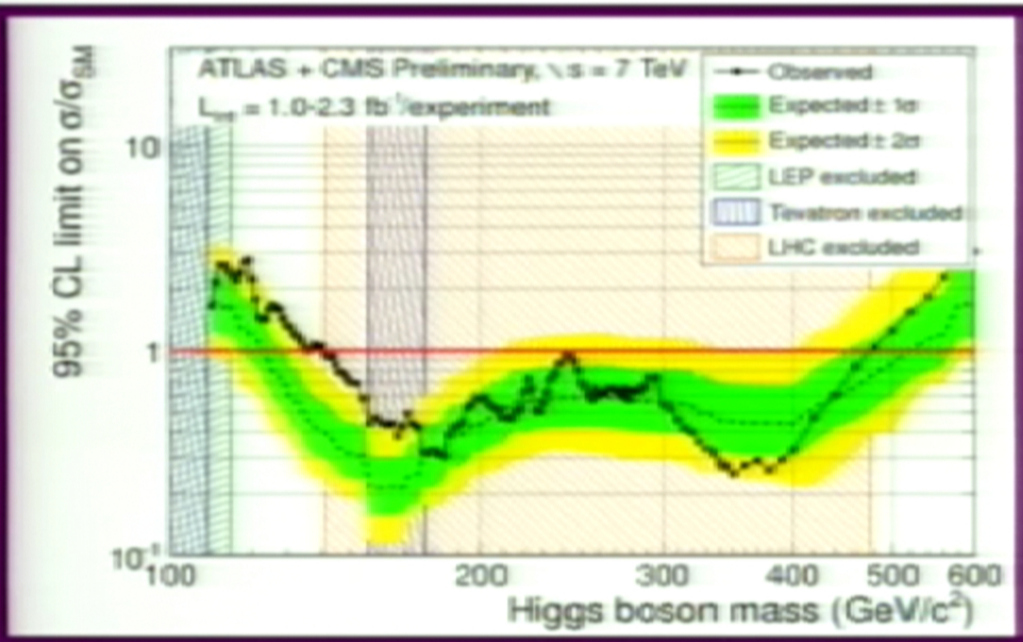

November 2011
CMS PAS HIG-11-023,
ATLAS-CONF-201-157

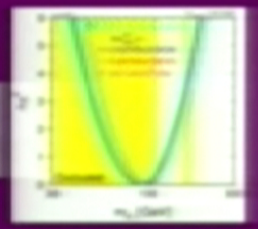

LEP (95%CL)
$m_H > 114.4$ GeV

Tevatron exclusion (95%CL):
$100 < m_H < 109$ GeV
$156 < m_H < 177$ GeV

First ATLAS+CMS combination: based on data recorded until end August 2011:
up to ~2.3 fb^{-1} per experiment

Excluded 95% CL : 141-476 GeV
Excluded 99% CL : 146-443 GeV (except ~222, 238-248, ~295 GeV)
Expected 95% CL : 124-520 GeV → max deviation from background-only: ~ 3σ (m_H~144 GeV)

Over the last months ...

Huge efforts to improve understanding of detector performance:

- 2011 data recorded with very different conditions compared to 2010, in particular the latest period with higher pile-up
- several measurements with 2010 data already dominated by systematic uncertainty → need to dismantle systematics

→ Improved knowledge (of many subtle effects...) propagated to simulation and reconstruction: detailed simulation of in- and out-of-time pile-up including bunch-train structure; new alignment; accurate simulation of absorber plates in the EM calorimeter (→ better agreement data-MC for e/γ showers); modeling varying detector conditions in MC; etc. etc.

Necessary, high-priority work for the full ATLAS physics programme based on the 2011 data

Higgs searches:
We updated the most sensitive channels in the best motivated (EW fit) and not-yet-excluded low-mass region: $H \to \gamma\gamma$ (4.9 fb^{-1}), $H \to 4l$ (4.8 fb^{-1}), $H \to WW \to l\nu l\nu$ (2.1 fb^{-1})

10

Micro-summary of present Higgs searches in ATLAS

Channel	m_H range (GeV)	Int. lumi fb^{-1}	Main backgrounds	Number of signal events after cuts	S/B after cuts	Expected σ/σ_{SM} sensitivity
$H \to \gamma\gamma$	110-150	4.9	$\gamma\gamma$, γj, jj	~70	~0.02	1.6-2
$H \to \tau\tau \to ll+\nu$	110-140	1.1	$Z \to \tau\tau$, top	~0.8	~0.02	30-60
$H \to \tau\tau \to l\tau_{had}$	100-150	1.1	$Z \to \tau\tau$	~10	~5 10^{-3}	10-25
W/ZH → bbl(l)	110-130	1.1	W/Z+jets, top	~6	~5 10^{-3}	15-25
$H \to WW^{(*)} \to l\nu l\nu$	110-300	2.1	WW, top, Z+jet	~20 (130 GeV)	~0.3	0.3-8
$H \to ZZ^{(*)} \to 4l$	110-600	4.8	ZZ*, top, Zbb	~2.5 (130 GeV)	~1.5	0.7-10
$H \to ZZ \to ll\,\nu\nu$	200-600	2.1	ZZ, top, Z+jets	~20 (400 GeV)	~0.3	0.8-4
$H \to ZZ \to ll\,qq$	200-600	2.1	Z+jets, top	2-20 (400 GeV)	0.05-0.5	2-6
$H \to WW \to l\nu qq$	240-600	1.1	W+jets, top, jets	~45 (400 GeV)	10^{-3}	5-10

- Based on (conservative) cut-based selections
- Large and sometimes not well-known backgrounds estimated mostly with data-driven techniques using signal-free control regions

$H \to WW^{(*)} \to l\nu l\nu$ ($e\nu e\nu$, $\mu\nu\mu\nu$, $e\nu\mu\nu$)

$110 < m_H < 300$ GeV

- Most sensitive channel over ~ 125-180 GeV ($\sigma \sim 200$ fb)
- However: challenging: $2\nu \to$ no mass reconstruction/peak $\to$ "counting channel"
- 2 isolated opposite-sign leptons, large E_T^{miss}
- Main backgrounds: WW, top, Z+jets, W+jets
  - $\to m_{ll} \neq m_Z$, b-jet veto, ...
  - $\to$ Topological cuts against "irreducible" WW background:
    p_{Tll}, m_{ll}, $\Delta\phi_{ll}$ (smaller for scalar Higgs), m_T (ll, E_T^{miss})

rucial experimental aspects:

- understanding of E_T^{miss} (genuine and fake)
- excellent understanding of background in signal region $\to$ use signal-free control regions in data to constrain MC $\to$ use MC to extrapolate to the signal region

2.1 fb^{-1}

Control region	MC expectation	Observed in data
WW 0-jet	296±36	296
WW 1-jet	171±21	184
Top 1-jet	270±69	249

After leptons, m_Z and E_T^{miss} cuts

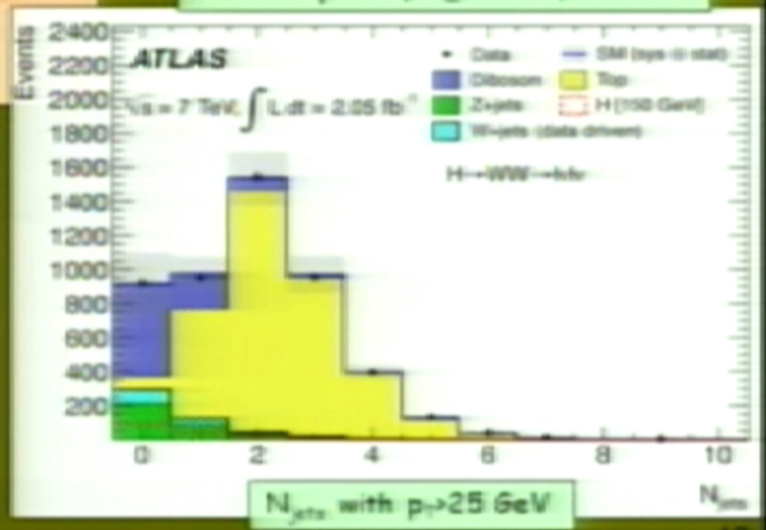

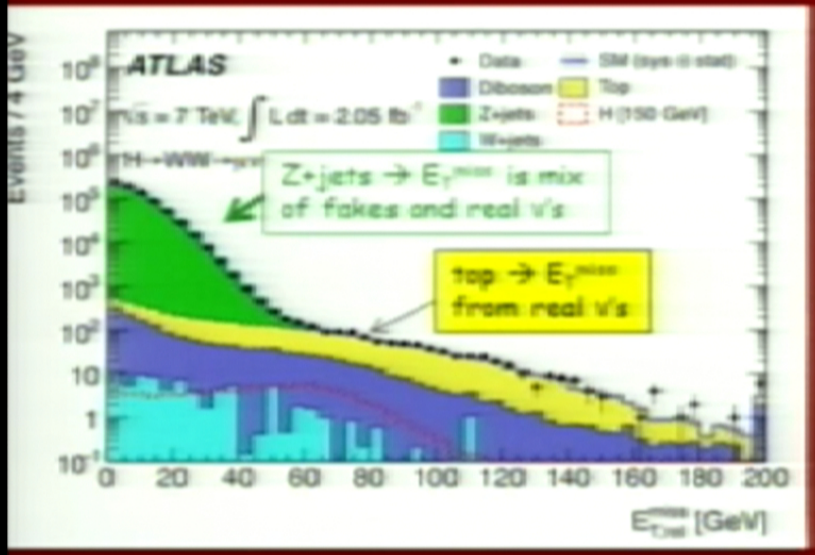

E_T^{miss} spectrum in data for inclusive events with $\mu^+\mu^-$ pair well described (over 5 orders of magnitude) by the various background components.
Dominated by real E_T^{miss} from ν's starting at E_T^{miss} ~ 50 GeV
→ little tails from detector effects

E_T^{miss} spectrum and resolution very sensitive to pile-up → we will include Period-B data when understanding at similar level as Period A

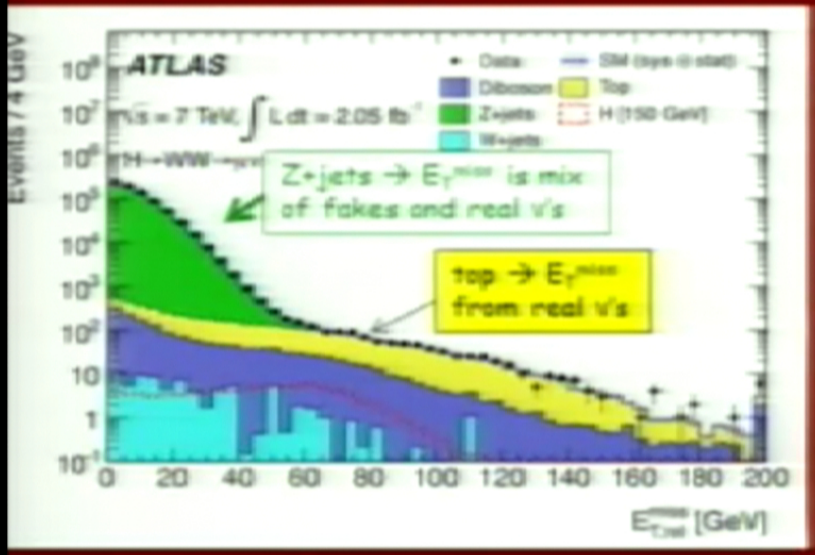

E_T^{miss} spectrum in data for inclusive events with $\mu^+\mu^-$ pair well described (over 5 orders of magnitude) by the various background components.
Dominated by real E_T^{miss} from ν's starting at $E_T^{miss} \sim 50$ GeV
→ little tails from detector effects

E_T^{miss} spectrum and resolution very sensitive to pile-up → we will include Period-B data when understanding at similar level as Period A

2.1 fb^{-1}

After all cuts (selection for m_{H}=130 GeV)

Observed in data	94 events 10 ee, 42 eμ, 42 μμ
Expected background	76 (±11)
Expected signal m_H=130 GeV	19 (±4)

Transverse mass spectrum after all cuts (except M_T)

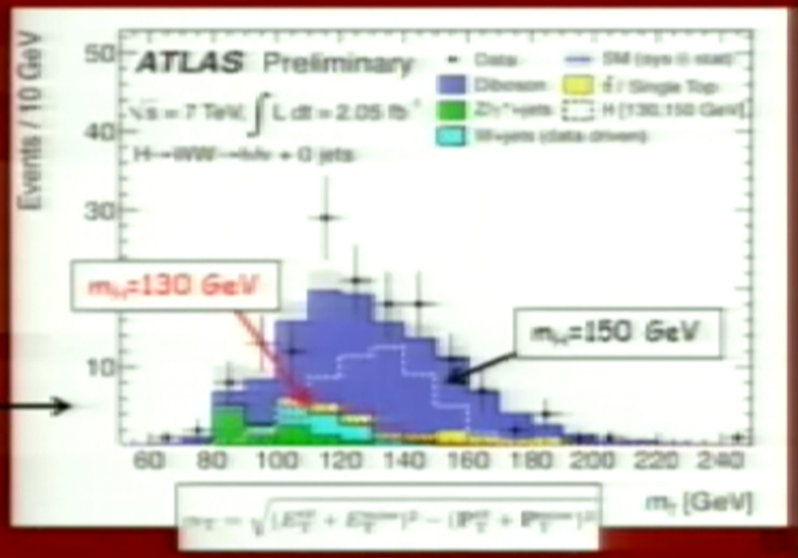

After all cuts (selection for m_H=130 GeV) 2.1 fb^{-1}

Observed in data	94 events 10 ee, 42 eμ, 42 μμ
Expected background	76 (±11)
Expected signal m_H=130 GeV	19 (±4)

Consistency of the data with the background-only expectation

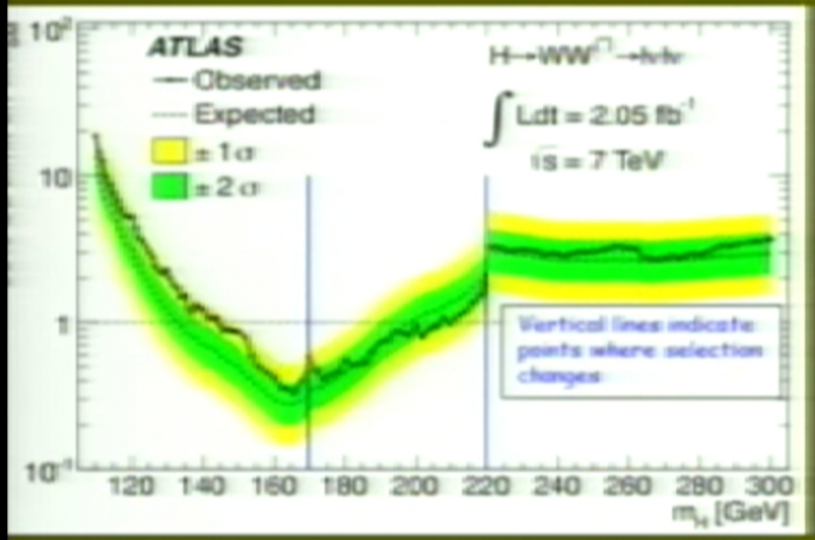

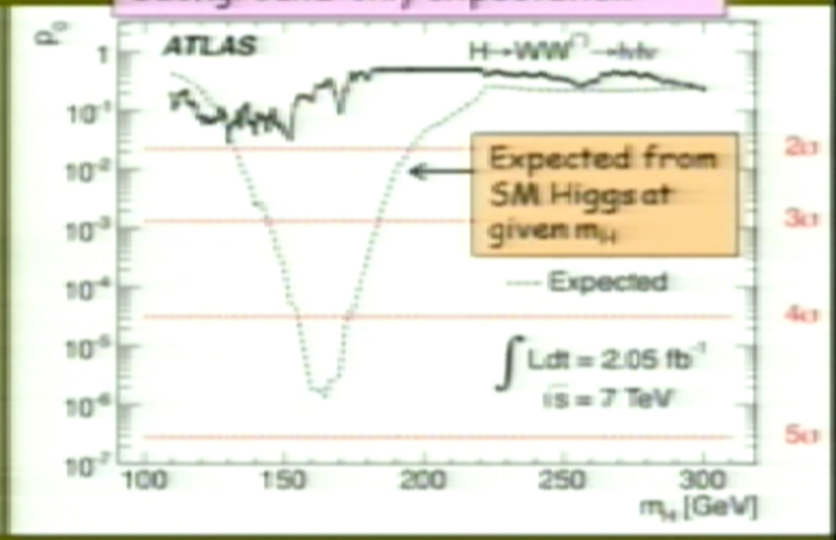

- Excluded (95% CL): 145 < m_H < 206 GeV (expected: 134-200 GeV)
- Observed limit within 2σ of expected: max deviation 1.9 σ for m_H ~ 130 GeV

14

After all cuts (selection for m_H=130 GeV) 2.1 fb^{-1}

Observed in data	94 events 10 ee, 42 eμ, 42 μμ
Expected background	76 (±11)
Expected signal m_H=130 GeV	19 (±4)

Consistency of the data with the background-only expectation

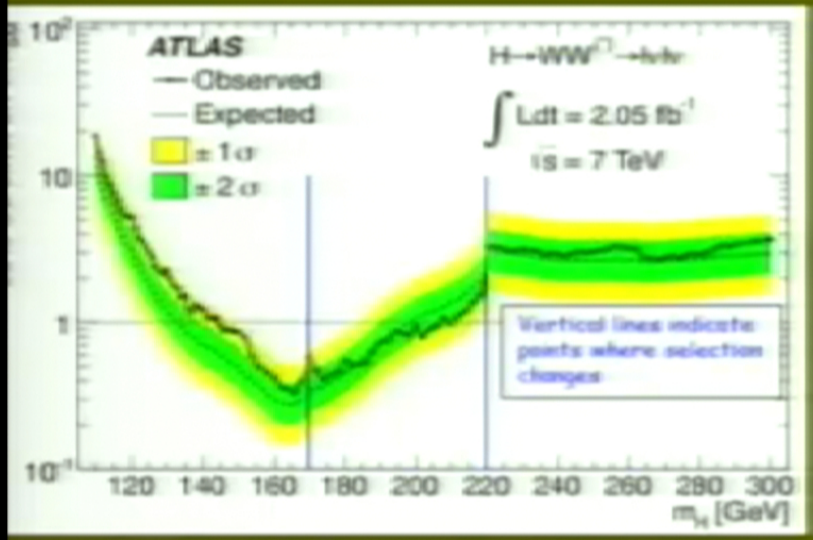

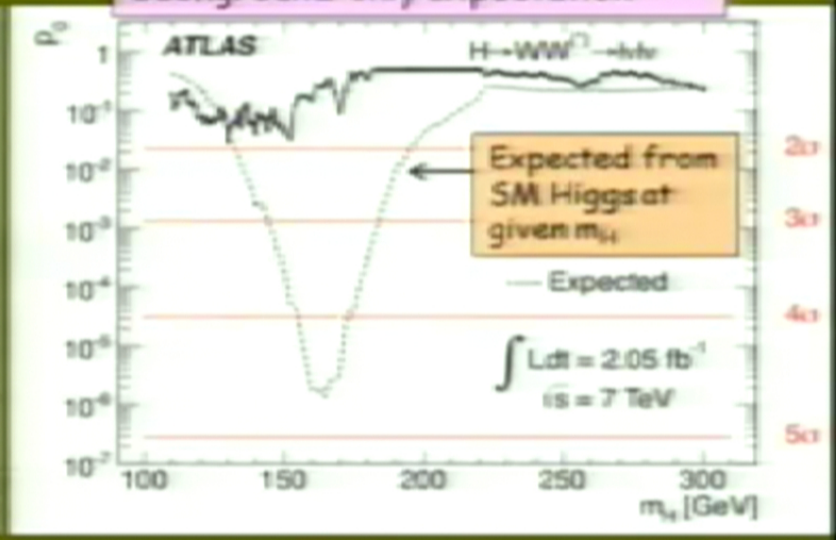

- Excluded (95% CL): 145 < m_H < 206 GeV (expected: 134–200 GeV)
- Observed limit within 2σ of expected: max deviation 1.9 σ for m_H ~ 130 GeV

14

$H \rightarrow \gamma\gamma$

$110 \leq m_H \leq 150$ GeV

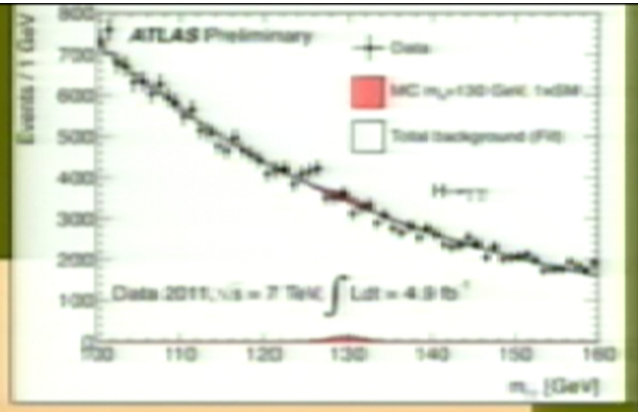

- Small cross-section: $\sigma \sim 40$ fb
- Simple final state: two high-p_T isolated photons
  $E_T(\gamma_1, \gamma_2) > 40, 25$ GeV
- Main background: $\gamma\gamma$ continuum (irreducible, smooth, ...)
- Events divided into 9 categories based on η-photon (e.g. central, rest, ...), converted/unconverted, $p_T^{\gamma\gamma}$ perpendicular to $\gamma\gamma$ thrust axis
- ~70 signal events expected in 4.9 fb^{-1} after all selections for m_H=125 GeV
  ~ 3000 background events in signal mass window → S/B ~ 0.02

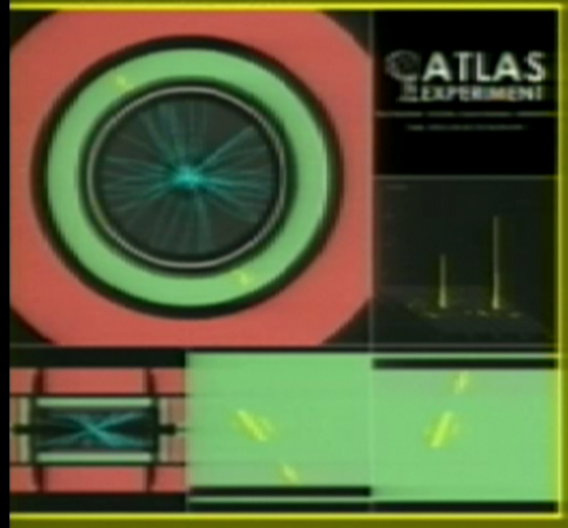

Crucial experimental aspects:

- excellent $\gamma\gamma$ mass resolution to observe narrow signal peak above irreducible background
- powerful γ/jet separation to suppress γj and jj background with jet → π^0 faking single γ

15

$m^2_{\gamma\gamma} = 2\,E_1\,E_2\,(1-\cos\alpha)$

m_H=120 GeV	$\sigma(m_{\gamma\gamma})$ GeV	Event fraction in $\pm 1.4\,\sigma(m_{\gamma\gamma})$
ll	1.7	80 %
est category unconverted central)	1.4	84%
Vorst category (~10%) 1 γ converted, ≥ 1 γ near arrel/end-cap transition)	2.3	70%

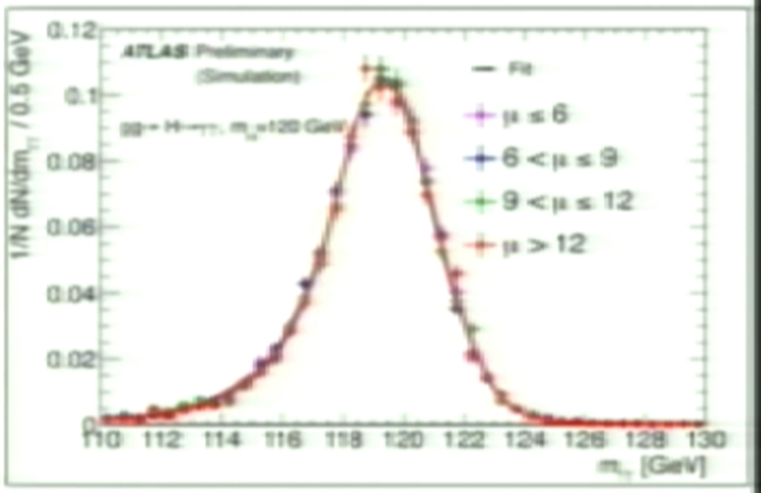

$m^2_{\gamma\gamma} = 2 E_1 E_2 (1-\cos\alpha)$

m_H=120 GeV	$\sigma(m_{\gamma\gamma})$ GeV	Event fraction in $\pm 1.4\,\sigma(m_{\gamma\gamma})$
ll	1.7	80 %
est category unconverted central)	1.4	84%
Vorst category (~10%) ≥ 1 γ converted, ≥ 1 γ near arrel/end-cap transition)	2.3	70%

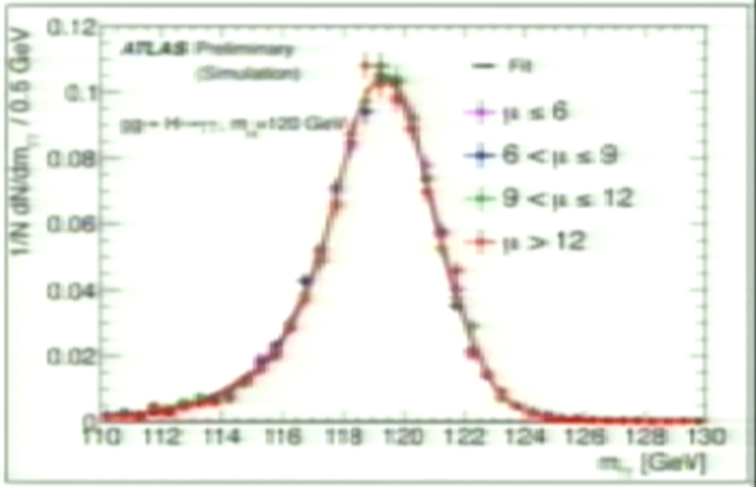

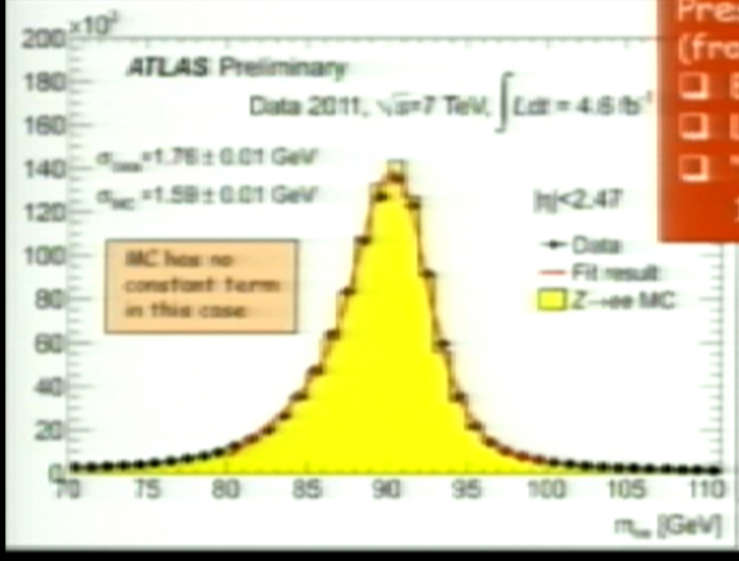

Present understanding of calorimeter E response (from Z, J/ψ → ee, W→ eν data and MC):

- Energy scale at m_Z known to ~ 0.5%
- Linearity better than 1% (over few GeV-few 100 GeV)
- "Uniformity" (constant term of resolution): 1% (barrel) -1.7 % (end-cap)

Electron scale and resolution transported to photons using MC
(systematics few from material effects)

16

$m^2_{\gamma\gamma} = 2 E_1 E_2 (1-\cos\alpha)$

m_H=120 GeV	$\sigma(m_{\gamma\gamma})$ GeV	Event fraction in $\pm 1.4\,\sigma(m_{\gamma\gamma})$
ll	1.7	80 %
est category unconverted central)	1.4	84%
Vorst category (~10%) ≥ 1 γ converted, ≥ 1 γ near arrel/end-cap transition)	2.3	70%

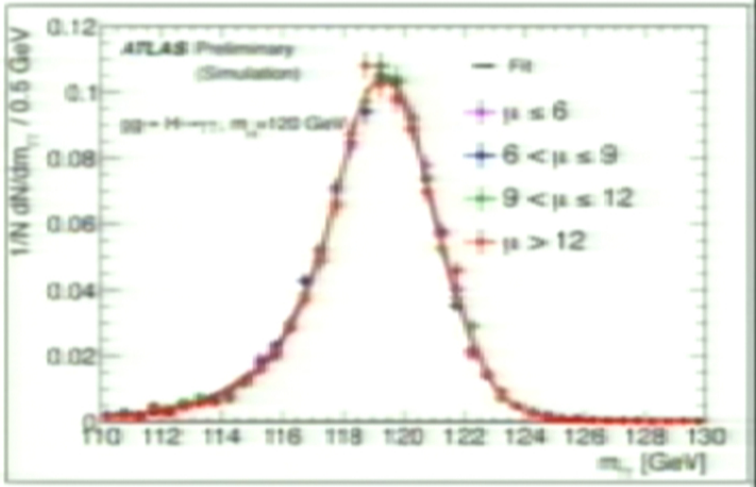

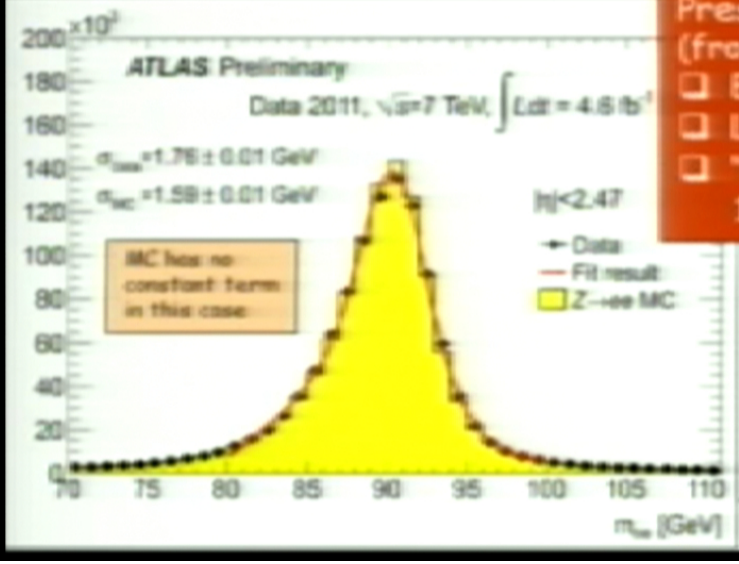

Present understanding of calorimeter E response (from Z, J/ψ → ee, W→ eν data and MC):

- Energy scale at m_Z known to ~ 0.5%
- Linearity better than 1% (over few GeV-few 100 GeV)
- "Uniformity" (constant term of resolution): 1% (barrel) -1.7 % (end-cap)

Electron scale and resolution transported to photons using MC
(systematics few from material effects)

16

$m^2_{\gamma\gamma} = 2\,E_1\,E_2\,(1-\cos\alpha)$

α=opening angle of the two photons

Use longitudinal (and lateral) segmentation of EM calorimeter to measure photon polar angle ϑ crucial at high pile-up: many vertices distributed over σ_z (LHC beam spot) ~ 5.6 cm → difficult to know which one produced the γγ pair

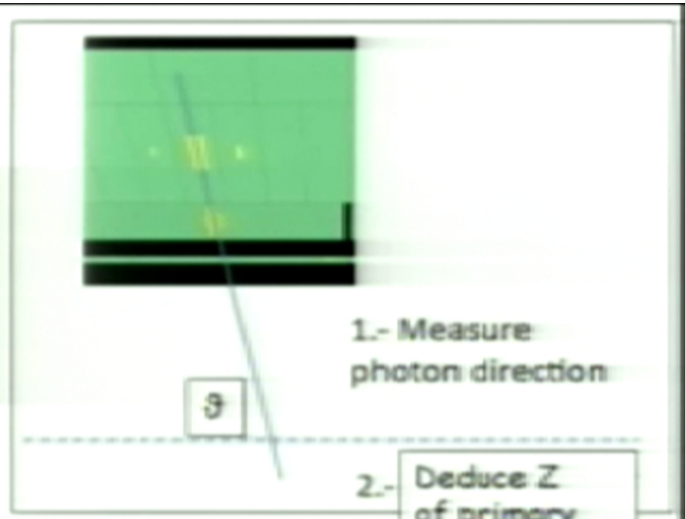

Z-vertex as measured in γγ events after selection from calorimeter "pointing"

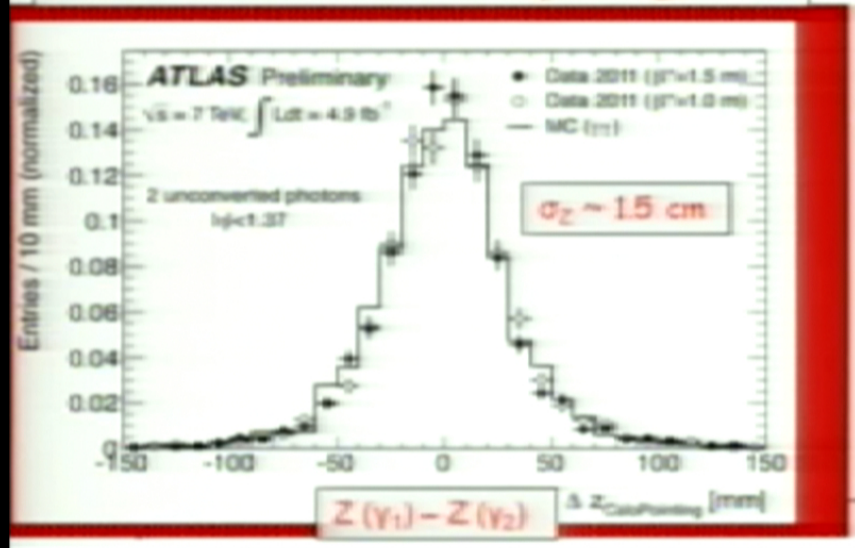

- Calorimeter pointing capability reduces vertex uncertainty from ~ 5.6 cm (LHC beam spot) to ~ 1.5 cm
- → Contribution to mass resolution from angular term is negligible with calo pointing (γ →ee vertex also used)
- Robust against pile-up

17

$m^2_{\gamma\gamma} = 2\,E_1\,E_2\,(1-\cos\alpha)$

α=opening angle of the two photons

Use longitudinal (and lateral) segmentation of EM calorimeter to measure photon polar angle ϑ crucial at high pile-up: many vertices distributed over σ_z (LHC beam spot) ~ 5.6 cm → difficult to know which one produced the γγ pair

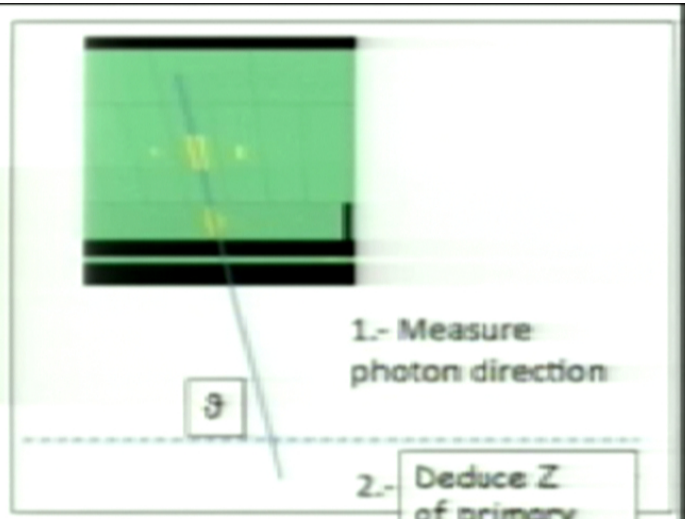

Z-vertex as measured in γγ events after selection from calorimeter "pointing"

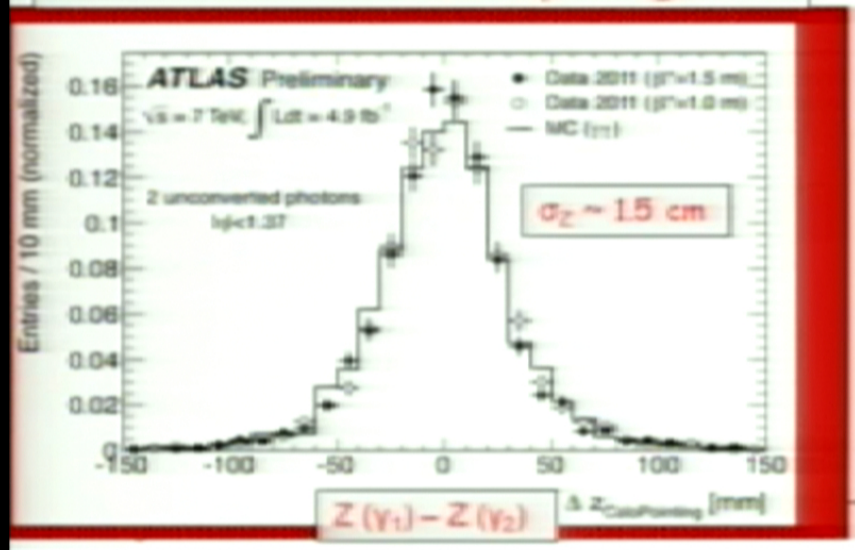

- Calorimeter pointing capability reduces vertex uncertainty from ~ 5.6 cm (LHC beam spot) to ~ 1.5 cm
- → Contribution to mass resolution from angular term is negligible with calo pointing (γ →ee vertex also used)
- Robust against pile-up

$m^2_{\gamma\gamma} = 2\,E_1\,E_2\,(1-\cos\alpha)$

α=opening angle of the two photons

Use longitudinal (and lateral) segmentation of EM calorimeter to measure photon polar angle ϑ crucial at high pile-up: many vertices distributed over σ_z (LHC beam spot) ~ 5.6 cm → difficult to know which one produced the γγ pair

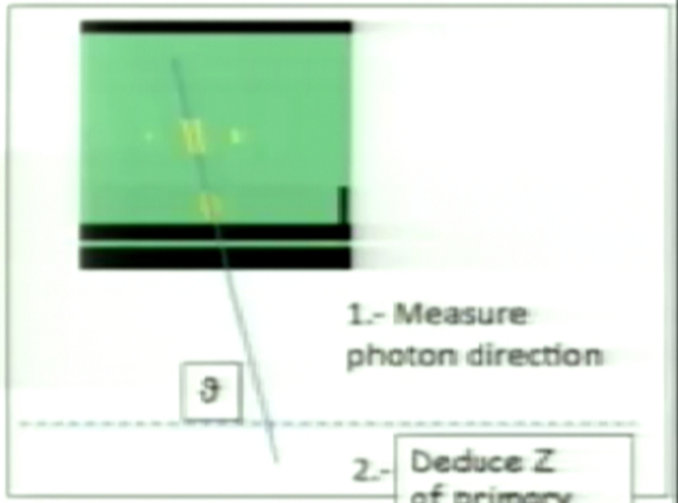

Z-vertex as measured in γγ events after selection from calorimeter "pointing"

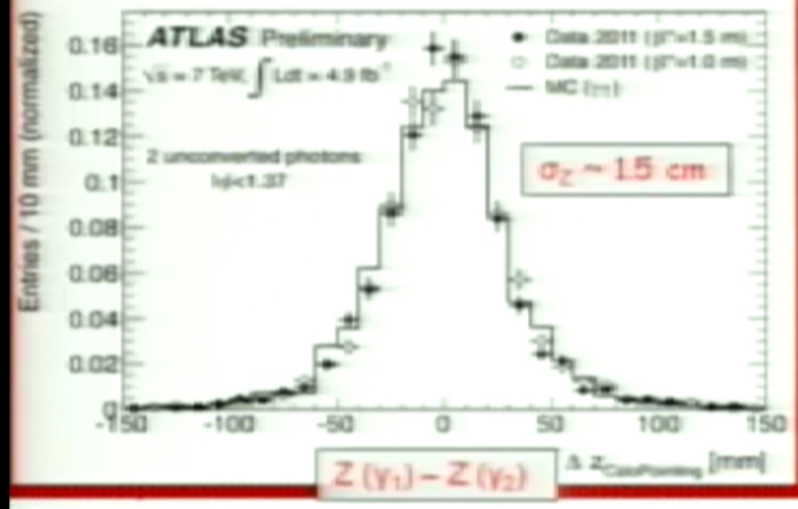

- Calorimeter pointing capability reduces vertex uncertainty from ~ 5.6 cm (LHC beam spot) to ~ 1.5 cm
- → Contribution to mass resolution from angular term is negligible with calo pointing (γ →ee vertex also used)
- Robust against pile-up

17

otentially huge background from γj and jj production with jets fragmenting into a single ard π^0 and the π^0 faking single photon

etermined choice of fine lateral segmentation (4mm η-strips) f the first compartment of ATLAS EM calorimeter

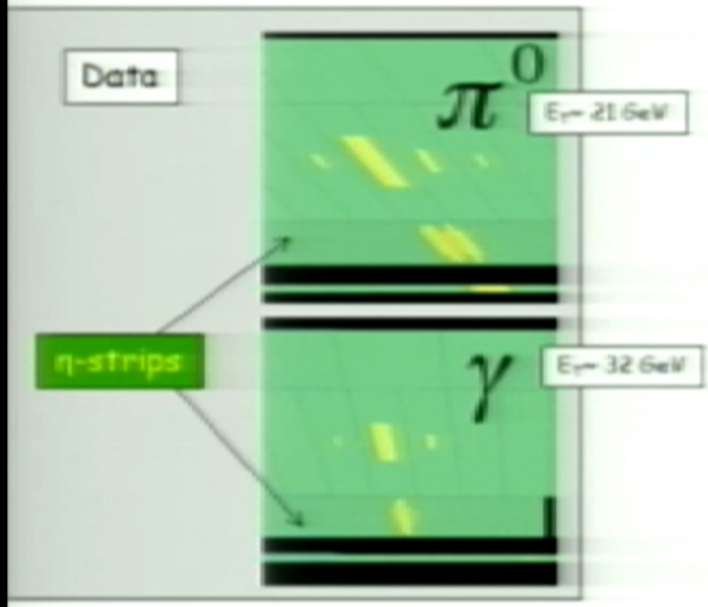

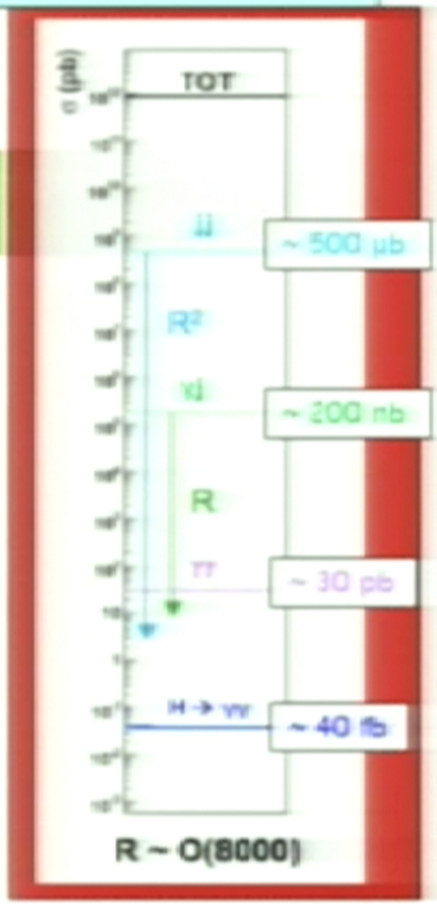

However: huge uncertainties on σ (γj, jj) !! → not obvious γj, jj could be suppressed well below irreducible γγ until we measured with data

After all cuts: 22489 events with $100 < m_{\gamma\gamma} < 160$ GeV observed in the data

Sample composition estimated from data using control samples

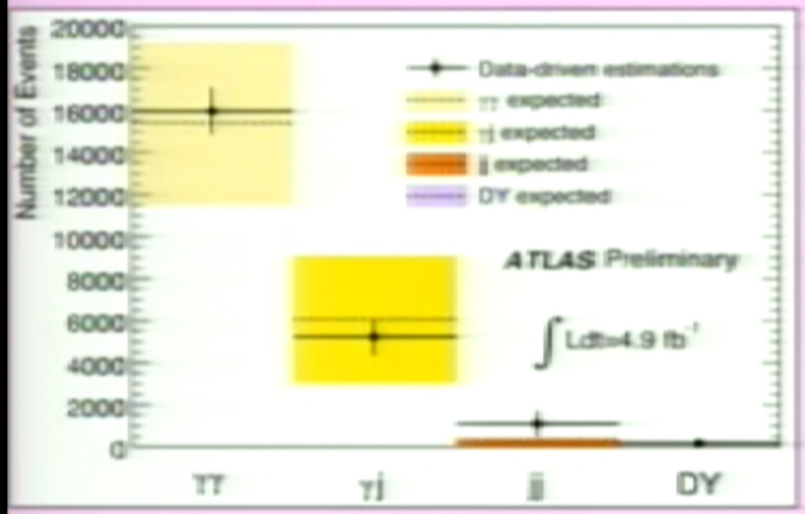

	Number of events	Fraction
γγ	16000 ± 1120	71 ±5 %
γj	5230 ± 890	23 ±4 %
jj	1130 ± 600	5 ±3 %
DY/Z	165 ± 8	0.7 ±0.1 %

γj + jj « γγ irreducible (purity ~ 70%)

Photon identification efficiency: ~ 85±5% from MC, cross-checked with data ($Z \to ee$, $Z \to ee\gamma$, $\mu\mu\gamma$)

After all cuts: 22489 events with $100 < m_{\gamma\gamma} < 160$ GeV observed in the data

Sample composition estimated from data using control samples

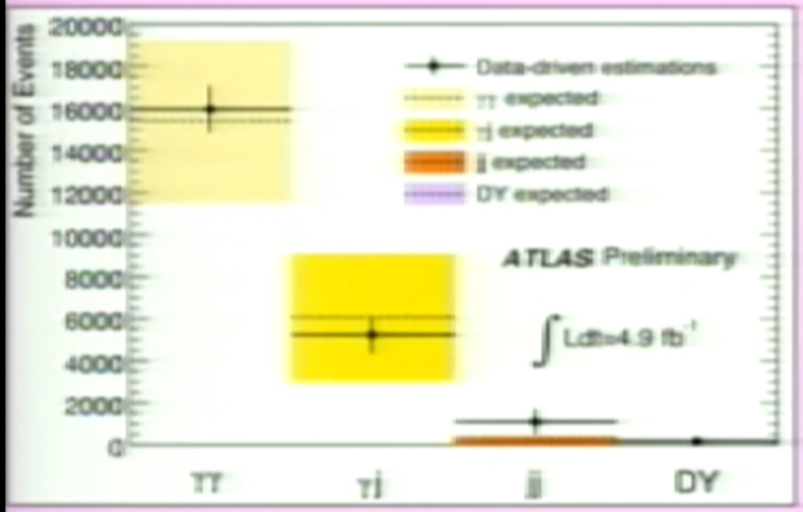

	Number of events	Fraction
γγ	16000 ± 1120	71 ±5 %
γj	5230 ± 890	23 ±4 %
jj	1130 ± 600	5 ±3 %
DY/Z	165 ± 8	0.7 ±0.1 %

γj + jj << γγ irreducible (purity ~ 70%)

Photon identification efficiency: ~ 85±5% from MC, cross-checked with data ($Z \to ee$, $Z \to ee\gamma$, $\mu\mu\gamma$)

After all selections: kinematic cuts, γ identification and isolation

- 22489 events with $100 < m_{\gamma\gamma} < 160$ GeV observed in the data
- expected signal efficiency: ~ 35% for m_{H}=125 GeV

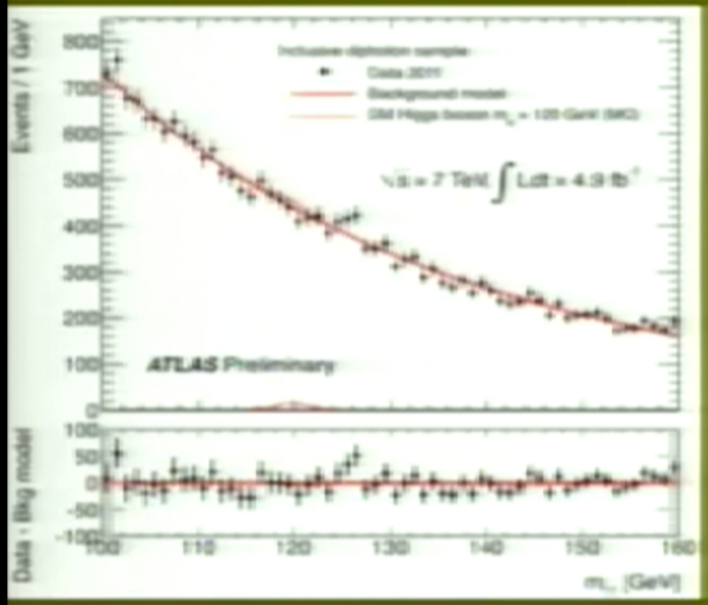

$m_{\gamma\gamma}$ spectrum fit with exponential function for background plus Crystal Ball + Gaussian for signal
→ background determined directly from data

Systematic uncertainties on signal expectation

Event yield	
Photon reconstruction and identification	±11%
Effect of pileup on photon identification	±4%
Isolation cut efficiency	±5%
Trigger efficiency	±1%
Higgs boson cross section	+15%/−11%
Higgs boson p_T modeling	±1%
Luminosity	±3.9%
Mass resolution	
Calorimeter energy resolution	±12%
Photon energy calibration	±6%
Effect of pileup on energy resolution	±3%
Photon angular resolution	±1%
Migration	
Higgs boson p_T modeling	±8%
Conversion reconstruction	±4.5%

Main systematic uncertainties

Expected signal yield : ~ 20%
H→ γγ mass resolution : ~ 14%
H→ γγ p_T modeling : ~ 8%
Background modeling : ±0.1-5.6 events

21

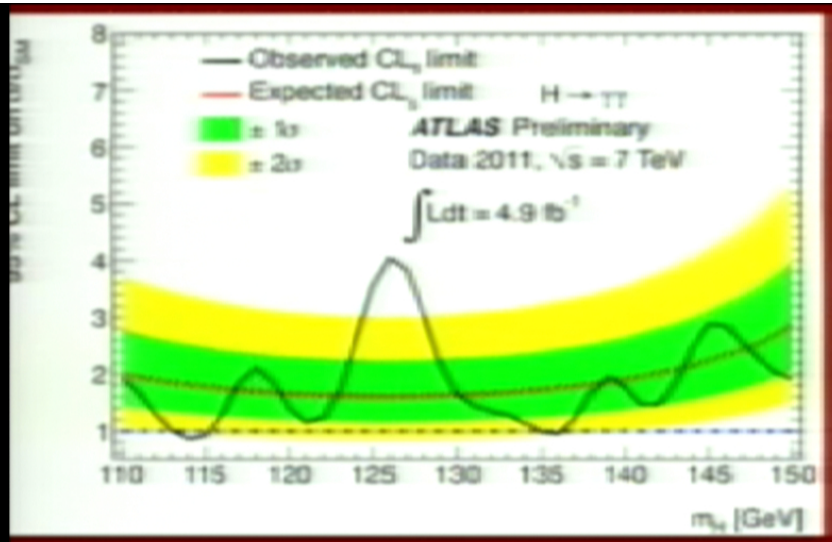

Excluded (95% CL):
$114 \leq m_{H} \leq 115$ GeV, $135 \leq m_{H} \leq 136$ GeV

Consistency of the data with the background-only expectation

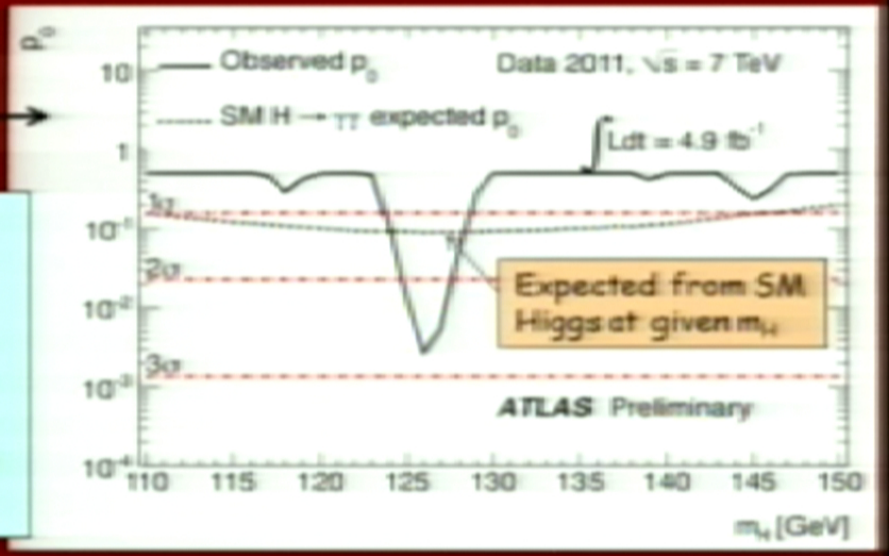

Maximum deviation from background-only expectation observed for m_H~126 GeV:
- local p_0-value: 0.27% or 2.8σ
- expected from SM Higgs: ~ 1.4σ local
- global p_0-value: includes probability for such an excess to appear anywhere in the investigated mass range (110-150 GeV) ("Look-Elsewhere-Effect"): ~7% (1.5σ)

$H \rightarrow ZZ^{(*)} \rightarrow 4l$ (4e, 4μ, 2e2μ)

$110 < m_{4l} < 600$ GeV

- $\sigma \sim 2\text{-}5$ fb
- However:
  - -- mass can be fully reconstructed → events would cluster in a (narrow) peak
  - -- pure: $S/B \sim 1$
- 4 leptons: $p_T^{1,2,3,4} > 20,20,7,7$ GeV; $m_{12} = m_Z \pm 15$ GeV; $m_{34} > 15\text{-}60$ GeV (depending on m_{4l})
- Main backgrounds:
  - -- $ZZ^{(*)}$ (irreducible)
  - -- $m_{4l} < 2m_Z$: Zbb, Z+jets, tt with two leptons from b/q-jets → l

→ Suppressed with isolation and impact parameter cuts on two softest leptons

- Signal acceptance x efficiency: ~ 15 % for $m_{4l} \sim 125$ GeV

rucial experimental aspects:

High lepton reconstruction and identification efficiency down to lowest p_T

Good lepton energy/momentum resolution

Good control of reducible backgrounds (Zbb, Z+jets, tt) in low-mass region:

→ cannot rely on MC alone (theoretical uncertainties, b/q-jet → l modeling, ..)

→ need to compare MC to data in background-enriched control regions (but: low statistics ..)

Conservative/stringent p_T and m(ll) cuts used at this stage

23

Identification efficiency from
J/ψ → ee, W → eν, Z→ ee data samples

Crucial to understand low-p_T electrons
(affected by material) with data

Electron performance

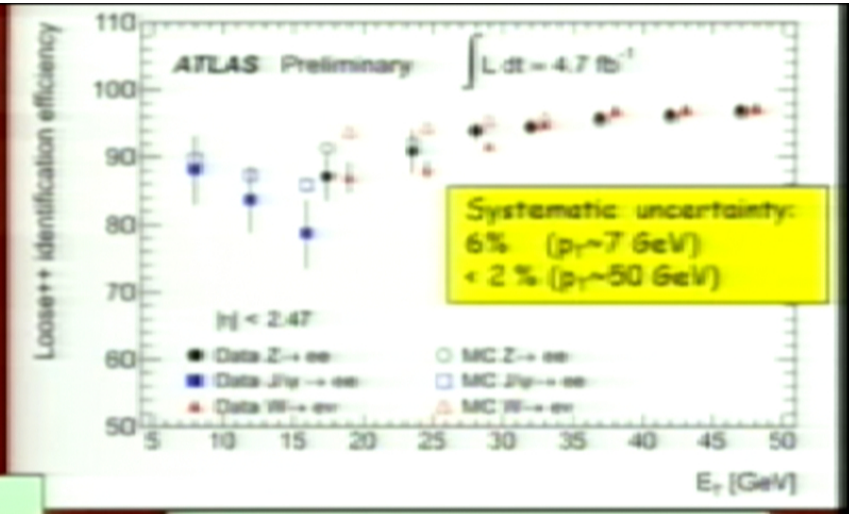

ariation of electron efficiency with
ile-up (cuts not re-tuned yet) well modeled by
imulation: from Z→ ee data and MC samples

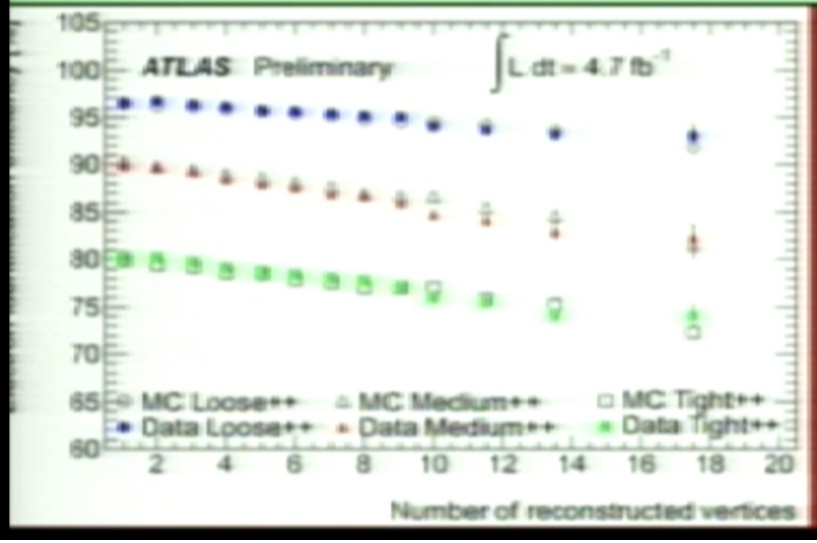

H→ 4e mass resolution: 2.5 GeV
Event fraction in ±2σ: ~ 82%

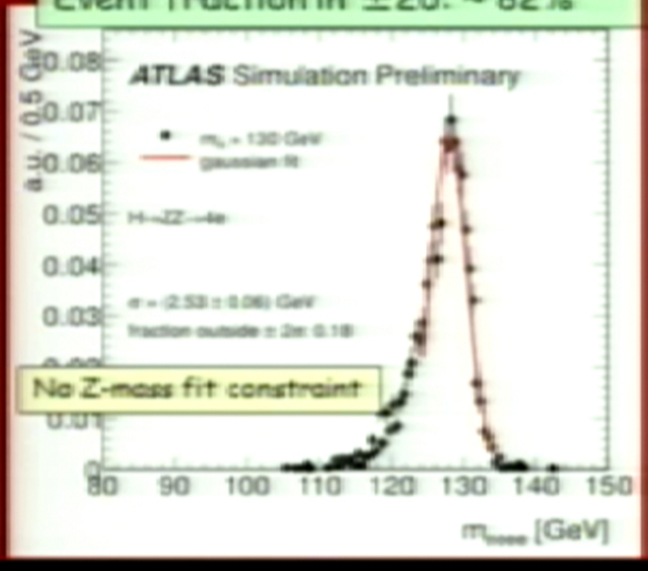

After all selections: kinematic cuts, isolation, impact parameter

Full mass range
Observed: 71 events: 24 4μ + 30 2e2μ + 17 4e
Expected from background: 62±9

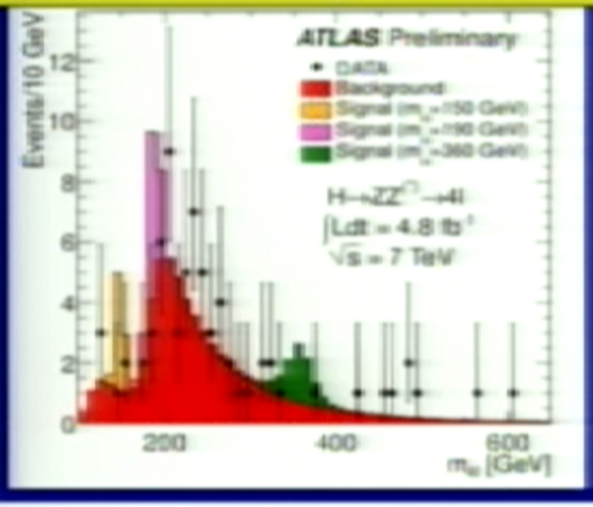

m(4l) < 180 GeV
Observed: 8 events: 3 4μ + 3 2e2μ + 2 4e
Expected from background: 9.3±1.5

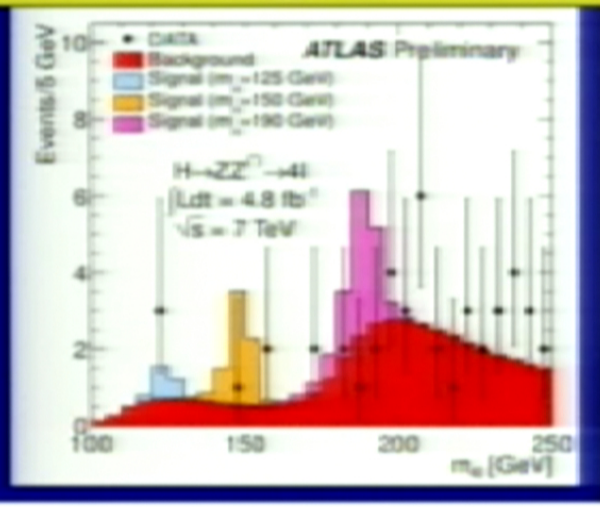

In the region $m_{4\mu}$ < 141 GeV (not already excluded at 95% C.L.) 3 events are observed:
two 2e2μ events (m=123.6 GeV, m=124.3 GeV) and one 4μ event (m=124.6 GeV)

In the region 117< m_{4l} <128 GeV
(containing ~90% of a m_H=125 GeV signal):
- similar contributions expected from signal and background: ~ 1.5 events each
- S/B ~ 2 (4μ), ~ 1 (2e2μ), ~ 0.3 (4e)
- Background dominated by ZZ* (4μ and 2e2μ), ZZ* and Z+jets (4e)

Main systematic uncertainties

Higgs cross-section	: ~ 15%
Electron efficiency	: ~ 2-8%
ZZ* background	: ~ 15%
Zbb, +jets backgrounds	: ~ 40%

After all selections: kinematic cuts, isolation, impact parameter

Full mass range
Observed: 71 events: 24 4μ + 30 2e2μ + 17 4e
Expected from background: 62±9

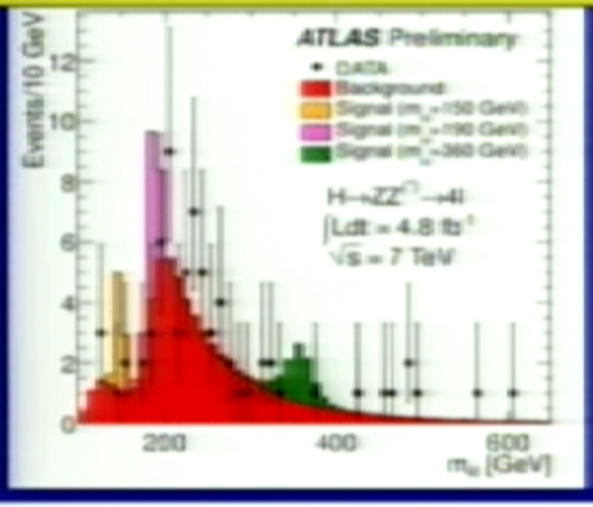

m(4l) < 180 GeV
Observed: 8 events: 3 4μ + 3 2e2μ + 2 4e
Expected from background: 9.3±1.5

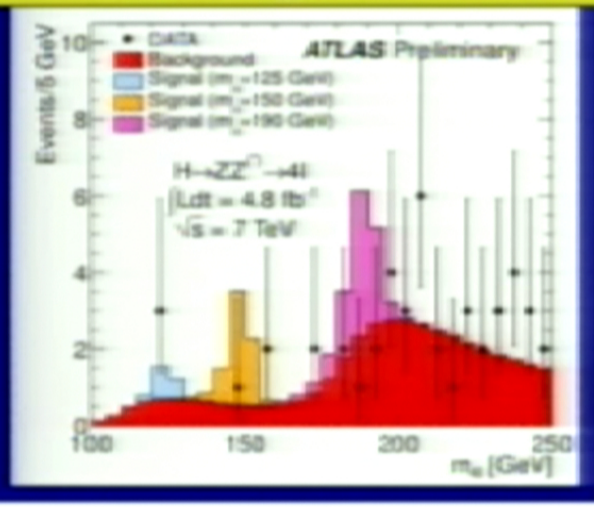

In the region $m_{4\mu}$ < 141 GeV (not already excluded at 95% C.L.) 3 events are observed:
two 2e2μ events (m=123.6 GeV, m=124.3 GeV) and one 4μ event (m=124.6 GeV)

In the region 117< m_{4l} <128 GeV
(containing ~90% of a m_H=125 GeV signal):
- similar contributions expected from signal and background: ~ 1.5 events each
- S/B ~ 2 (4μ), ~ 1 (2e2μ), ~ 0.3 (4e)
- Background dominated by ZZ* (4μ and 2e2μ), ZZ* and Z+jets (4e)

Main systematic uncertainties

Higgs cross-section	: ~ 15%
Electron efficiency	: ~ 2-8%
ZZ* background	: ~ 15%
Zbb, +jets backgrounds	: ~ 40%

4μ candidate with $m_{4\mu}$= 124.6 GeV

p_T (μ^-, μ^+, μ^+, μ^-)= 61.2, 33.1, 17.8, 11.6 GeV
m_{12}= 89.7 GeV, m_{34}= 24.6 GeV

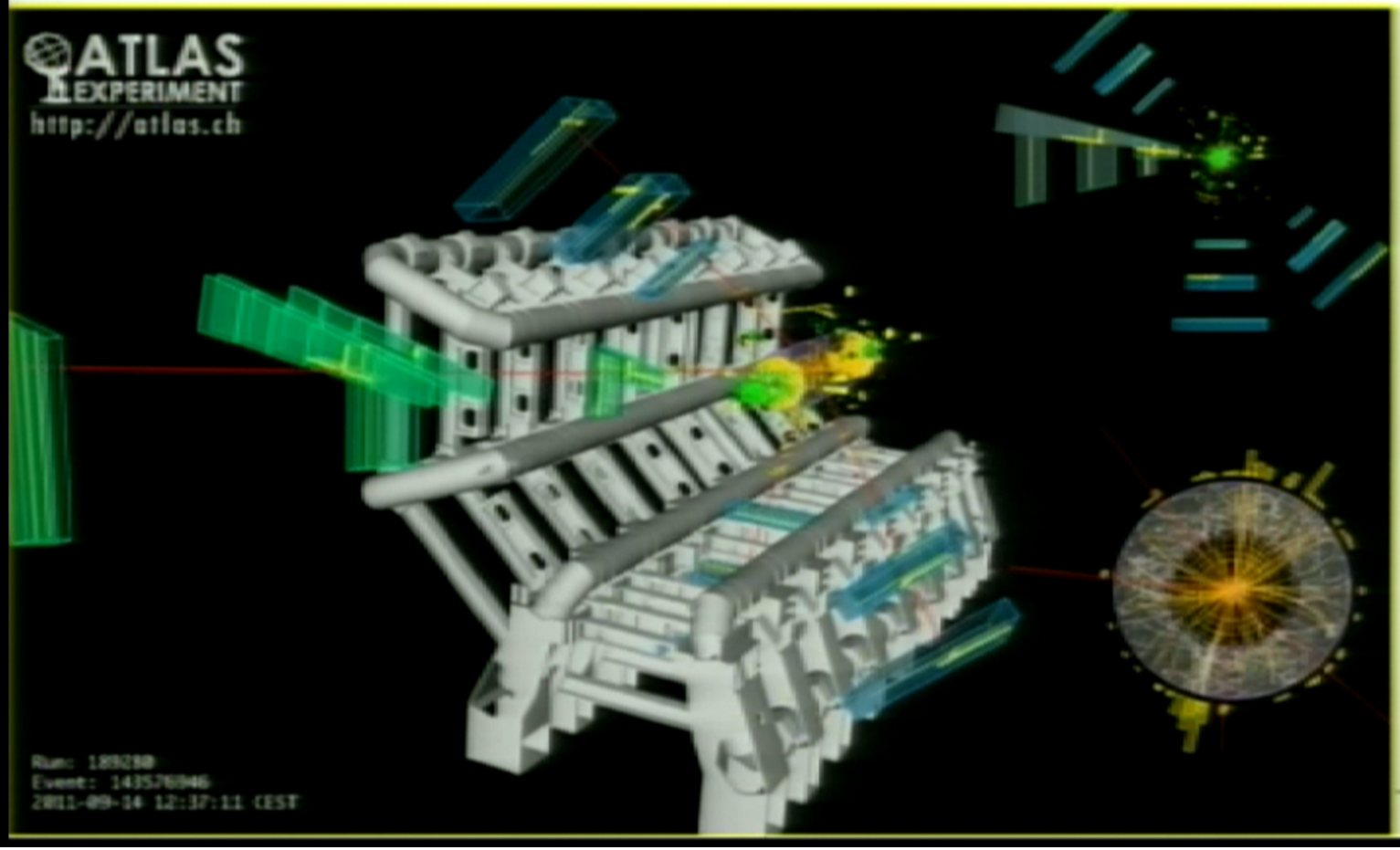

27

2e2μ candidate with $m_{2e2\mu}$= 124.3 GeV

p_T (e^+, e^-, μ^-, μ^+)= 41.5, 26.5, 24.7, 18.3 GeV
m(e^+e^-)= 76.8 GeV, m($\mu^+\mu^-$) = 45.7 GeV

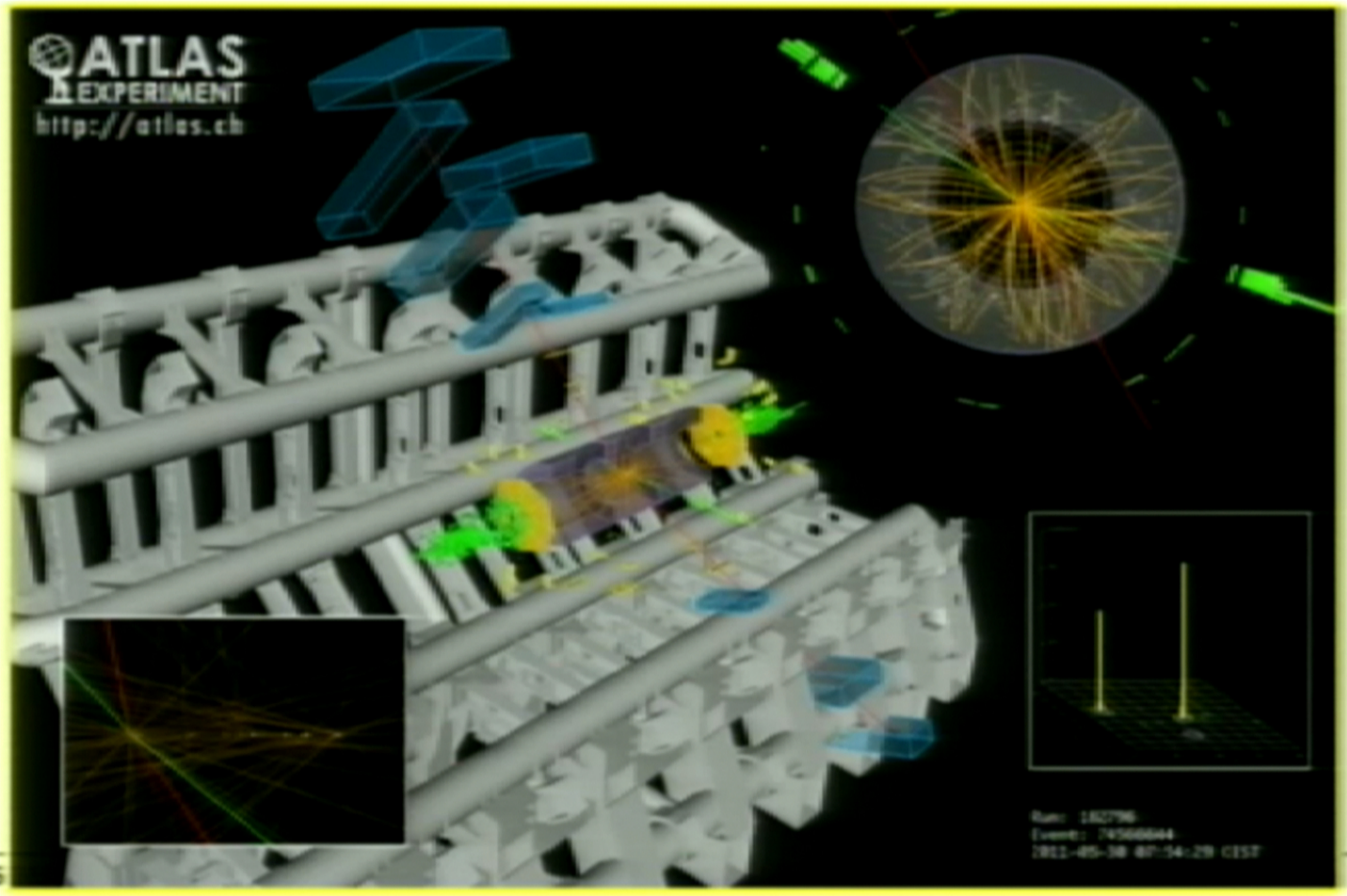

Reducible backgrounds from Zbb, Z+jets, tt giving 2 genuine + 2 fake leptons measured using background-enriched-signal-depleted control regions in data mimicking as much as possible the kinematics of the signal region → compromise between statistics and "purity"

Zbb+Z+jets control regions: events with:

- 2 opposite-sign same-flavour leptons, $m_{ll}=m_Z \pm 15$ GeV
- 2 additional same-flavour leptons passing all cuts but isolation and impact parameter
  → below plots of their invariant mass (m_{34})

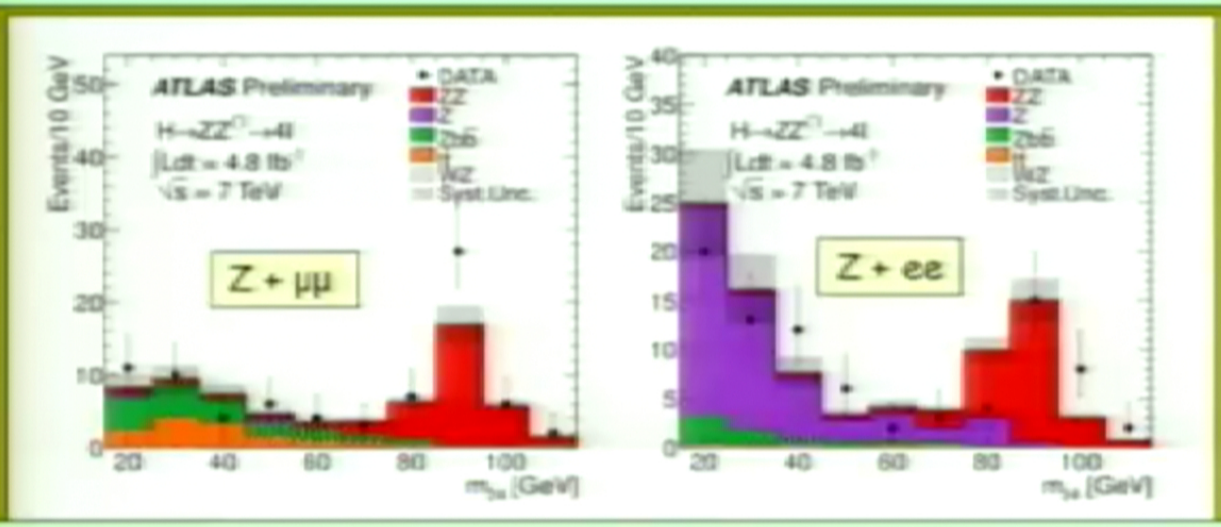

- Low-mass regions dominated by Zbb ($Z+\mu^+\mu^-$ sample) and Z+jet ($Z+e^+e^-$ sample)
- Data well reproduced by MC (within uncertainties)
- Samples of Z+μ and Z+e then used to compare efficiencies of isolation and impact parameter cuts between data and MC → Good agreement

→ MC used to estimate background contamination in signal region

	Data	MC
Z+μ	20 ± 1%	20.3 ± 0.4%
Z+e	29.9 ± 0.6%	30.4 ± 0.4%

29

From fit of signal and background expectations to 4l mass spectrum

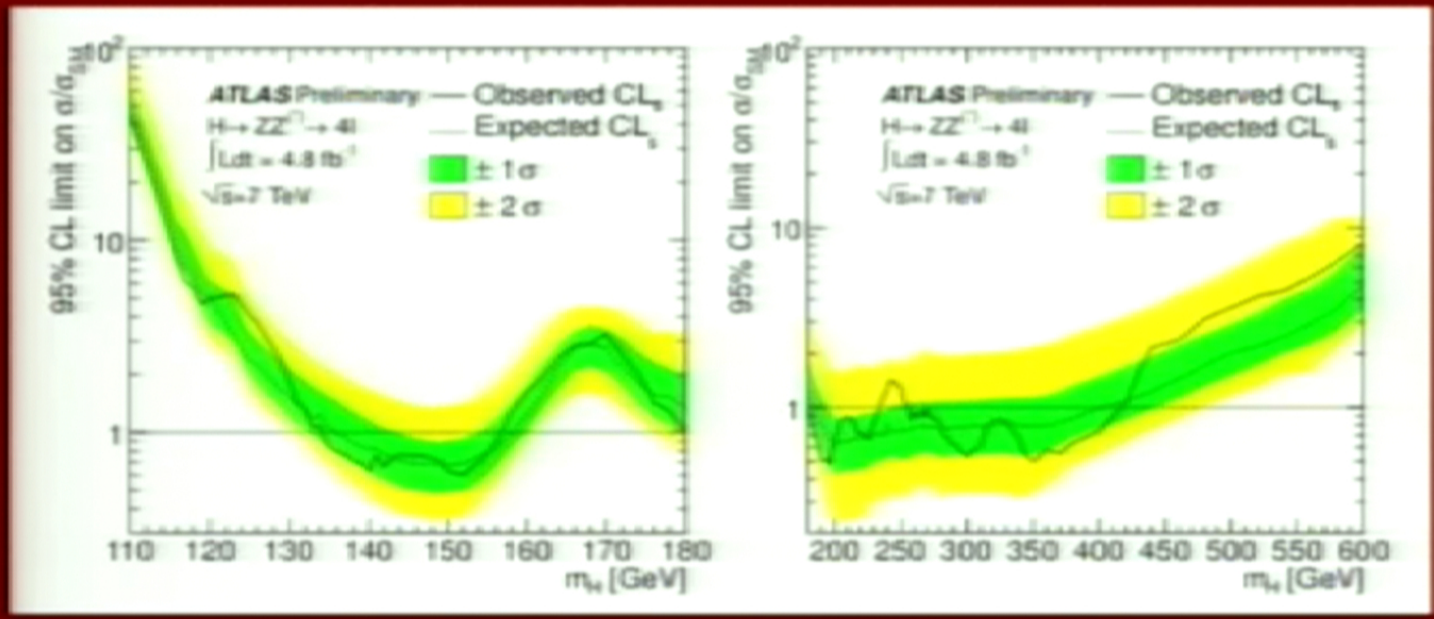

Excluded (95% CL): $135 < m_H < 156$ GeV and $181 < m_H < 415$ GeV (except 234-255 GeV)
Expected (95% CL): $137 < m_H < 158$ GeV and $185 < m_H < 400$ GeV

Consistency of the data with the background-only expectation

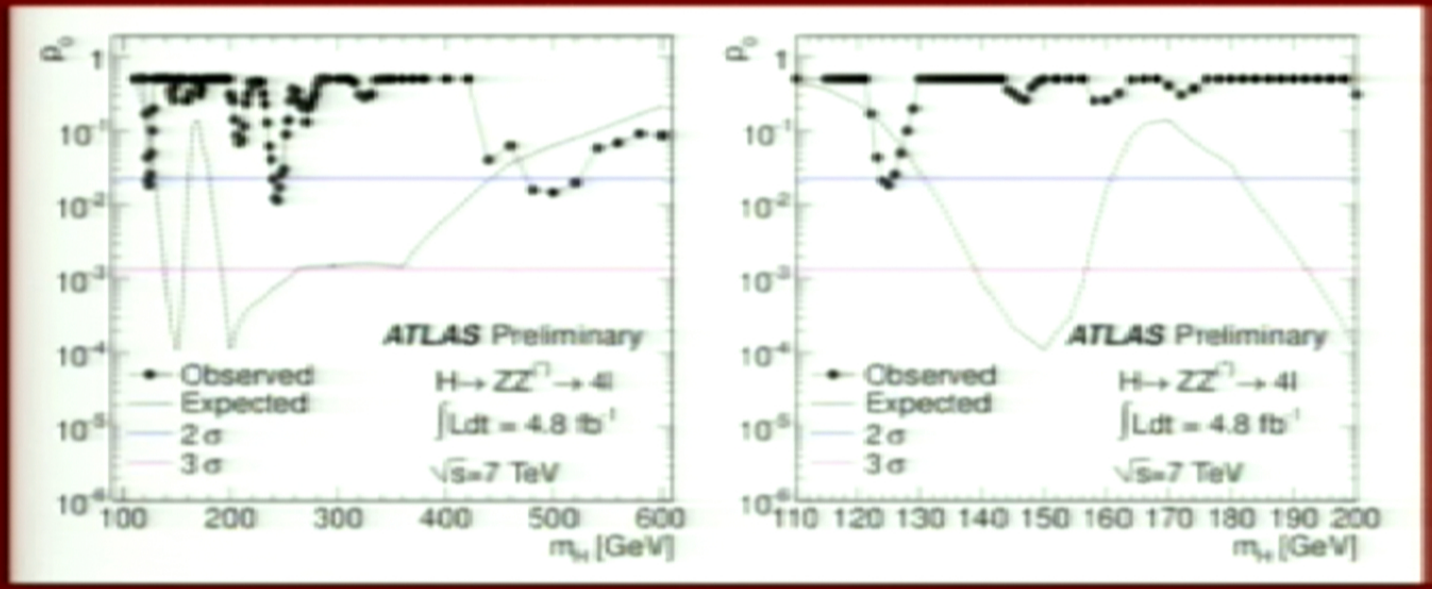

Maximum deviations from background-only expectations

m_H (GeV)	Local (global) p_0	Local significance	Expected from SM Higgs
125	1.8% (~50%)	2.1 σ	1.4σ
244	1.1% (~50%)	2.3 σ	3.2σ
500	1.4% (~50%)	2.2 σ	1.5σ

Excluded at 95% C.L. by ATLAS+CMS combination

LEE estimated over mass range: 110-600 GeV

Consistency of the data with the background-only expectation

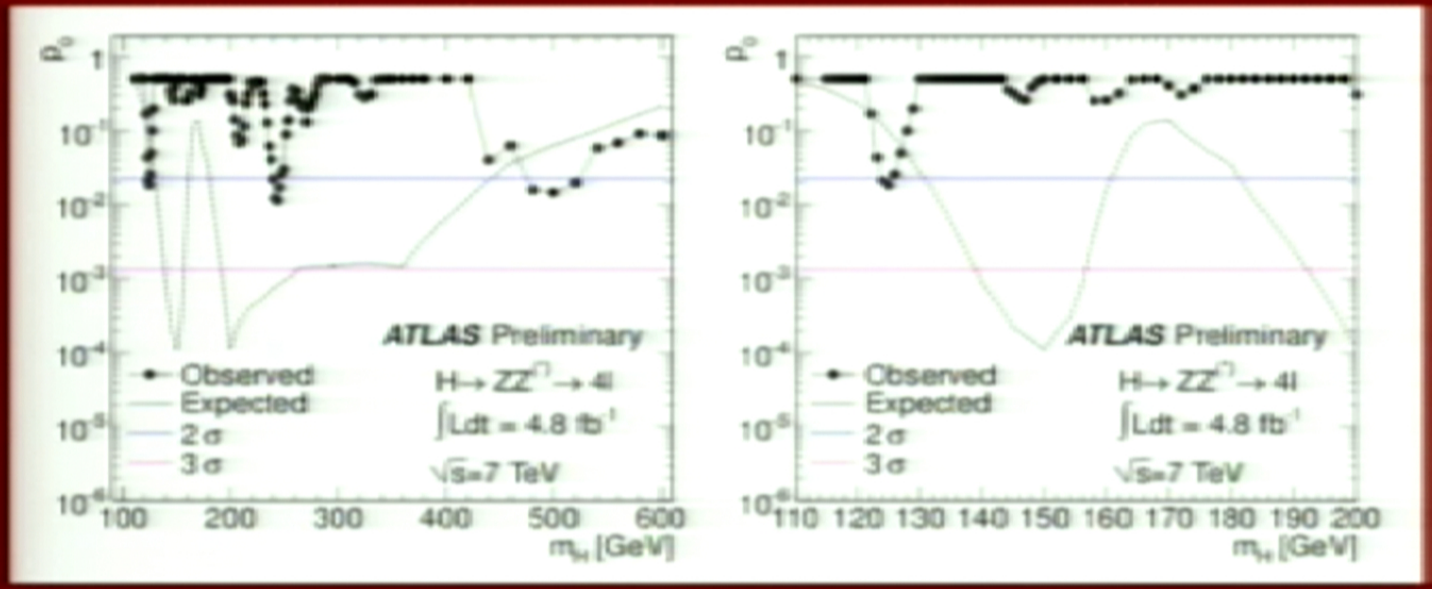

Maximum deviations from background-only expectations

m_H (GeV)	Local (global) p_0	Local significance	Expected from SM Higgs
125	1.8% (~50%)	2.1 σ	1.4σ
244	1.1% (~50%)	2.3 σ	3.2σ
500	1.4% (~50%)	2.2 σ	1.5σ

Excluded at 95% C.L. by ATLAS+CMS combination

LEE estimated over mass range: 110-600 GeV

Putting all channels together → combined constraints

H→γγ, H→ ττ
H→ WW(*)→ lνlν
H→ ZZ(*) → 4l, H→ ZZ → llνν
H→ ZZ → llqq, H→ WW→lνqq
W/ZH→ lbb+X not included

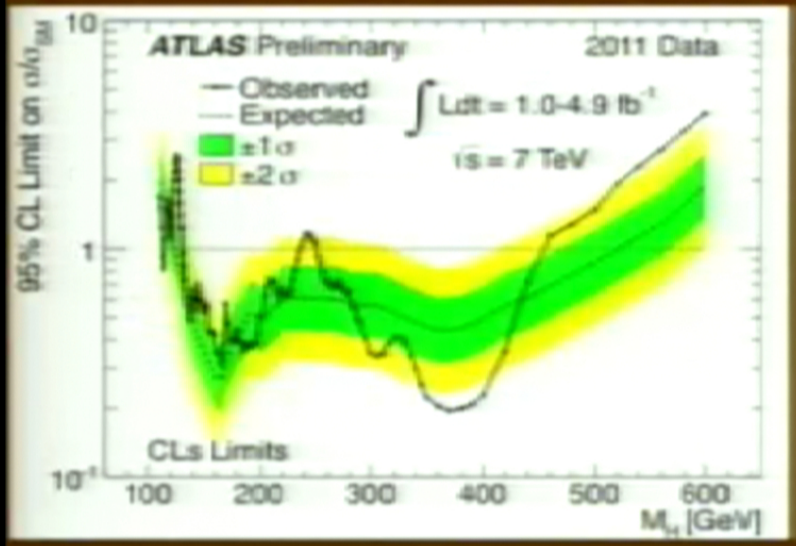

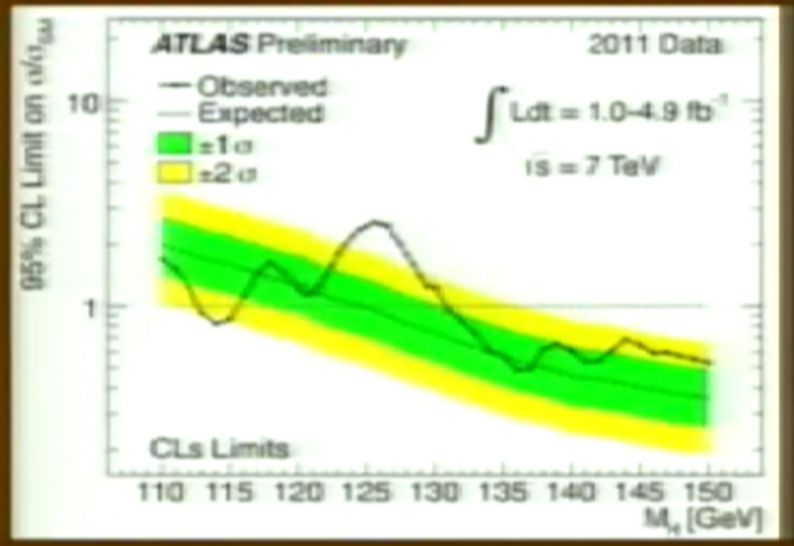

Excluded at 95% CL	112.7 < m_H < 115.5 GeV 131 < m_H < 453 GeV, except 237-251 GeV
Expected if no signal	124.6-520 GeV
Excluded at 99% CL	133 < m_H < 230 GeV, 260 < m_H < 437 GeV

Putting all channels together → combined constraints

H→γγ, H→ ττ
H→ WW(*)→ lνlν
H→ ZZ(*) → 4l, H→ ZZ → llνν
H→ ZZ → llqq, H→ WW→lνqq
W/ZH→ lbb+X not included

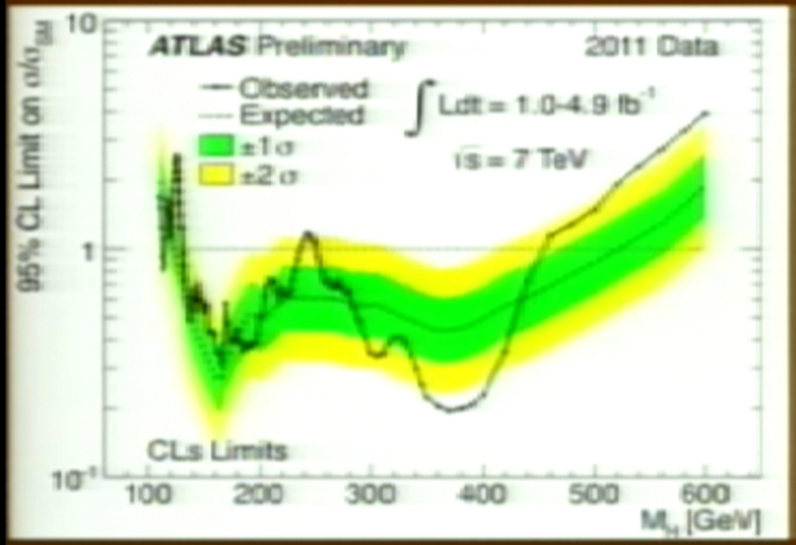

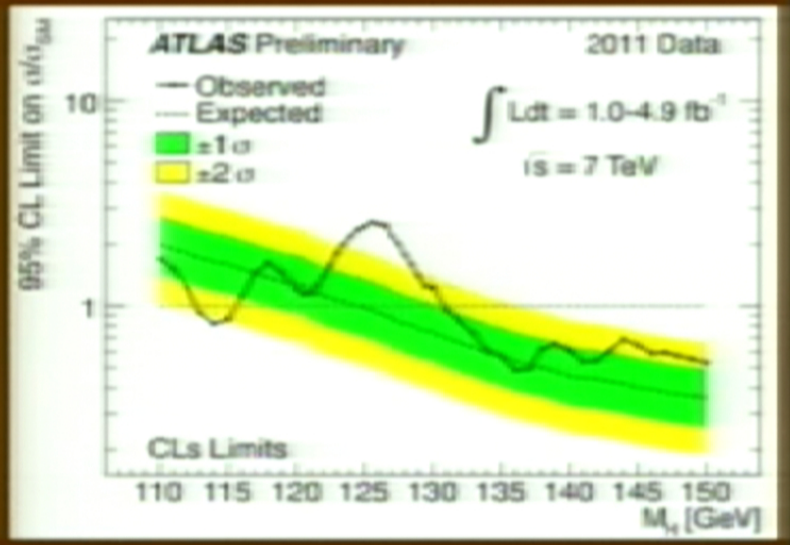

Excluded at 95% CL	112.7 < m_H < 115.5 GeV 131 < m_H < 453 GeV, except 237-251 GeV
Expected if no signal	124.6-520 GeV
Excluded at 99% CL	133 < m_H < 230 GeV, 260 < m_H < 437 GeV

32

Putting all channels together → combined constraints

H→γγ, H→ ττ
H→ WW(*)→ lνlν
H→ ZZ(*) → 4l, H→ ZZ → llνν
H→ ZZ → llqq, H→ WW→lνqq
W/ZH→ lbb+X not included

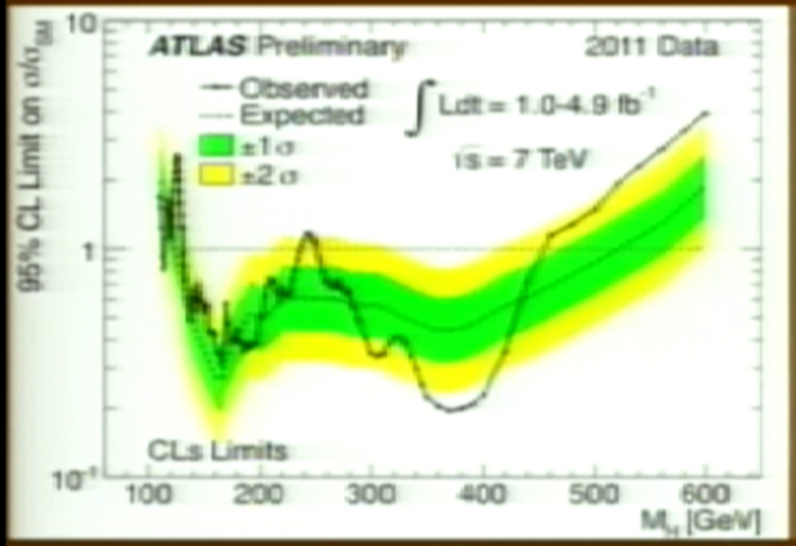

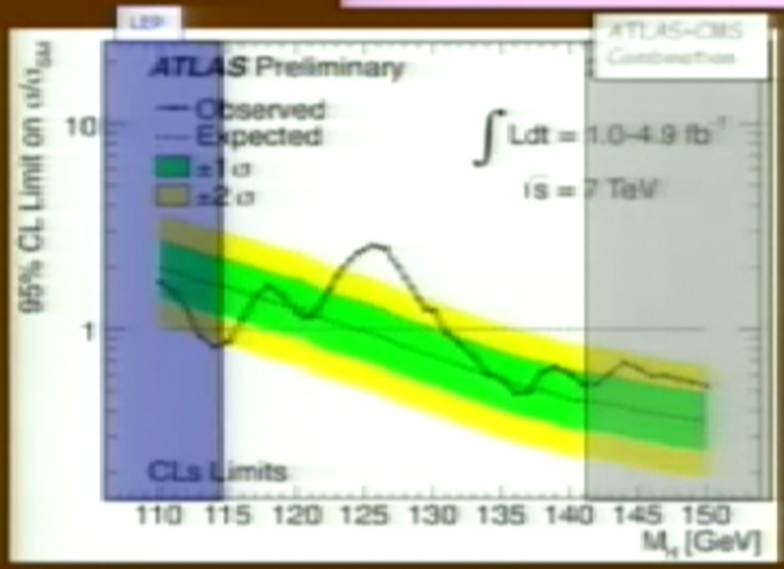

Excluded at 95% CL	112.7 < m_H < 115.5 GeV 131 < m_H < 453 GeV, except 237-251 GeV
Expected if no signal	124.6-520 GeV
Excluded at 99% CL	133 < m_H < 230 GeV, 260 < m_H < 437 GeV

32

Putting all channels together → combined constraints

H→γγ, H→ ττ
H→ WW(*)→ lνlν
H→ ZZ(*) → 4l, H→ ZZ → llνν
H→ ZZ → llqq, H→ WW→lνqq
W/ZH→ lbb+X not included

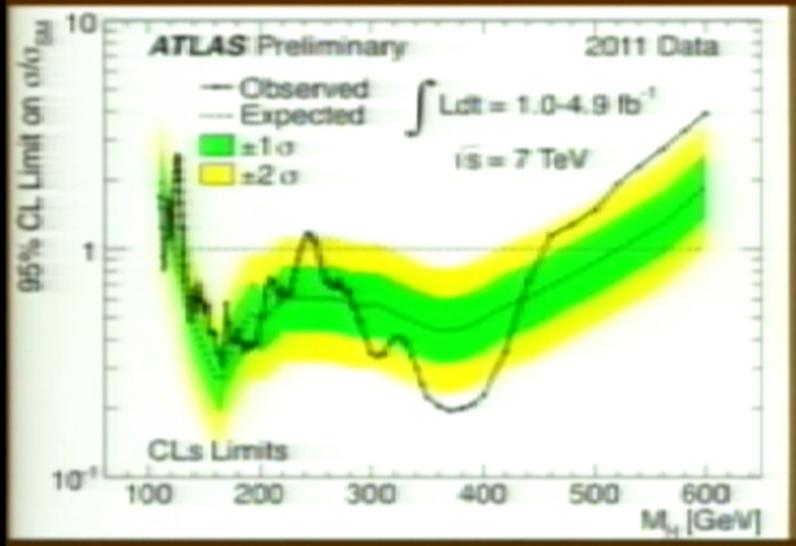

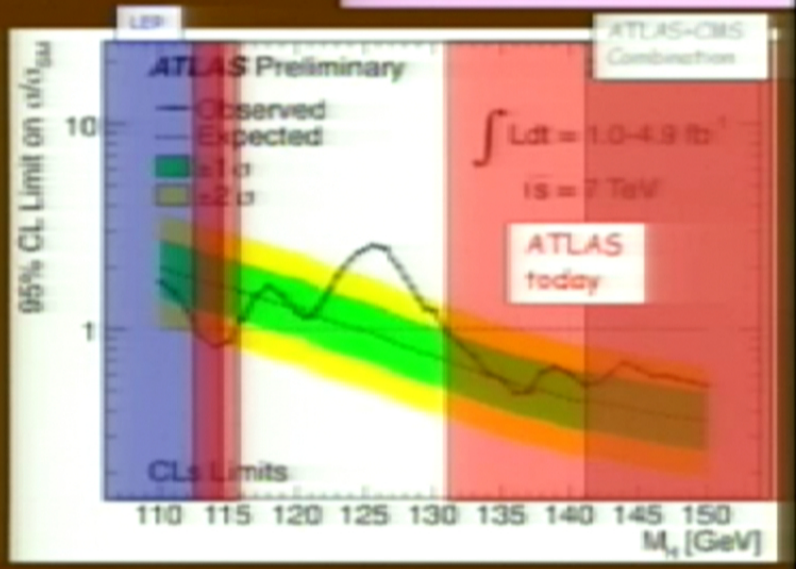

Excluded at 95% CL	112.7 < m_H < 115.5 GeV 131 < m_H < 453 GeV, except 237-251 GeV
Expected if no signal	124.6-520 GeV
Excluded at 99% CL	133 < m_H < 230 GeV, 260 < m_H < 437 GeV

32

Putting all channels together → combined constraints

H→γγ, H→ ττ
H→ WW(*)→ lνlν
H→ ZZ(*) → 4l, H→ ZZ → llνν
H→ ZZ → llqq, H→ WW→lνqq
W/ZH→ lbb+X not included

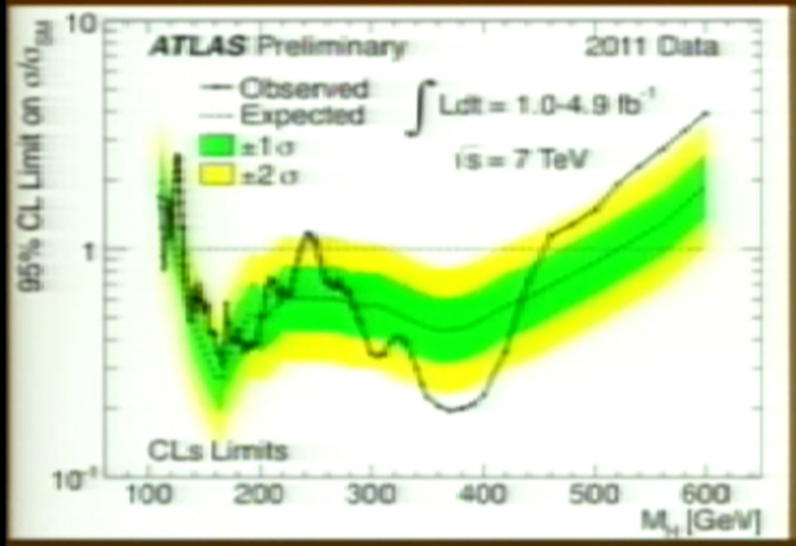

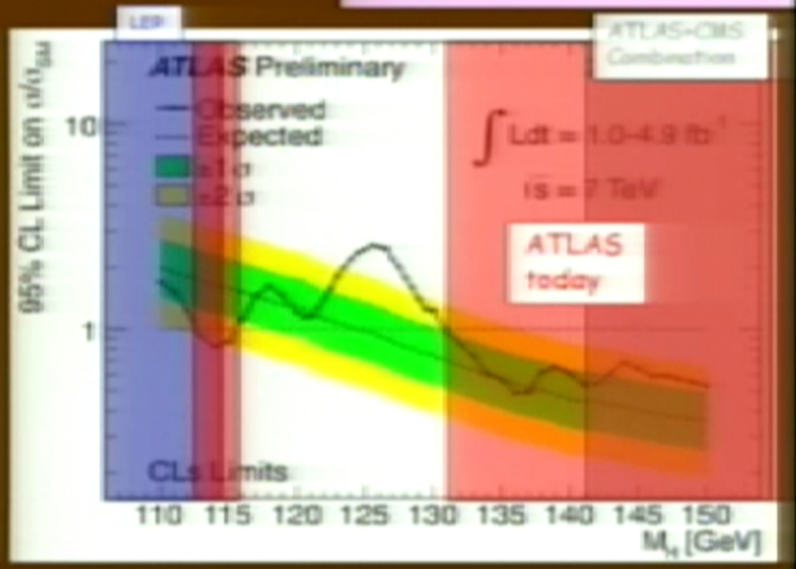

Excluded at 95% CL	112.7 < m_H < 115.5 GeV 131 < m_H < 453 GeV, except 237-251 GeV
Expected if no signal	124.6-520 GeV
Excluded at 99% CL	133 < m_H < 230 GeV, 260 < m_H < 437 GeV

32

Consistency of the data with the background-only expectation

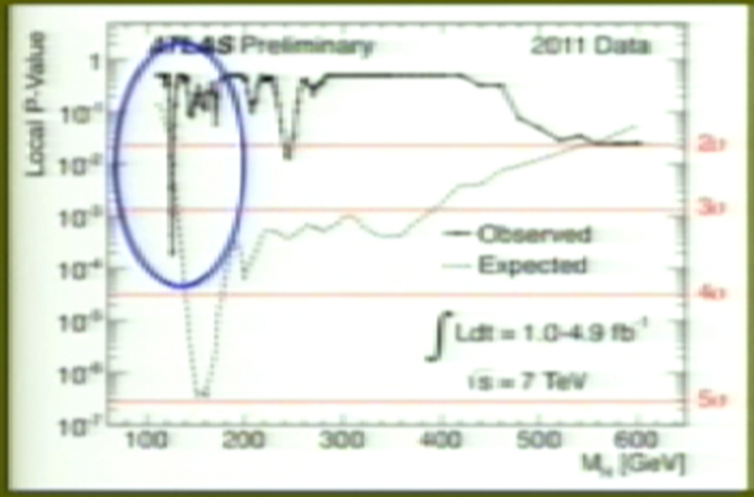

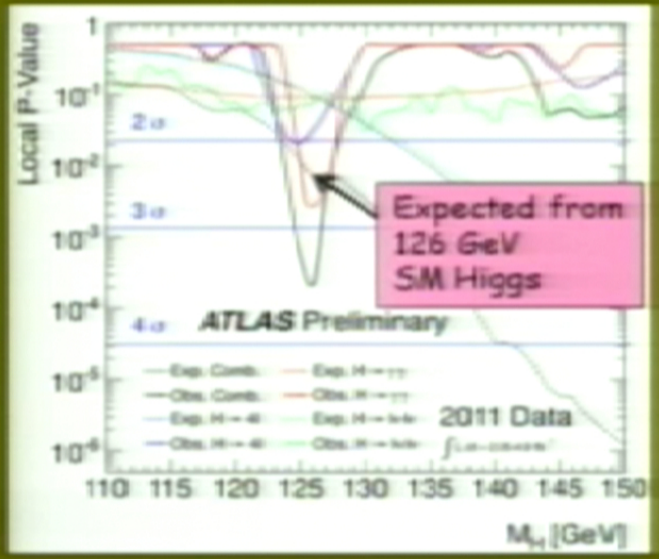

Maximum deviation from background-only expectation observed for m_H~126 GeV

Local p_0-value: $1.9\ 10^{-4}$
→ local significance of the excess: 3.6σ
~ 2.8σ H→ γγ, 2.1σ H→ 4l, 1.4σ H→ lνlν

Expected from SM Higgs: ~2.4σ local (~1.4σ per channel)

Global p_0-value : 0.6% →2.5σ LEE over 110-146 GeV
Global p_0-value : 1.4% →2.2σ LEE over 110-600 GeV

Consistency of the data with the background-only expectation

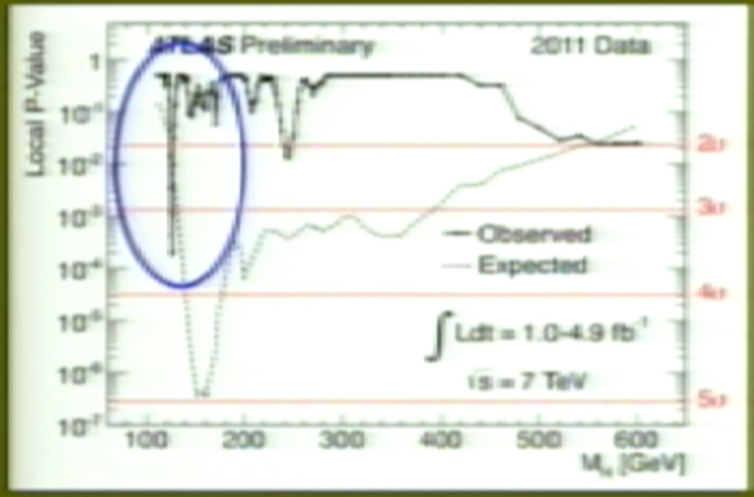

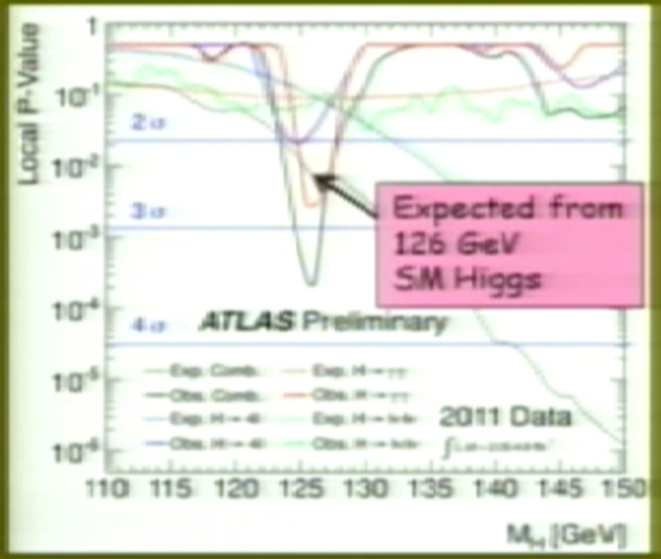

Maximum deviation from background-only expectation observed for m_H~126 GeV

Local p_0-value: $1.9\ 10^{-4}$
→ local significance of the excess: 3.6σ
~ 2.8σ H→ γγ, 2.1σ H→ 4l, 1.4σ H→ lνlν

Expected from SM Higgs: ~2.4σ local (~1.4σ per channel)

Global p_0-value : 0.6% →2.5σ LEE over 110-146 GeV
Global p_0-value : 1.4% →2.2σ LEE over 110-600 GeV

Consistency of the data with the background-only expectation

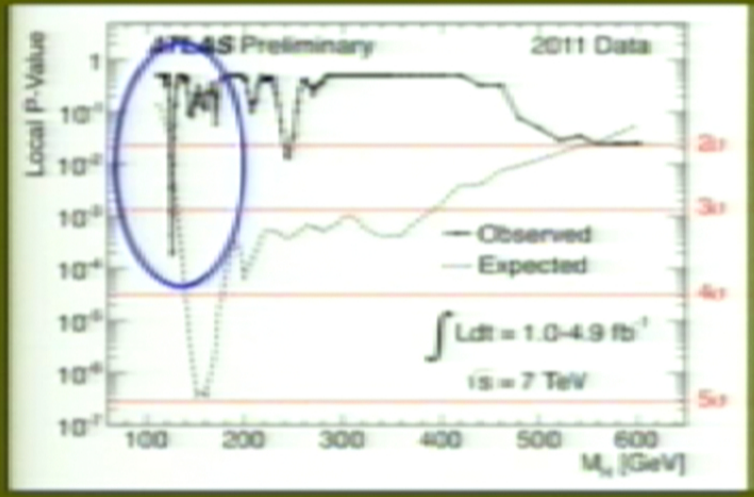

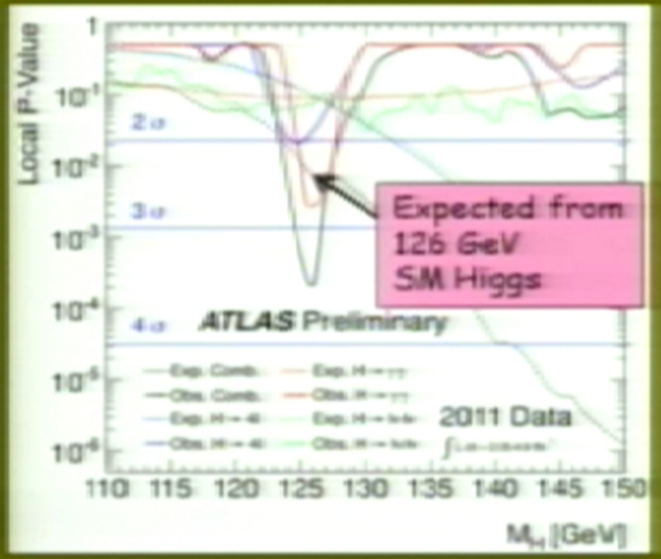

Maximum deviation from background-only expectation observed for m_H~126 GeV

Local p_0-value: $1.9\ 10^{-4}$
→ local significance of the excess: 3.6σ
~ 2.8σ H→ γγ, 2.1σ H→ 4l, 1.4σ H→ lνlν

Expected from SM Higgs: ~2.4σ local (~1.4σ per channel)

Global p_0-value : 0.6% →2.5σ LEE over 110-146 GeV
Global p_0-value : 1.4% →2.2σ LEE over 110-600 GeV

Compatibility of the observation with the expected strength of a SM Higgs signal

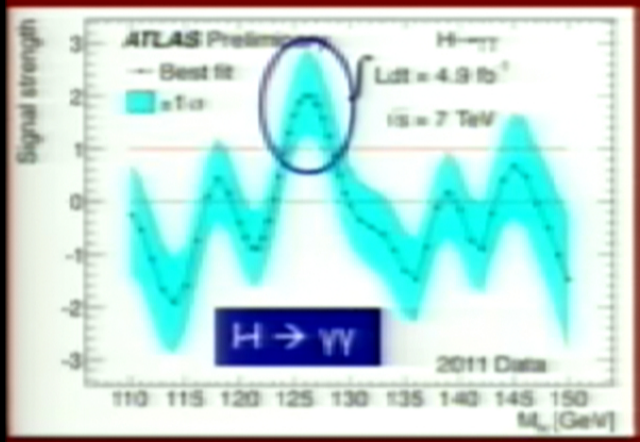

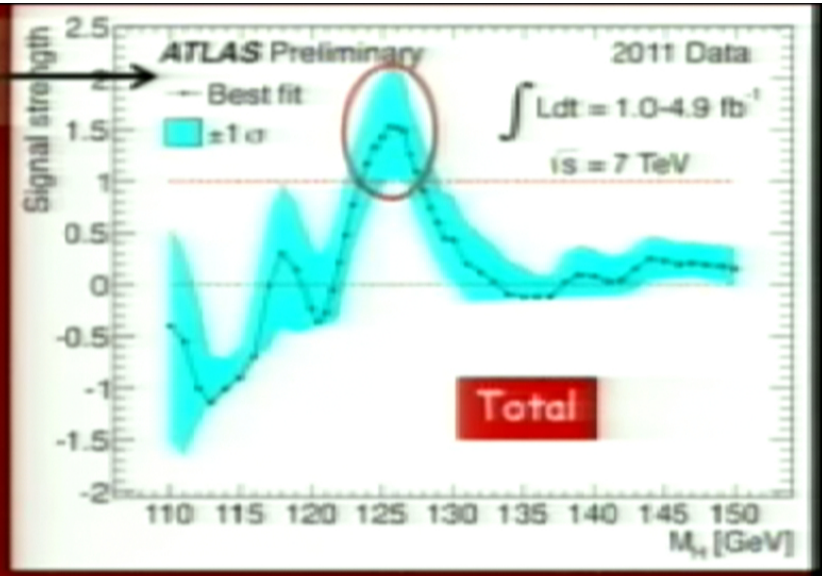

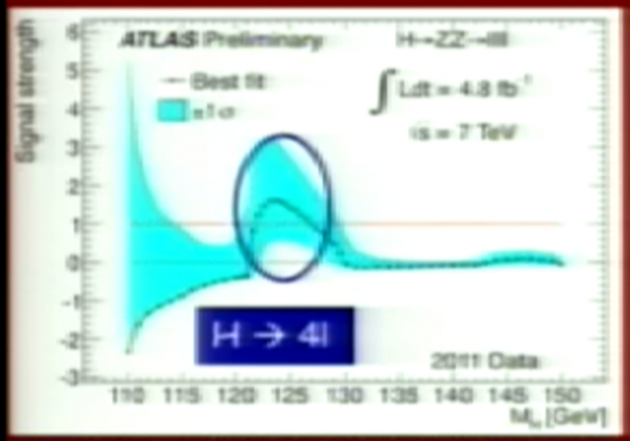

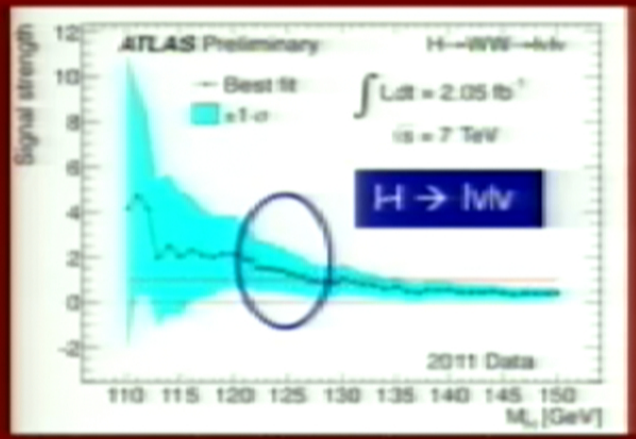

The observed excess is slightly larger (2±0.8) than expected in the H→γγ channel and compatible within 1σ for the other channels and the combined result

La suite …

Improve analysis sensitivities:

- update $H \to WW^{(*)} \to l\nu l\nu$, $W/ZH \to bb$ and $H \to \tau\tau$ to ~5 fb^{-1}
- relax kinematic cuts (e.g. lepton p_T) to increase acceptance at low masses
- multivariate techniques, exclusive channels (e.g $H \to \gamma\gamma$ + 0/1/2 jets), additional discriminating variables beyond mass spectra (p_T, angular distributions, etc.)

In parallel: improvements of the detector performance and modeling (a never-ending feat …)

One of the numerous lessons and outstanding achievements of the Tevatron:
how much better than expectation experiments can do with data and ingenuity !

Combine with CMS: being discussed …
Not before results from individual experiments are published

MORE DATA → 2012 run:

~ 20 fb^{-1} more per experiment of delivered luminosity needed for:

- 5σ discovery at m_H ~ 125 GeV with ~ 3σ per channel (ATLAS alone)
- 5σ discovery down to ~ 116 GeV (ATLAS+CMS combined)

"Contingency": analysis improvements; $\sqrt{s}$=8 TeV (brings ~ 10% sensitivity gain)

Conclusions

It has been a wonderful year for the LHC and ATLAS → THANKS LHC TEAM !

Conclusions

It has been a wonderful year for the LHC and ATLAS → THANKS LHC TEAM !

We have looked for a SM Higgs boson
- over the mass region 110-600 GeV
- in 11 distinct channels
- using up to 4.9 fb^{-1} of integrated luminosity

→ We have restricted the most likely mass region (95% CL) to **115.5-131 GeV**

We observe an excess of events around $m_H \sim 126$ GeV:
- local significance 3.6 σ, with contributions from the $H \to \gamma\gamma$ (2.8 σ), $H \to ZZ^* \to 4l$ (2.1 σ), $H \to WW^{(*)} \to l\nu l\nu$ (1.4 σ) analyses
- SM Higgs expectation: 2.4 σ local → observed excess compatible with signal strength within +1σ
- the global significance (taking into account Look-Elsewhere-Effect) is ~2.3σ

It would be a very nice region for the Higgs to be → accessible at LHC in $\gamma\gamma$, 4l, $l\nu l\nu$, bb, ττ


What an extraordinary time !
rgentina
rmenia
ustralia
ustria
zerbaijan
elarus
razil
anada
hile
hina
olombia
zech Republic
enmark
rance
eorgia
ermany
reece
srael
aly
apan
Morocco
Netherlands
Norway
Poland
Portugal
Romania
Russia
Serbia
Slowakia
Slowenia
South Africa
Spain
Sweden
Switzerland
Taiwan
Turkey
UK
USA
CERN
JINR
ATLAS
Collaboration
ATLAS Experiment

Outline of the talk

- Short introduction.
- Search for a SM Higgs boson in the high mass region.
- Search for a SM Higgs boson in the low mass region.
- Combination of the searches and new exclusion limits.
- Conclusion.

The SM Higgs boson

SM Higgs could be an excellent candidate to understand the ElectroWeak Symmetry Breaking mechanism.

Constraints from EWK precision measurements favour a light Higgs with Standard Model like couplings (WW, ZZ).

Recent exclusion limits based on the ATLAS+CMS Combination using 1.1-2.3fb^{-1} of data have costrained significantly the search.

I'll present preliminary results of our exploration in mass up to 600GeV but a special attention will be dedicated to the search of the SM Higgs Boson in the low mass region.

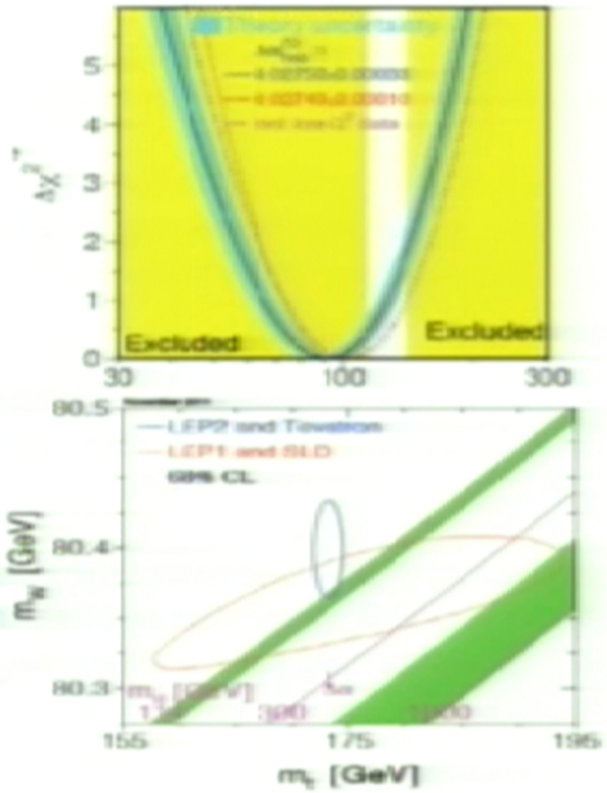

SM Higgs production at LHC

- Gluon fusion
- VBF
- VH
- ttH

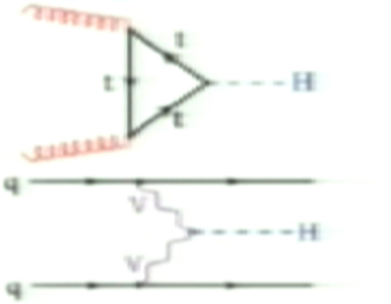

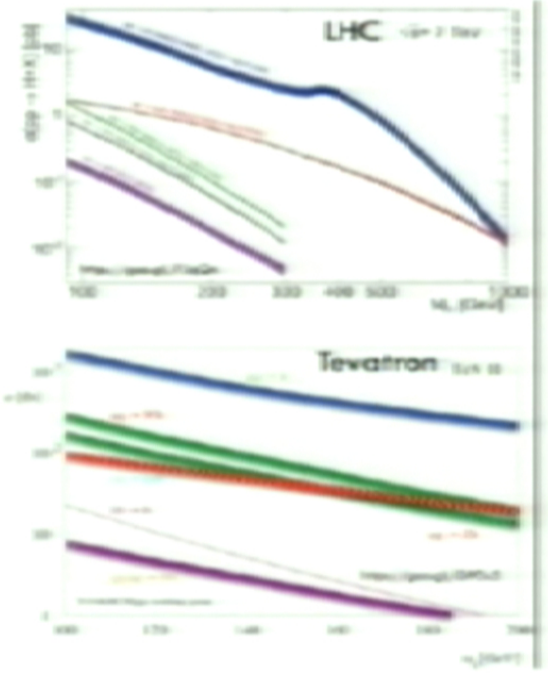

Gluon fusion (gg→ H) is the dominant production mechanism at LHC. Irreducible backgrounds in H → WW, ZZ, γγ are from qq annihilation. Signal to Noise better than at Tevatron except in VH. **VBF and VH also very useful at LHC**

The challenge

CMS Projected Sensitivity @5fb^{-1}

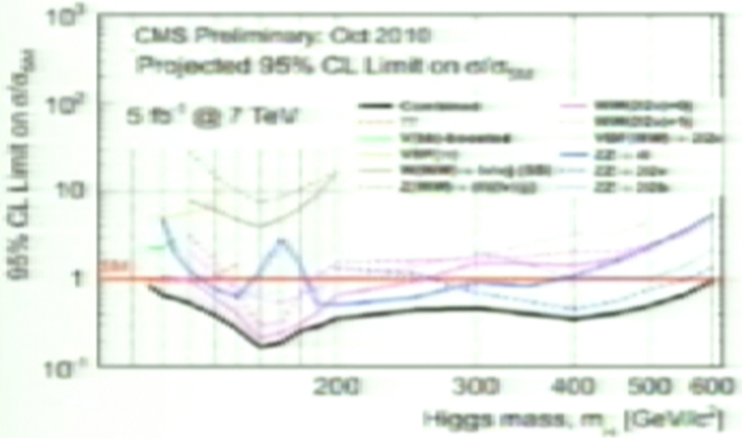

CMS Projected Significance @5fb^{-1}

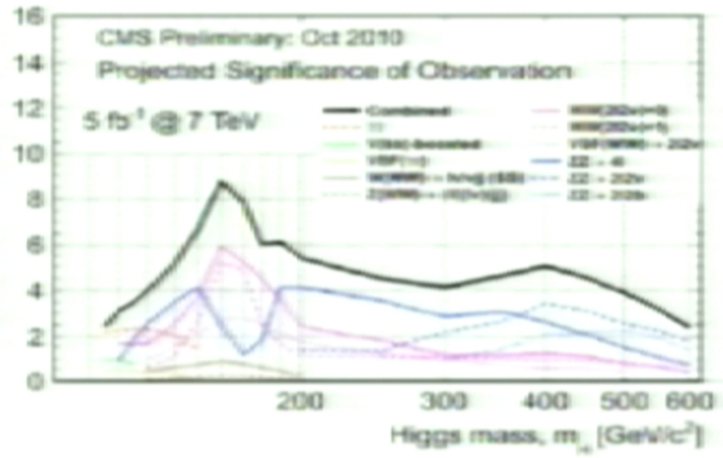

October 2010: with 5fb^{-1} delivered by LHC we could reach a sensitivity below 1xSM in the full mass range.

If the SM Higgs boson would be hidden in the low mass region we could start seeing excesses with a significance of 2-3 sigma.

Every single channel, particularly in the low mass region, brings very important information.

The challenge

CMS Projected Sensitivity @5fb^{-1}

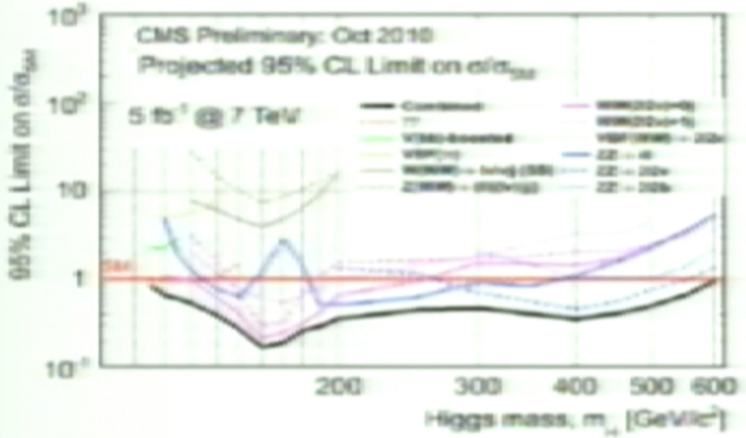

CMS Projected Significance @5fb^{-1}

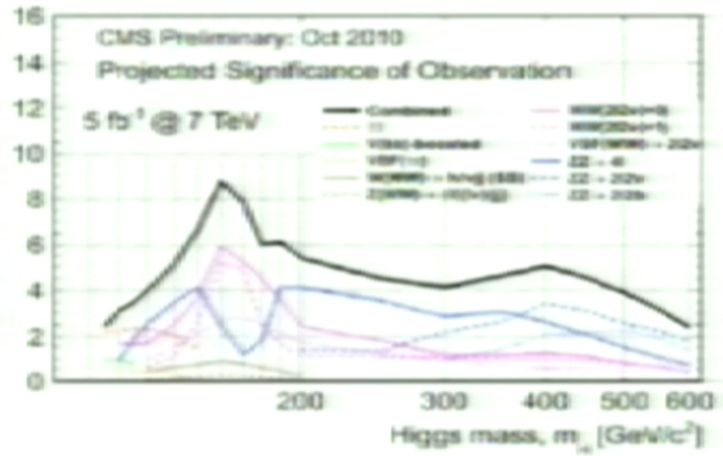

October 2010: with 5fb^{-1} delivered by LHC we could reach a sensitivity below 1xSM in the full mass range.

If the SM Higgs boson would be hidden in the low mass region we could start seeing excesses with a significance of 2-3 sigma.

Every single channel, particularly in the low mass region, brings very important information.

The challenge

CMS Projected Sensitivity @5fb^{-1}

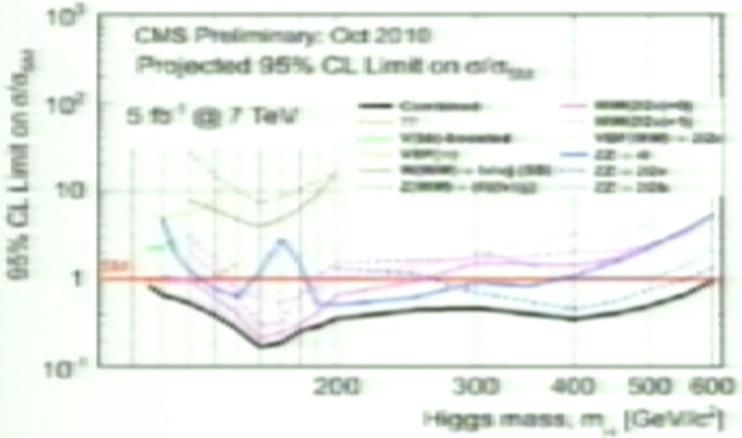

CMS Projected Significance @5fb^{-1}

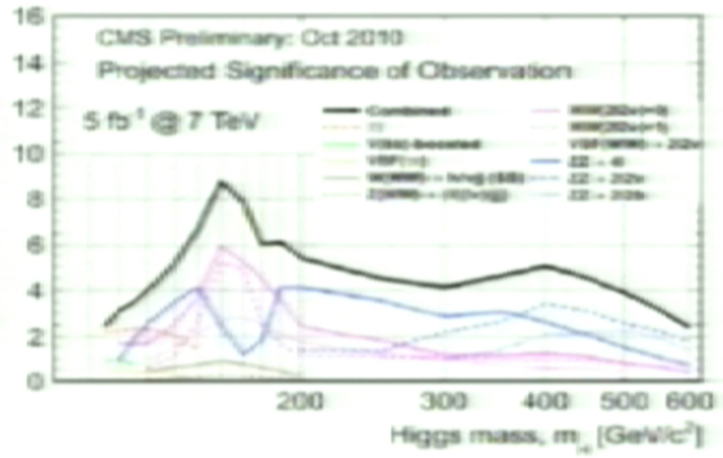

October 2010: with 5fb^{-1} delivered by LHC we could reach a sensitivity below 1xSM in the full mass range.

If the SM Higgs boson would be hidden in the low mass region we could start seeing excesses with a significance of 2-3 sigma.

Every single channel, particularly in the low mass region, brings very important information.

LHC/CMS operations pp@√s=7TeV 2011

5.72fb^{-1} delivered by LHC and 5.2fb^{-1} recorded by CMS. Overall data taking efficiency ~91%. Average fraction of operational channels per subsystem >98.5%

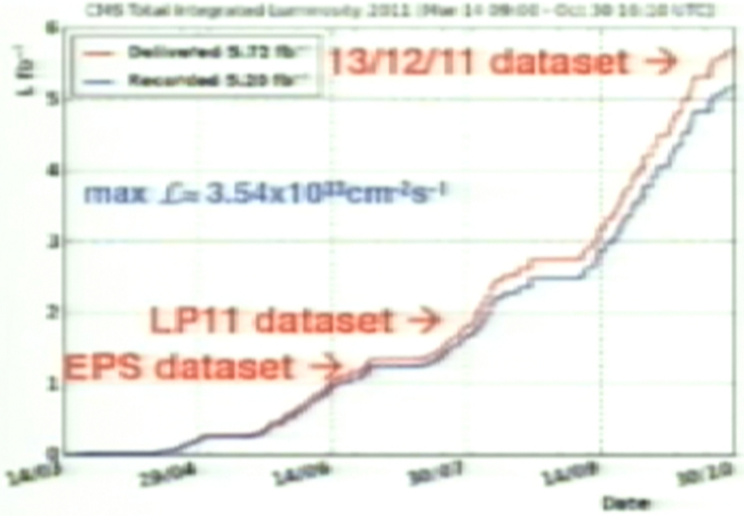

RPC	98.5
CSC	98.3
DT	99.4
HF	99.9
HE	100.0
HB	99.9
ES	95.9
EE	98.6
EB	99.1
STRIP	97.8
PIXEL	96.9

Results shown at this seminar use a large fraction of the full dataset.
Certified data for physics: Golden 4745pb^{-1} (91.2%), Muon 4965pb^{-1} (~96%).
Uncertainty on the luminosity determination 4.5%.

LHC/CMS operations pp@√s=7TeV 2011

5.72fb^{-1} delivered by LHC and 5.2fb^{-1} recorded by CMS. Overall data taking efficiency ~91%. Average fraction of operational channels per subsystem >98.5%

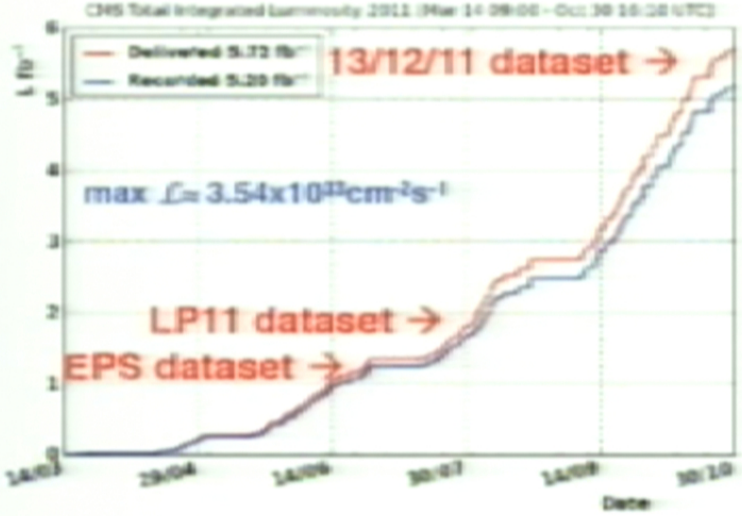

RPC	98.5
CSC	98.3
DT	99.4
HF	99.9
HE	100.0
HB	99.9
ES	95.9
EE	98.6
EB	99.1
STRIP	97.8
PIXEL	96.9

Results shown at this seminar use a large fraction of the full dataset.
Certified data for physics: Golden 4745pb^{-1} (91.2%), Muon 4965pb^{-1} (~96%).
Uncertainty on the luminosity determination 4.5%.

LHC/CMS operations pp@√s=7TeV 2011

5.72fb^{-1} delivered by LHC and 5.2fb^{-1} recorded by CMS. Overall data taking efficiency ~91%. Average fraction of operational channels per subsystem >98.5%

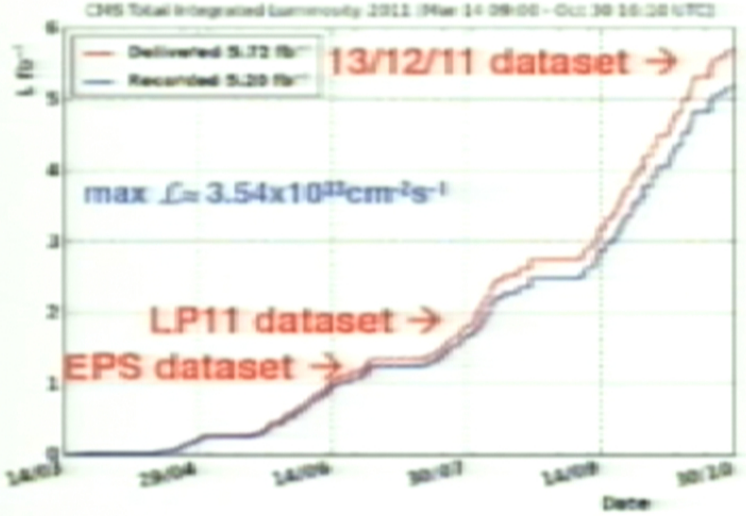

RPC	98.5
CSC	98.3
DT	99.4
HF	99.9
HE	100.0
HB	99.9
ES	95.9
EE	98.6
EB	99.1
STRIP	97.8
PIXEL	96.9

Results shown at this seminar use a large fraction of the full dataset.
Certified data for physics: Golden 4745pb^{-1} (91.2%), Muon 4965pb^{-1} (~96%).
Uncertainty on the luminosity determination 4.5%.

Excellent understanding of the physics "objects"

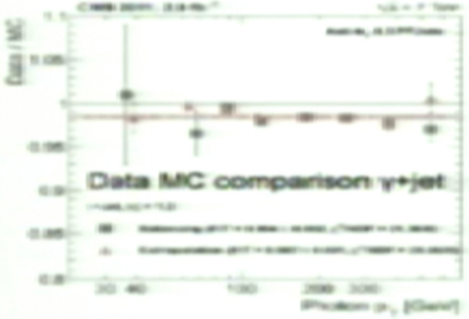

Jet Calibration with pileup

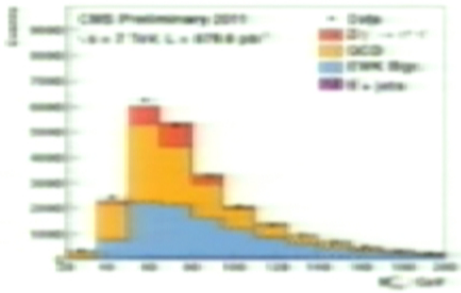

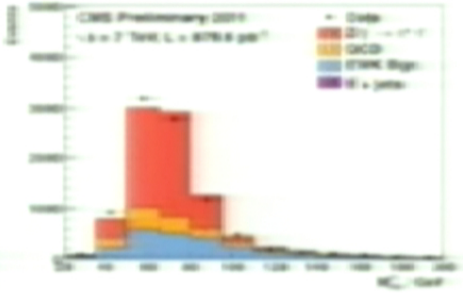

Tau efficiency with T&P on the Z measured to 6%

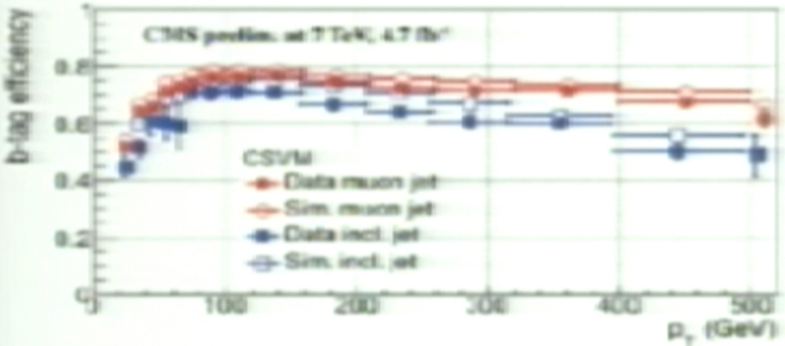

B- tagging efficiency measured to 10% up to 500 GeV

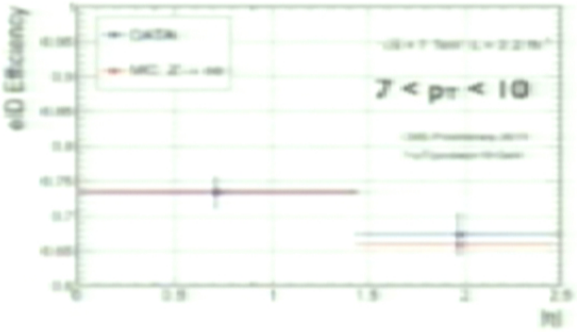

Electron efficiency with T&P on the Z measured down to 7 GeV

Excellent understanding of the physics "objects"

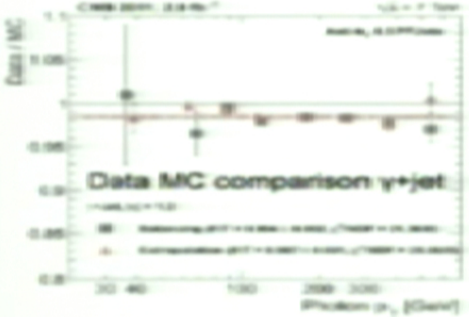

Jet Calibration with pileup

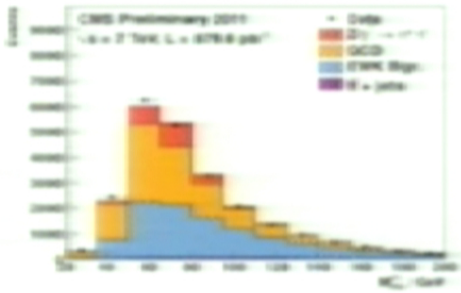

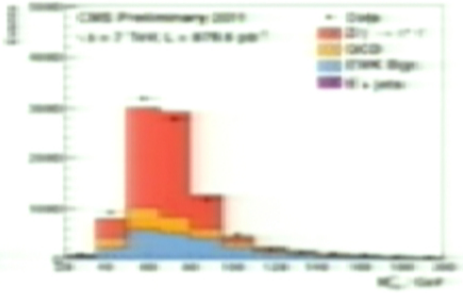

Tau efficiency with T&P on the Z measured to 6%

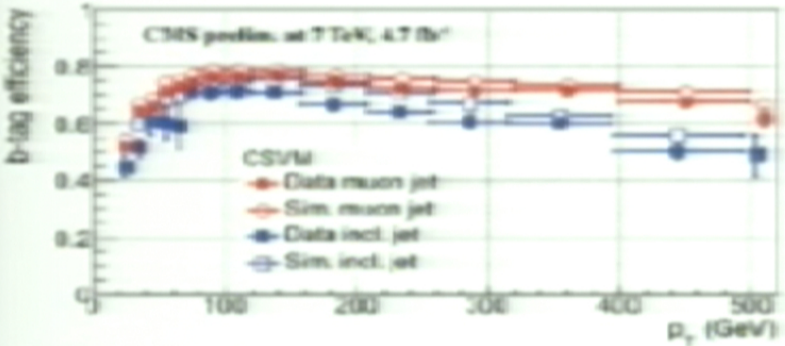

B- tagging efficiency measured to 10% up to 500 GeV

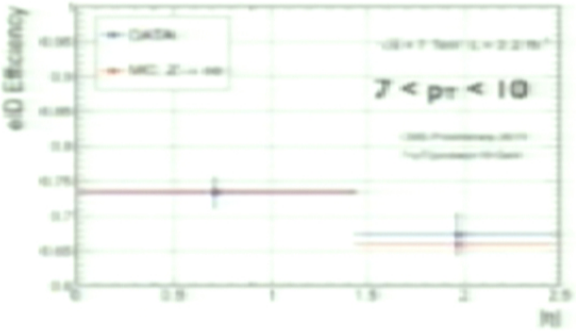

Electron efficiency with T&P on the Z measured down to 7 GeV

Some of the key SM background

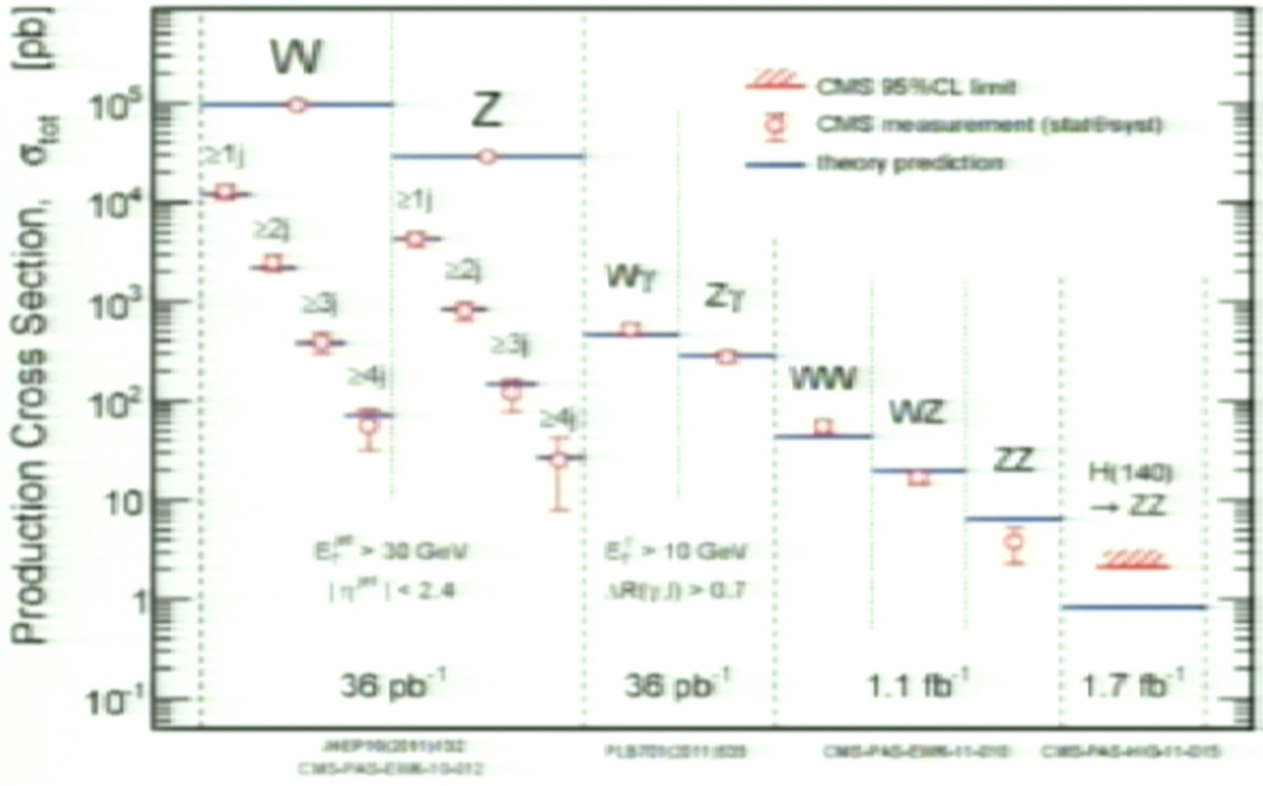

SM Higgs Decay Modes Vs Mass

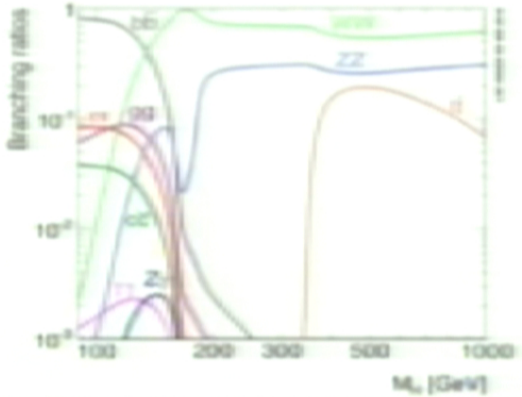

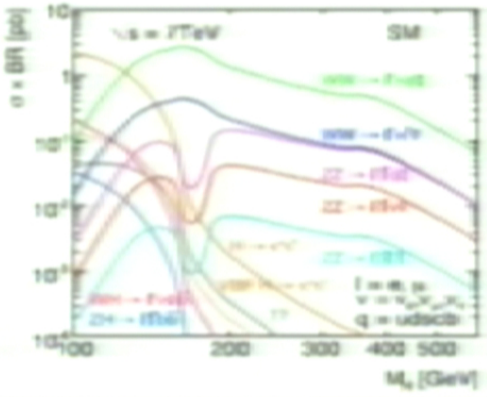

Mode	Mass Range	Data Used (fb^{-1})	CMS Document
H → γγ	110-150	4.7	HIG-11-030
H → bb	110-135	4.7	HIG-11-031
H → ττ	110-145	4.6	HIG-11-029
H → WW → 2l 2ν	110-600	4.6	HIG-11-024
H → ZZ → 4l	110-600	4.7	HIG-11-025
H → ZZ → 2l2τ	190-600	4.7	HIG-11-028
H → ZZ → 2l2j	130-165/200-600	4.6	HIG-11-027
H → ZZ → 2l2ν	250-600	4.6	HIG-11-026

SM Higgs Decay Modes Vs Mass

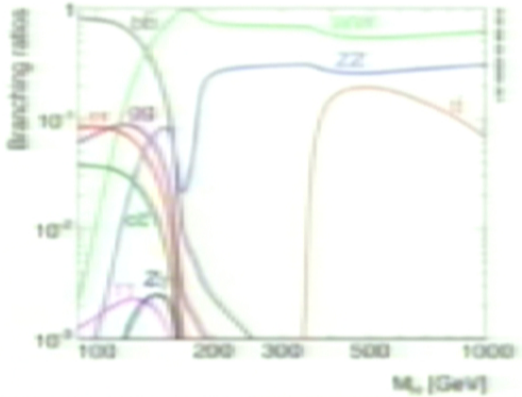

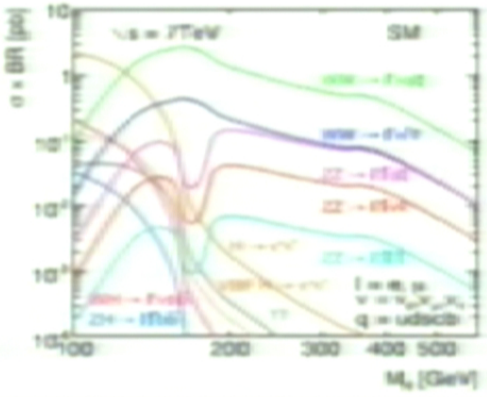

Mode	Mass Range	Data Used (fb^{-1})	CMS Document
H → γγ	110-150	4.7	HIG-11-030
H → bb	110-135	4.7	HIG-11-031
H → ττ	110-145	4.6	HIG-11-029
H → WW → 2l 2ν	110-600	4.6	HIG-11-024
H → ZZ → 4l	110-600	4.7	HIG-11-025
H → ZZ → 2l2τ	190-600	4.7	HIG-11-028
H → ZZ → 2l2j	130-165/200-600	4.6	HIG-11-027
H → ZZ → 2l2ν	250-600	4.6	HIG-11-026

Analyses presented here

Channel	m_H range (GeV/c^2)	Lumi (fb^{-1})	sub-channels	m_H resolution
$H \to \gamma\gamma$	110 – 150	4.7	4	1–3%
$H \to \tau\tau$	110 – 145	4.6	9	20%
$H \to bb$	110 – 135	4.7	5	10%
$H \to WW \to \ell\nu\ell\nu$	110 – 600	4.6	5	20%
$H \to ZZ \to 4\ell$	110 – 600	4.7	3	1–2%
$H \to ZZ \to 2\ell 2\tau$	190 – 600	4.7	8	10–15%
$H \to ZZ \to 2\ell 2\nu$	250 – 600	4.6	2	7%
$H \to ZZ \to 2\ell 2q$	130 – 164 200 – 600	4.6	6	3%

All 8 analyses yielded a preliminary result to be shown today, and contributed to the CMS combination documented in HIG-011-32.

High Mass Higgs: H → ZZ → 2l2ν

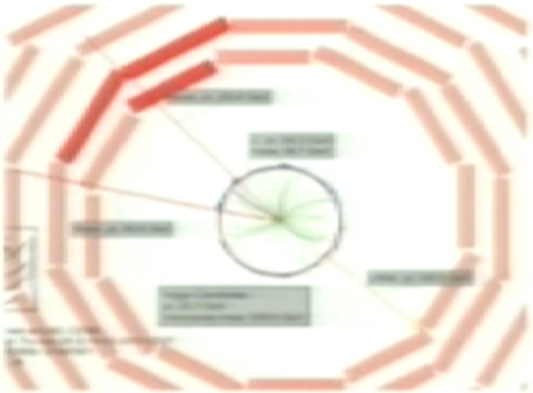

High sensitivity analysis for the high mass;

- **Z+jets background estimated from data**
- **M_T shape** analysis introduced
  - 10% improvement compared to cut-based analysis shown in LP

- M_Z ± 15 GeV; P_T (ll) >55 GeV
- Use $M_T^2 = (\sqrt{P_{TZ}^2 + M_Z^2} + \sqrt{MET^2 + M_Z^2})^2 - (\vec{P}_{TZ} + \vec{MET})^2$
- Major backgrounds: Z+Jets, ttbar & WW
  - ME_T requirement to suppress Z + jets by x10^5
  - Anti b-tag to suppress ttbar
- Backgrounds estimated from data
  - Z+jets (using γ + jets) ; eμ sample (for ttbar ++WW, single-top/W+jets/Ztautau)
- ZZ, WZ background estimate from MC

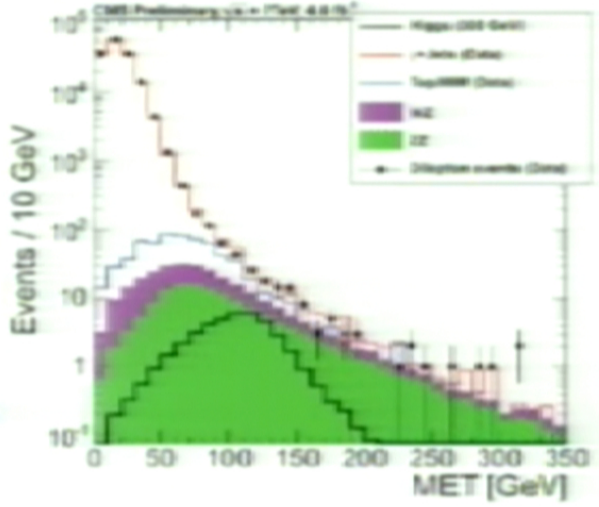

High Mass Higgs: H → ZZ → 2l2ν

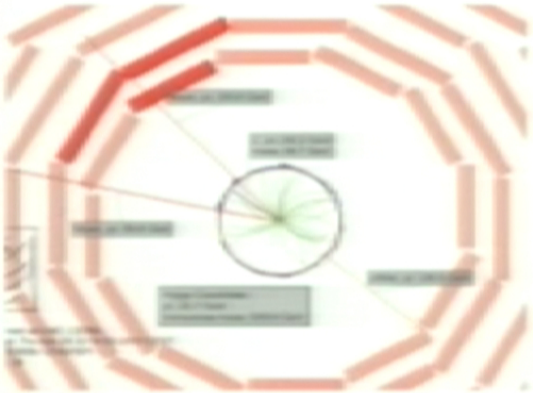

High sensitivity analysis for the high mass;

- **Z+jets background estimated from data**
- **M_T shape** analysis introduced
  - 10% improvement compared to cut-based analysis shown in LP

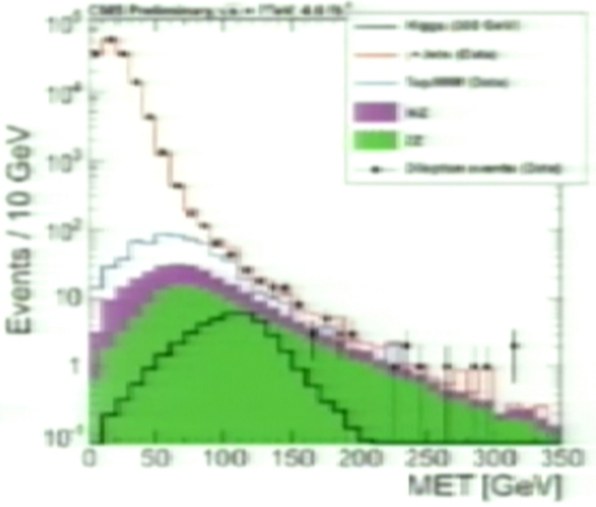

- $M_Z \pm 15$ GeV; P_T (ll) >55 GeV
- Use $M_T^2 = (\sqrt{P_{TZ}^2 + M_Z^2} + \sqrt{MET^2 + M_Z^2})^2 - (\vec{P}_{TZ} + \vec{MET})^2$
- Major backgrounds: Z+Jets, ttbar & WW
  - ME_T requirement to suppress Z + jets by x10^5
  - Anti b-tag to suppress ttbar
- Backgrounds estimated from data
  - Z+jets (using γ + jets) ; eμ sample (for ttbar ++WW, single-top/W+jets/Ztautau)
- ZZ, WZ background estimate from MC

High Mass Higgs: H → ZZ → 2l2ν

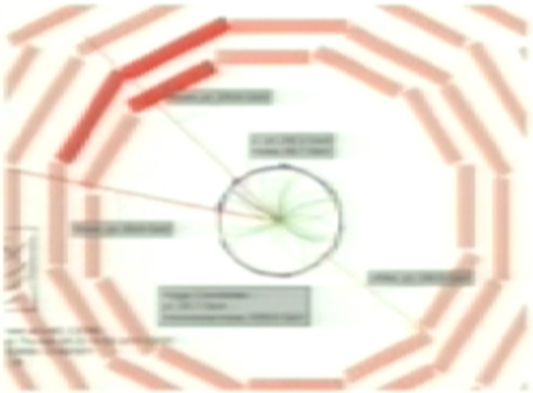

High sensitivity analysis for the high mass;

- **Z+jets background estimated from data**
- **M_T shape** analysis introduced
  - 10% improvement compared to cut-based analysis shown in LP

- $M_Z \pm 15$ GeV; P_T (ll) >55 GeV
- Use $M_T^2 = (\sqrt{P_{TZ}^2 + M_Z^2} + \sqrt{MET^2 + M_Z^2})^2 - (\vec{P}_{TZ} + \vec{MET})^2$
- Major backgrounds: Z+Jets, ttbar & WW
  - ME_T requirement to suppress Z + jets by x10^5
  - Anti b-tag to suppress ttbar
- Backgrounds estimated from data
  - Z+jets (using γ + jets) ; eμ sample (for ttbar ++WW, single-top/W+jets/Ztautau)
- ZZ, WZ background estimate from MC

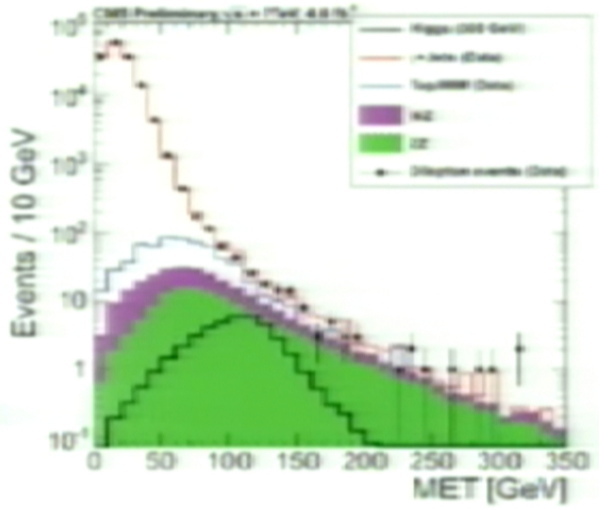

Results and Limits: H → ZZ→ 2l2ν

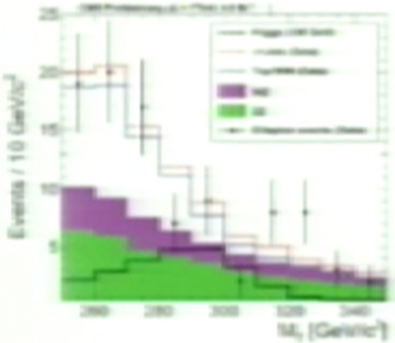

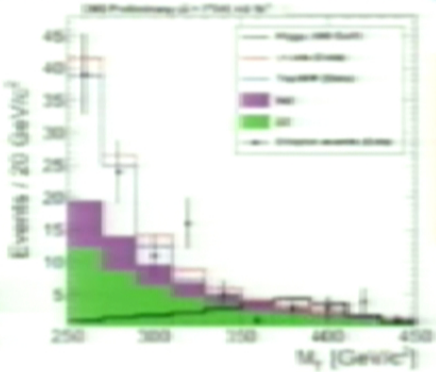

95%CL exclusion limits for a SM Higgs boson in the range 270-440 GeV (M_T shape based analysis)

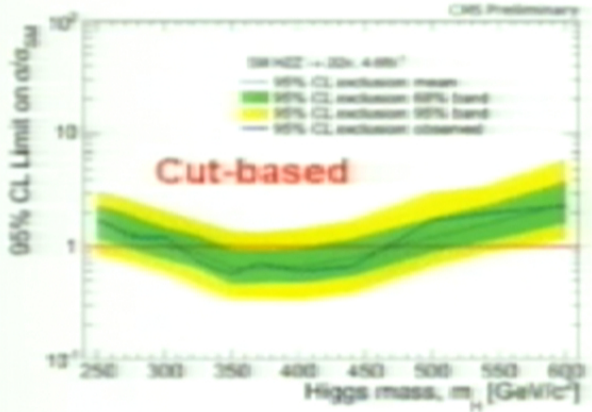

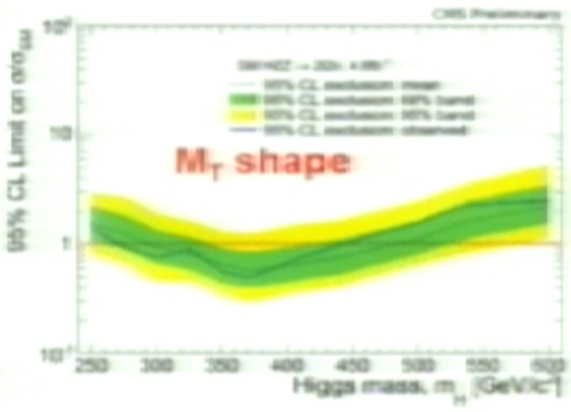

Results and Limits: H → ZZ→ 2l2ν

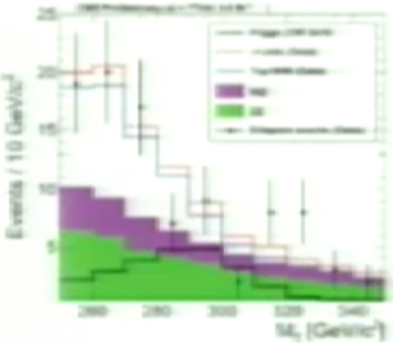

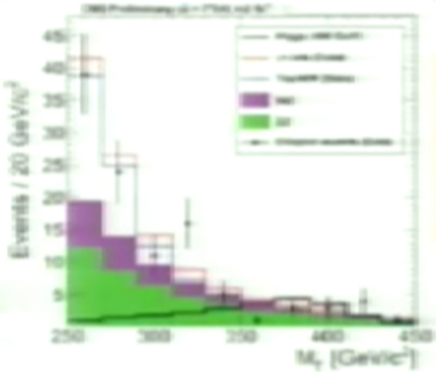

95%CL exclusion limits for a SM Higgs boson in the range 270-440 GeV (M_T shape based analysis)

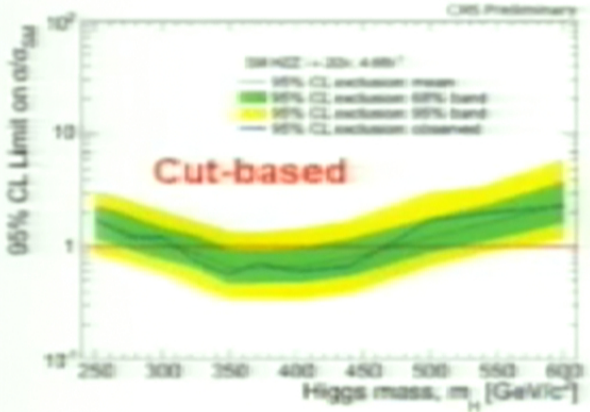

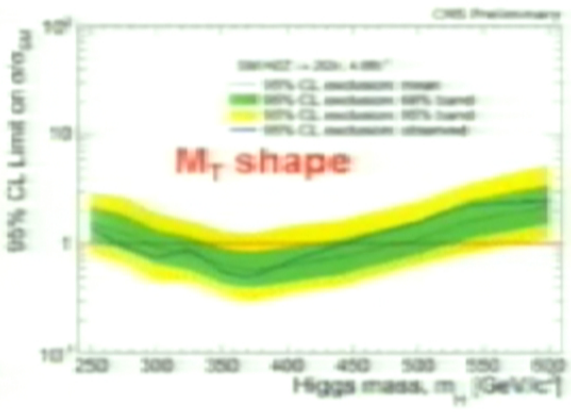

Results and Limits: H → ZZ→ 2l2ν

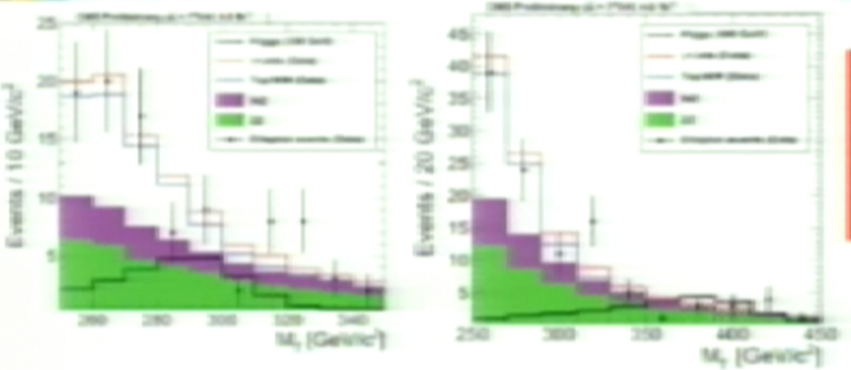

95%CL exclusion limits for a SM Higgs boson in the range 270-440 GeV (M_T shape based analysis)

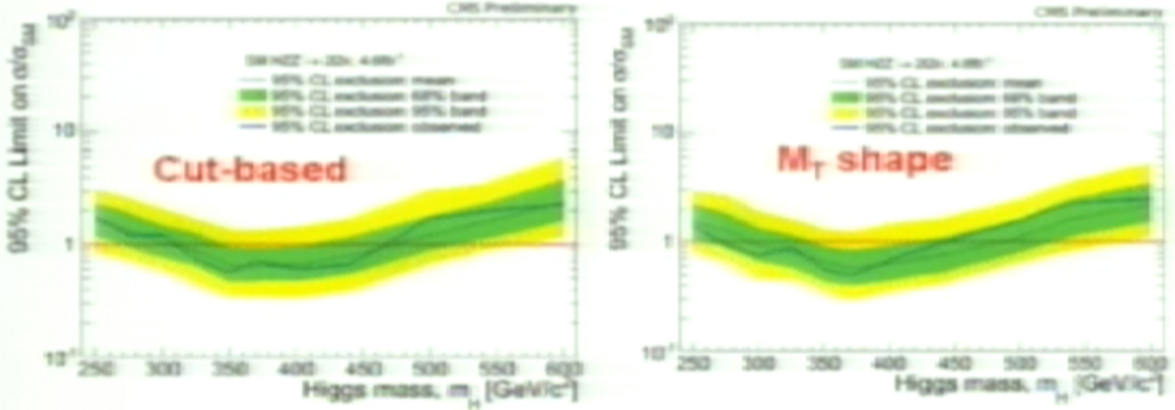

High Mass Higgs: H→ZZ→2l 2q

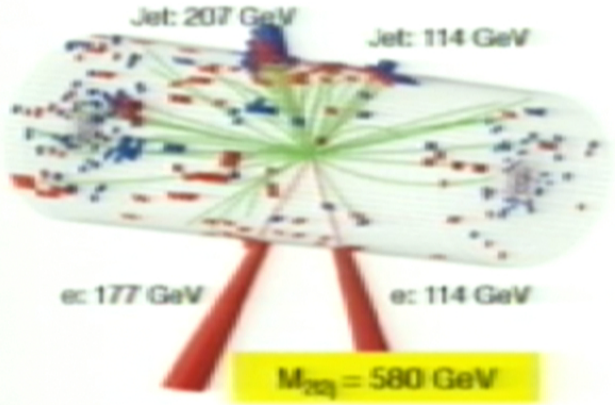

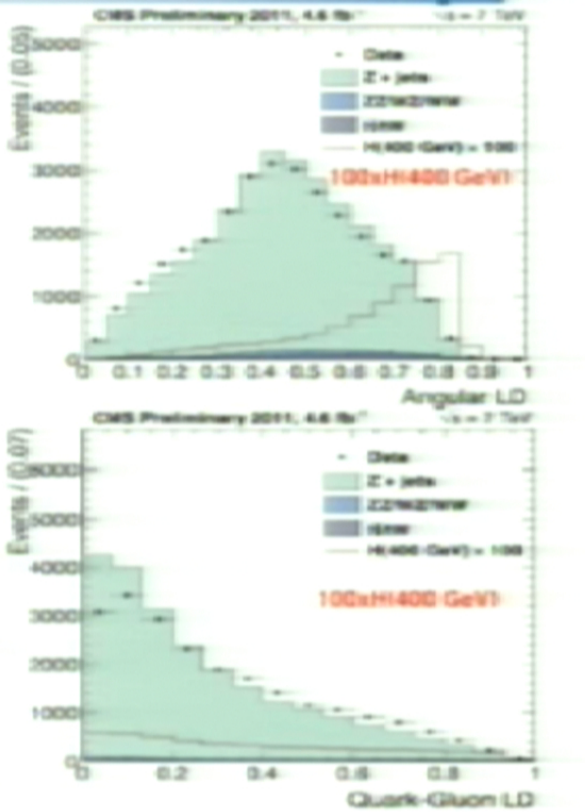

- Since LP: Added low mass in M_{2lq} distribution
- Events categorized by presence of 0, 1, 2 b-jets
- Major background: Z+jets ; ttbar suppressed by ME_T significance requirement
- Use 5 angles of scalar H → ZZ → 2l 2q in an angular likelihood discriminant
- Quark-gluon discriminant to reject Z +jets
- Background shape, normalization ← data sideband

High Mass Higgs: H→ZZ→2l 2q

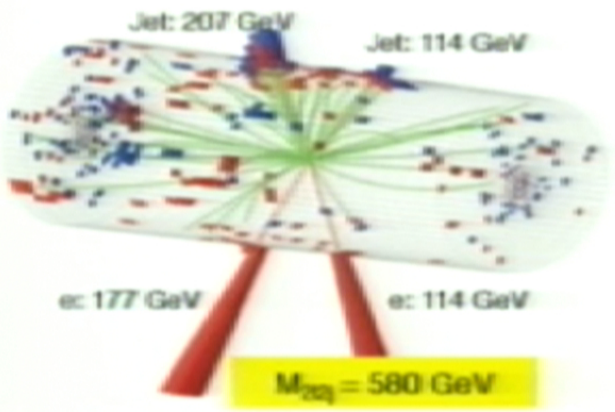

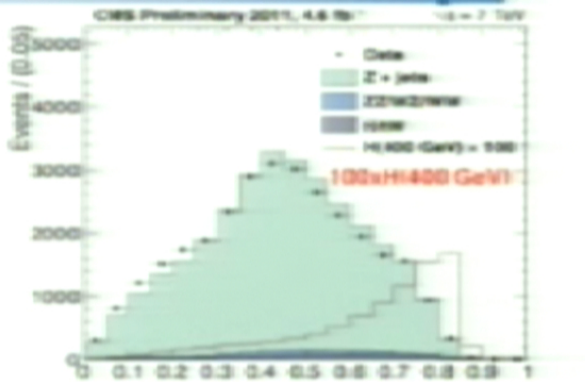

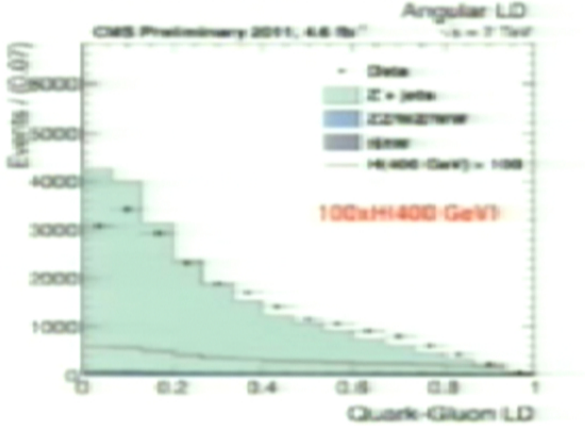

- Since LP: Added low mass in M_{2lq} distribution
- Events categorized by presence of 0, 1, 2 b-jets
- Major background: Z+jets ; ttbar suppressed by ME_T significance requirement
- Use 5 angles of scalar H → ZZ → 2l 2q in an angular likelihood discriminant
- Quark-gluon discriminant to reject Z +jets
- Background shape, normalization ← data sideband

H →ZZ→2l 2q: data and limits

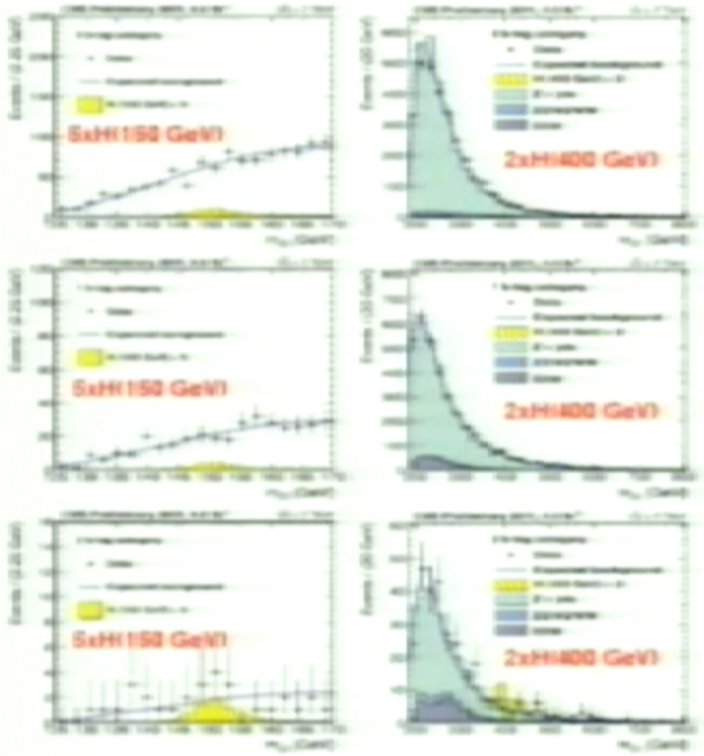

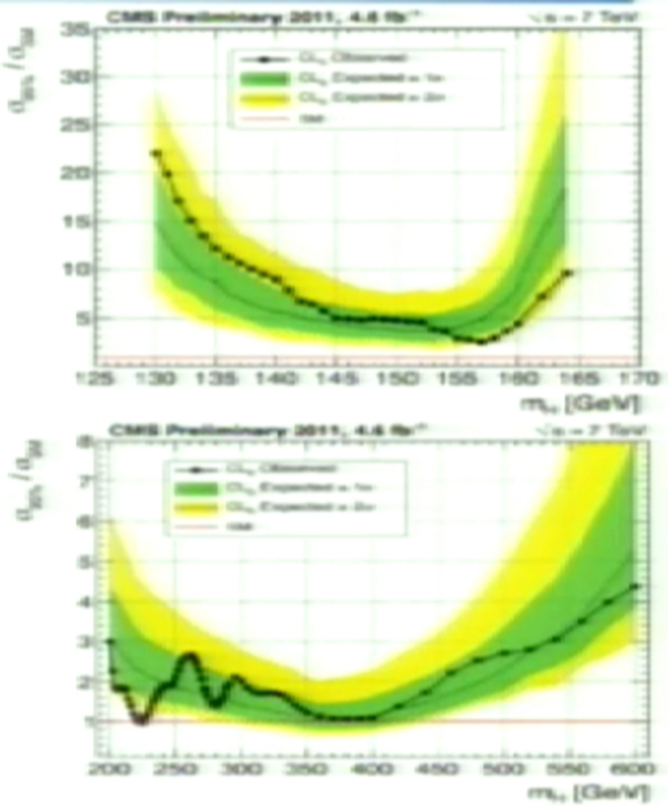

H →ZZ→2l 2q: data and limits

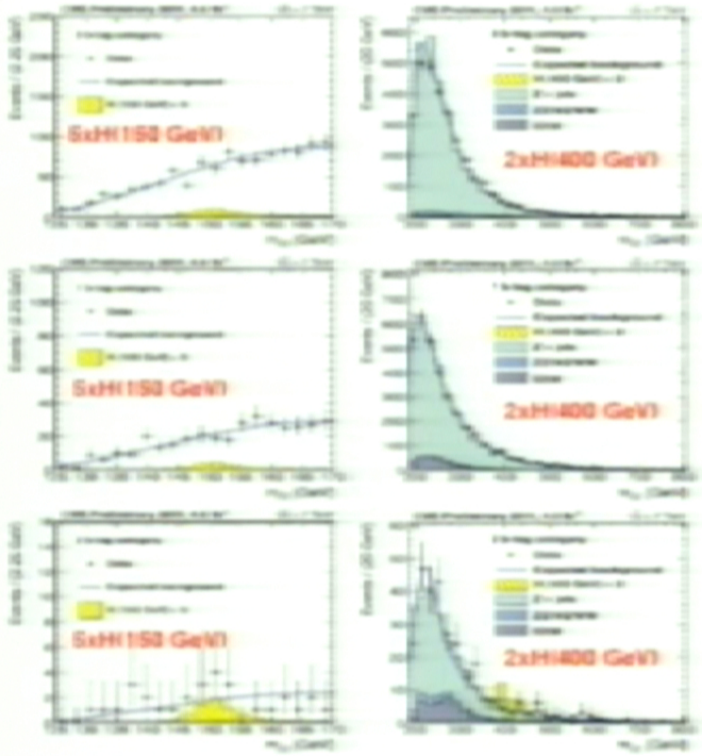

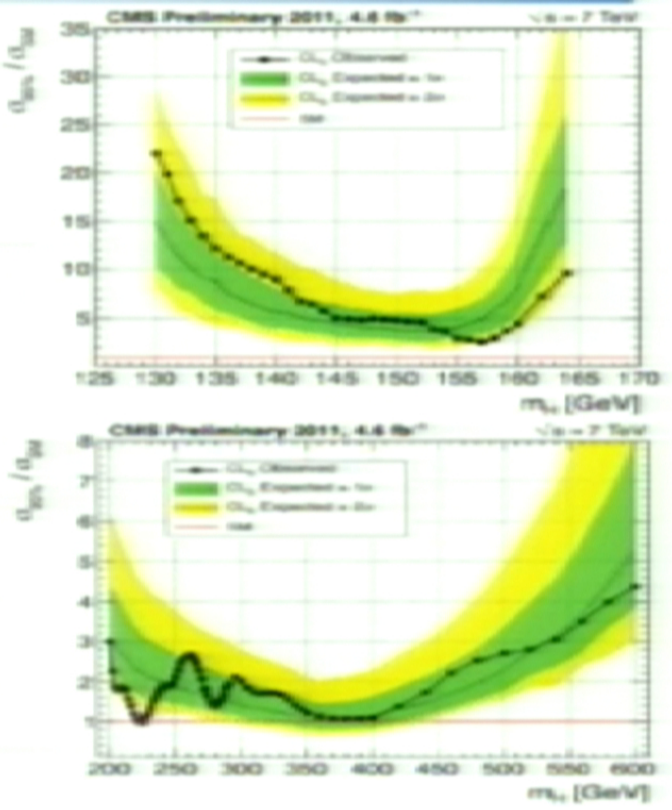

High Mass Higgs: H →ZZ→2l 2τ

eeeτ candidate

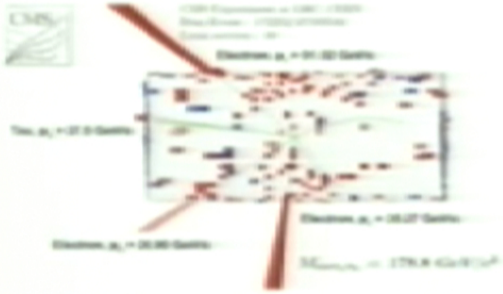

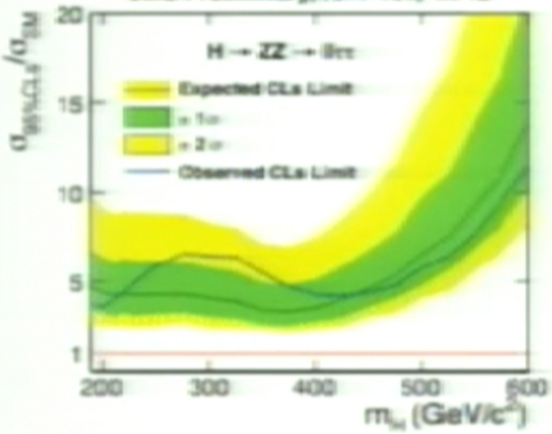

No major change w.r.t LP'11

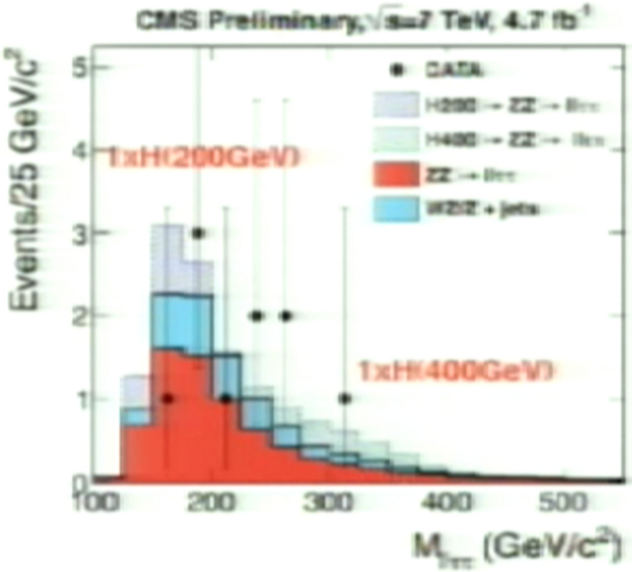

10 observed events, 10.2 expected background

Background shapes are taken from MC simulation and normalized to the values obtained using data-driven techniques.

H→ WW → 2l 2ν

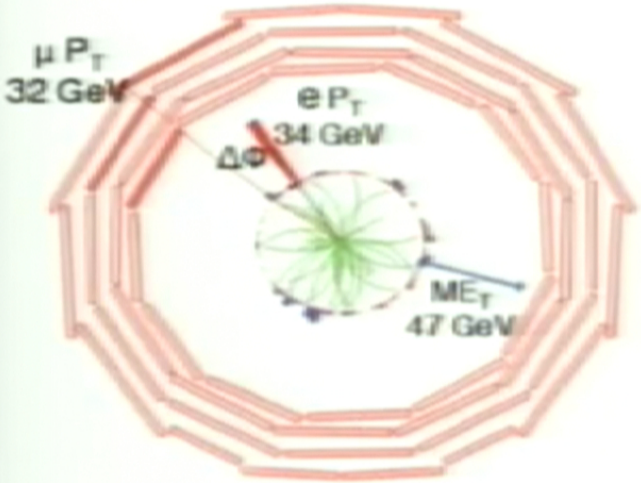

- Signal characteristics:
  - Only 2 opposite sign, isolated leptons
  - significant ME_T → No mass peak
  - No b-jets, no additional low P_T μ
  - With additional 0, 1 or 2 jets (VBF)
  - Small ΔΦ (l⁺l⁻) ← Higgs scalarity

- No signal mass peak (missing νν) → Counting expt.
- Challenge is to remove & control large backgrounds

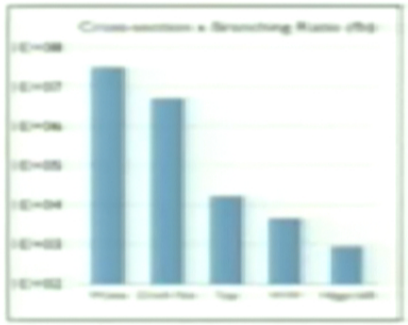

Major requirements:

- Lepton P_T > 15 GeV, tight ID & Isolation
  - removes QCD & W+jets contamination
- Large ME_T & Z → μμ, ee veto
  - removes Drell-Yan contamination
- Classification by # of jets (P_T > 30 GeV) & b-jet veto
  - removes Top contamination
- Kinematic discriminants: M_{ll} & ΔΦ (l⁺l⁻)
  - mitigates pp → WW background
- M_H–dependent cut optimization

H→ WW → 2l 2ν

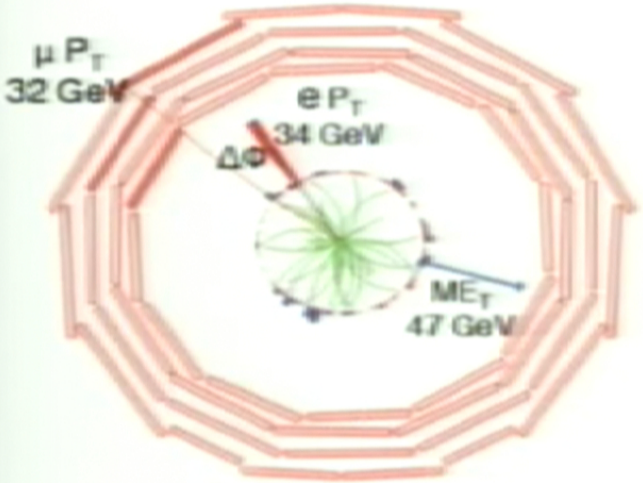

- Signal characteristics:
  - Only 2 opposite sign, isolated leptons
  - significant ME_T → No mass peak
  - No b-jets, no additional low P_T μ
  - With additional 0, 1 or 2 jets (VBF)
  - Small ΔΦ (l⁺l⁻) ← Higgs scalarity

- No signal mass peak (missing νν) → Counting expt.
- Challenge is to remove & control large backgrounds

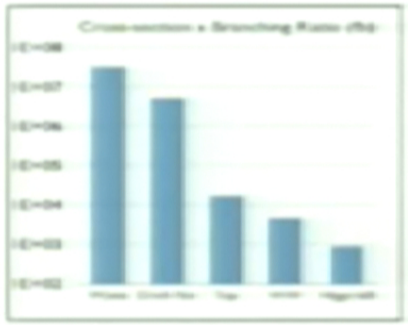

Major requirements:

- Lepton P_T > 15 GeV, tight ID & Isolation
  - removes QCD & W+jets contamination
- Large ME_T & Z → μμ, ee veto
  - removes Drell-Yan contamination
- Classification by # of jets (P_T > 30 GeV) & b-jet veto
  - removes Top contamination
- Kinematic discriminants: M_{ll} & ΔΦ (l⁺l⁻)
  - mitigates pp → WW background
- M_H–dependent cut optimization

H→ WW → 2l 2ν: improvements

- Objects Identification:
  - MVA-based electron identification (fakes reduced by 50%, same signal efficiency)
- Selections:
  - Pileup dependent MET cut
  - Minimum dilepton mass cut from 12→20 GeV for same-flavor events
  - Refined the top tagging procedure (less sensitive to PU)
  - Trailing lepton p_T from 10 to 15 GeV for SF and dilepton p_T cut at 45 GeV (suppressing Drell-Yan and W+jets)
- Backgrounds:
  - Refined DY and top estimation
  - Data driven normalization of DY→ττ and $W\gamma^*$
- **Major effort in understanding BDT Shape based analysis:**
  - **Shape variation for systematic uncertainty evaluation**
  - **Additional cross-checks: single variable shape analyses; matrix element analysis**

Data and limits in cut and count analysis

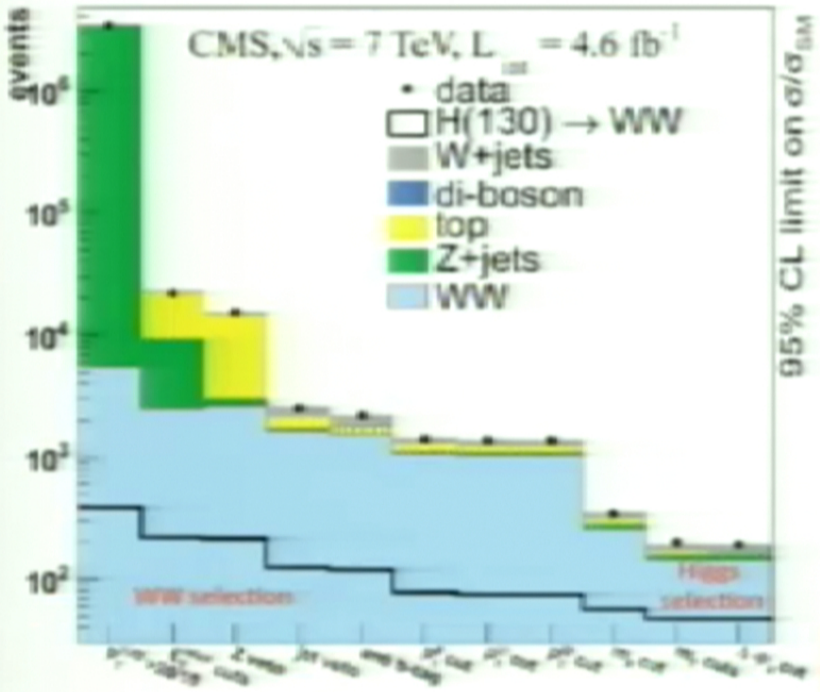

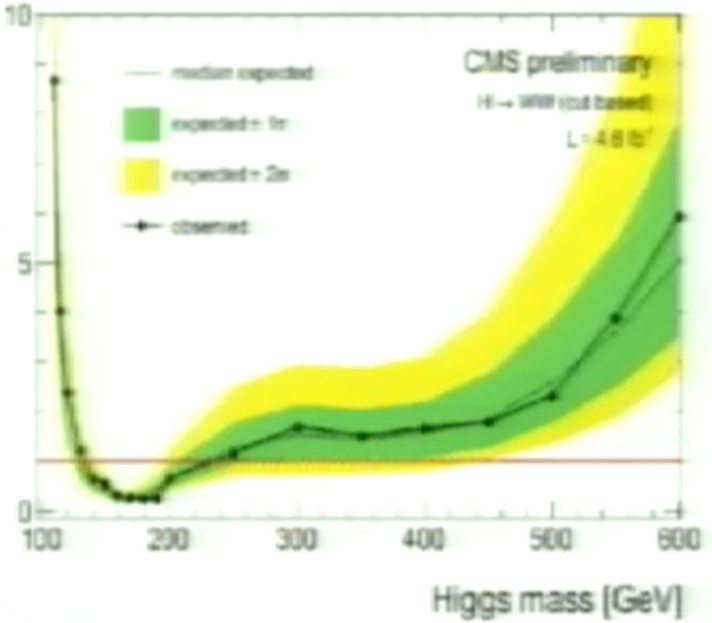

Expected range: 129 < M_H < 236 GeV
Observed range: 132< M_H < 238 GeV

Data describes predicted background well.

BDT Shape Comparison

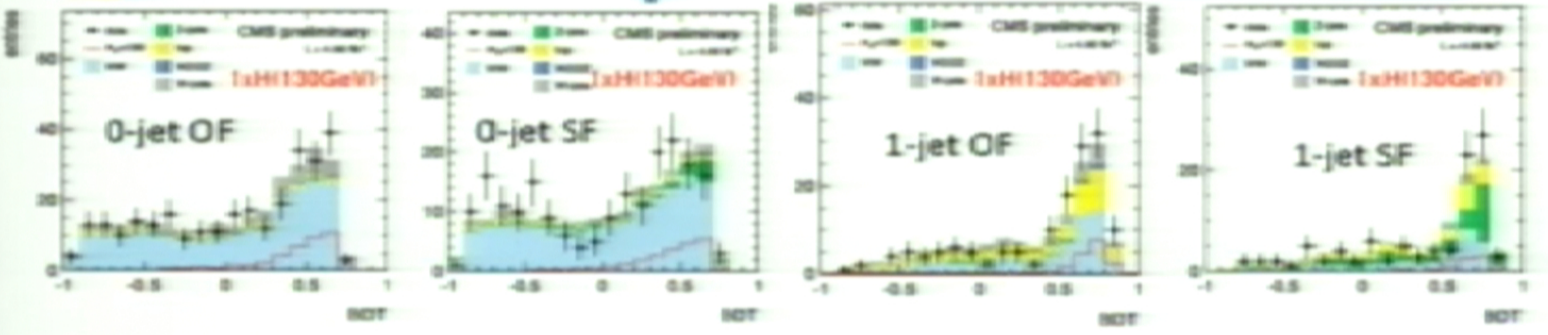

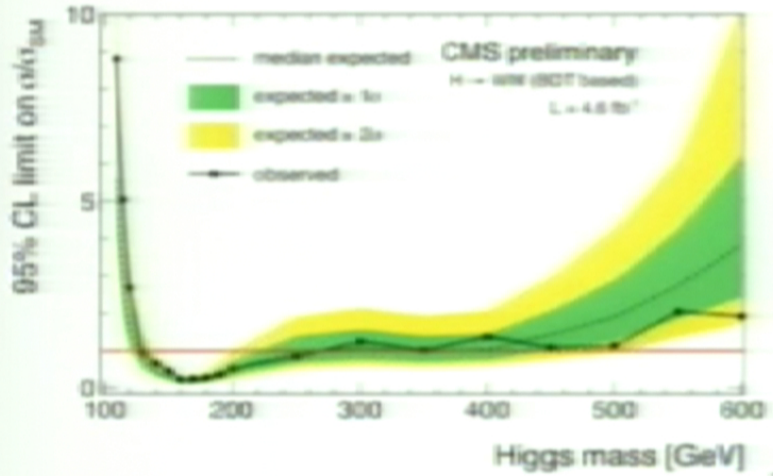

Expected range: $127 < M_H < 270$ GeV
Observed range: $129 < M_H < 270$ GeV

Low Mass Higgs Search : H→ ττ

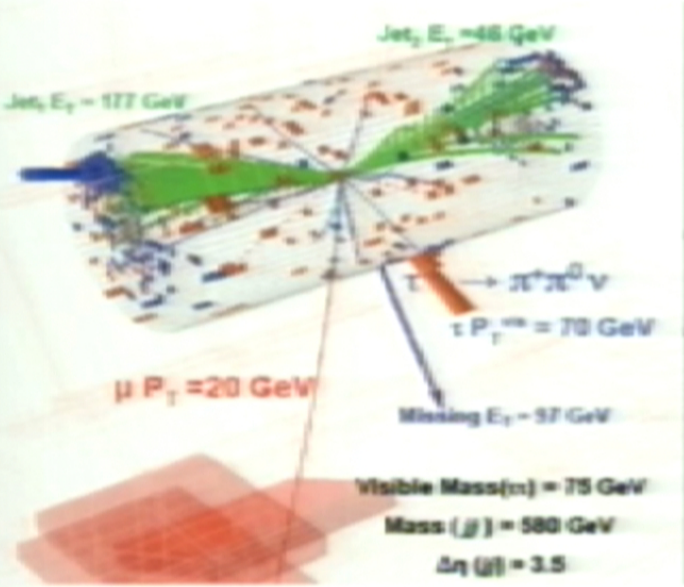

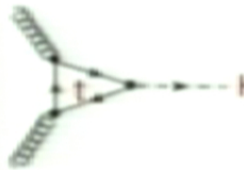

0 or 1 JET
0 jets>30GeV or 1jet<150GeV

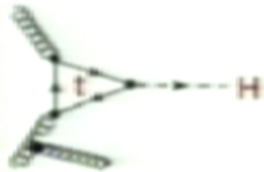

BOOSTED
One jet P_T>150GeV

VBF
>= 2jets >30GeV
Δη>4, M_{jj}>400GeV
No additional jets with P_T>30GeV
In the rapidity gap

- ττ selection: $\mu+\tau_{had}$, $\mu+\tau_{had}$, $\mu+e$
- SM-Boosted mode added
- VBF mode cleanest, most sensitive

H→ ττ : Mass Spectrum By Categories

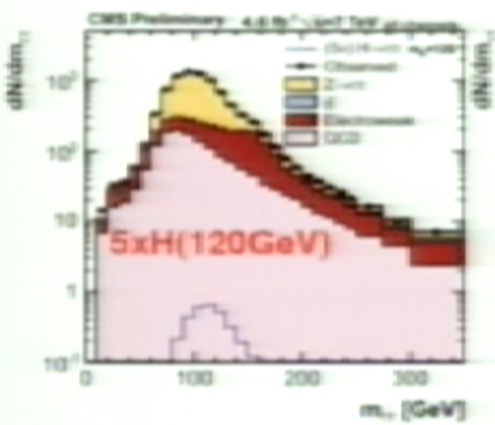

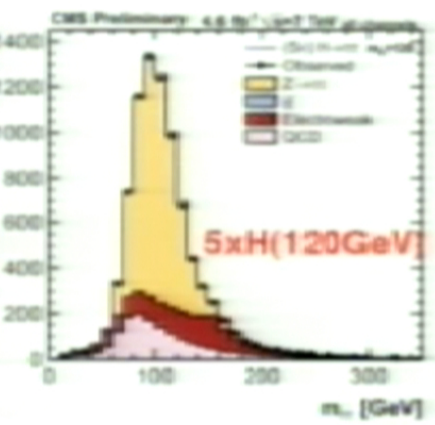

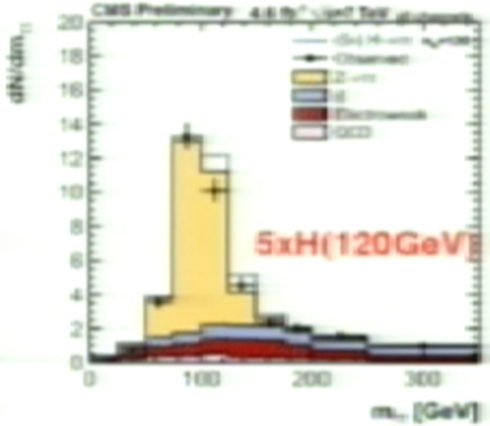

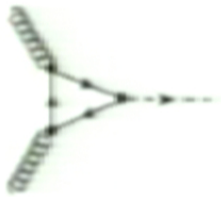

H→ ττ : data and limits

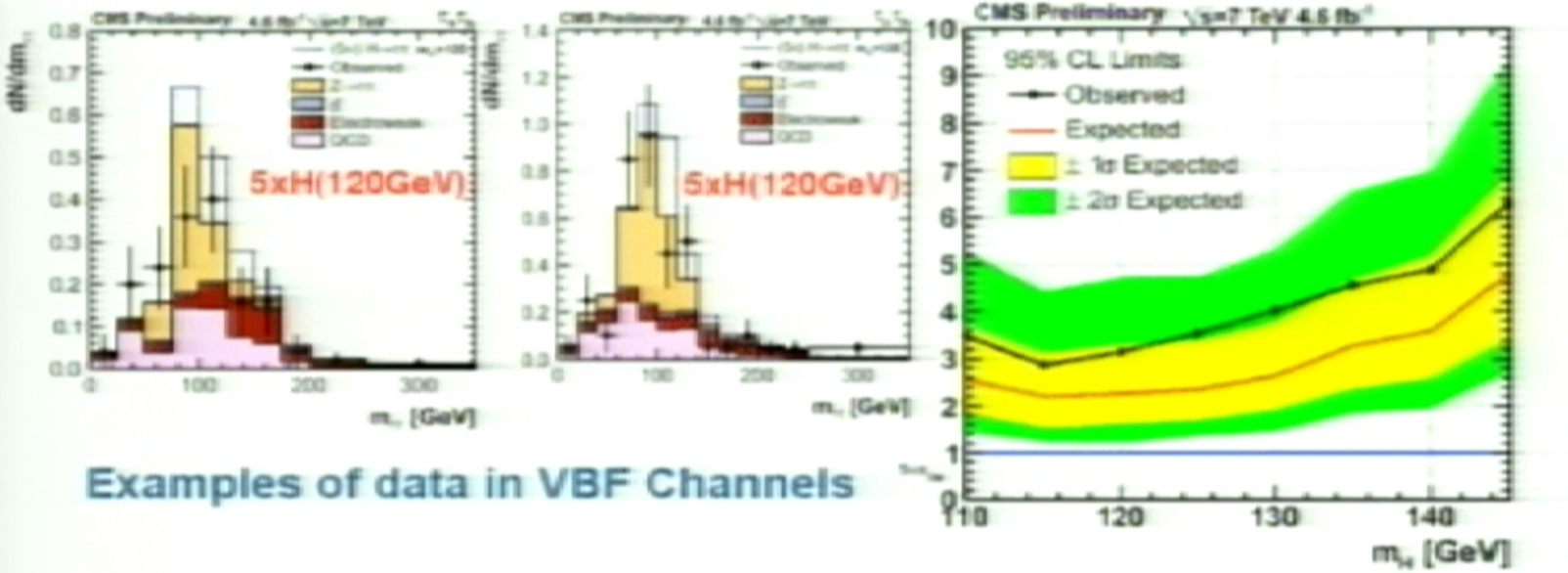

Examples of data in VBF Channels

Significant improvement in sensitivity since LP'11

Low Mass Higgs Search : H→ bb

- gg→ H→ bb and VBF are dominant production modes but overwhelmed by enormous QCD di-jet background
- Best option: qq→ VH; H → bb
  - Major backgrounds are V+jets, VV, ttbar
- Use
  - VH topology : ΔΦ(V,H) > 3
  - P_T(V)> 100-160 GeV (boosted W/Z)
  - Tight b-tagging & MET quality
  - Backgrounds estimated from control data

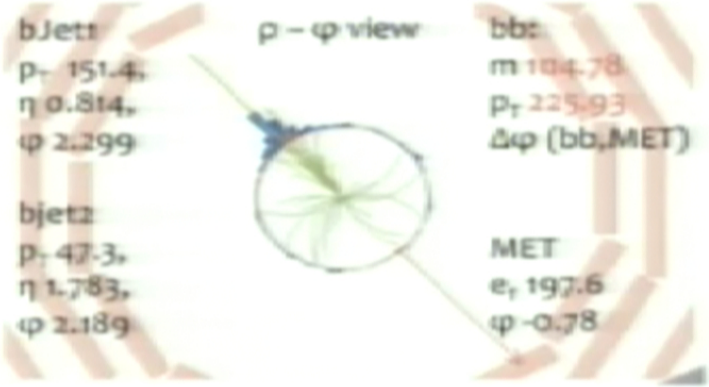

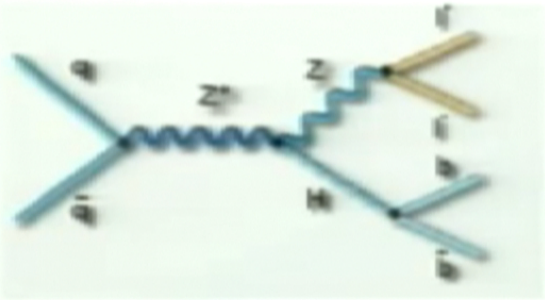

5 sub channels

Z(→*ll*); H→bb, *l* = μ, e
W(→lν) ; H→bb, *l* = μ, e
Z(→νν); H→bb

Analysis method largely unchanged w.r.t LP'11
Extensive use of data driven methods to control the backgrounds.

H→ bb: data and limits

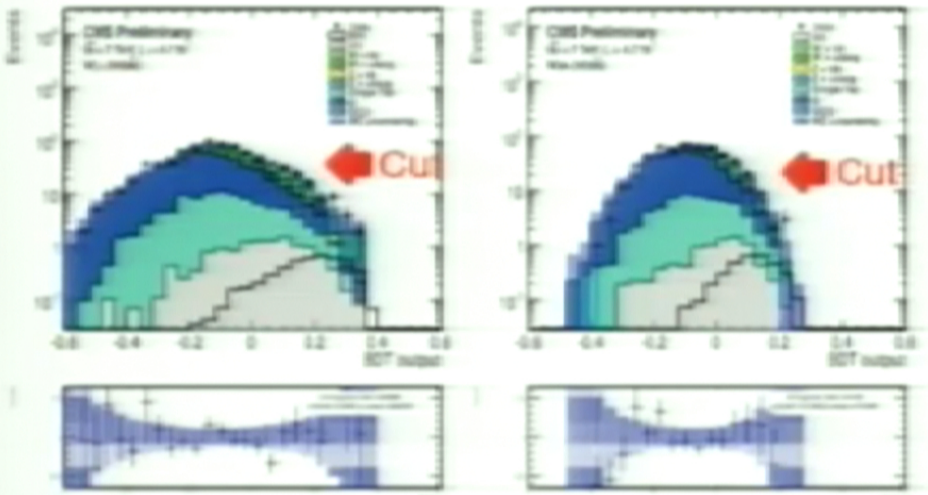

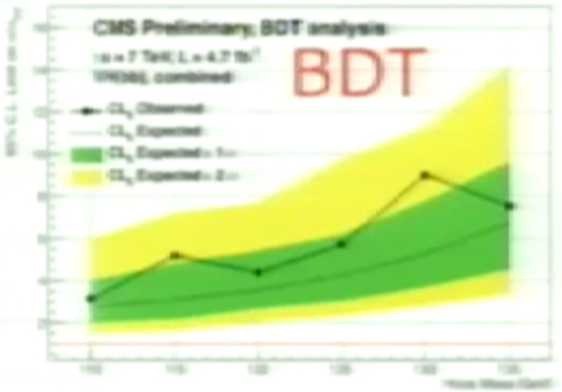

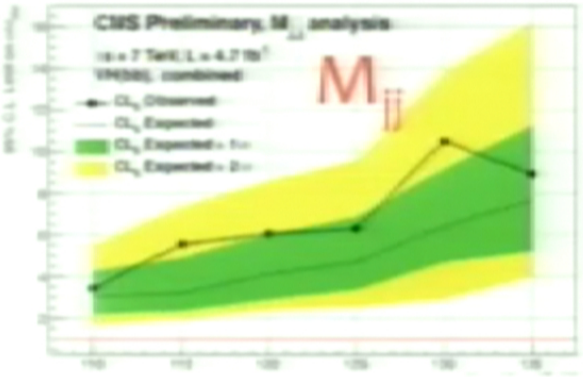

H → ZZ →4e, 4μ, 2e2μ: The Golden Channel

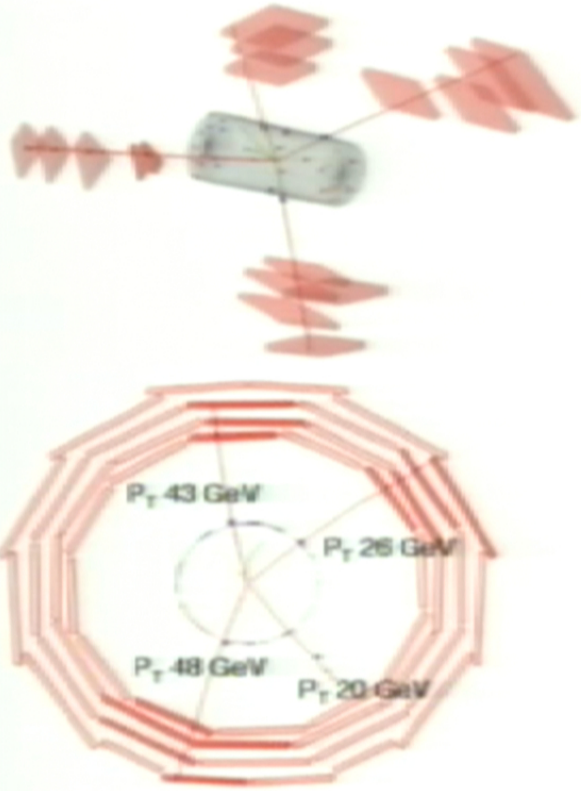

Improved sensitivity at low Higgs masses

- Reduce MZ_1 cut from 60 → 50GeV
- Reduce MZ_2 cut from 20 → 12GeV

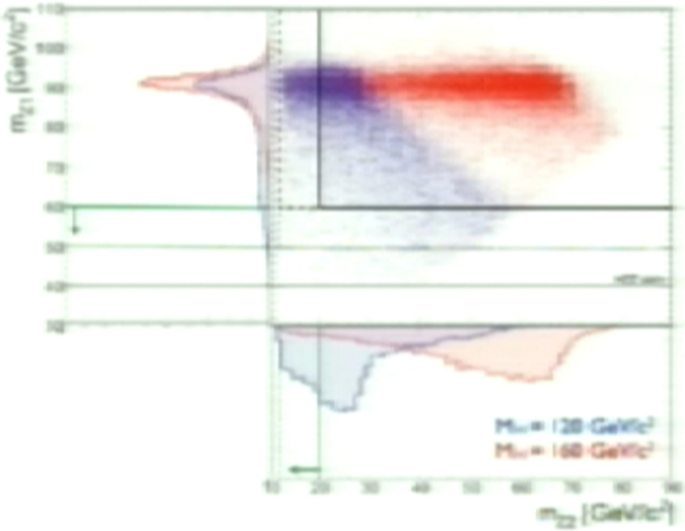

H→ZZ→4l: Baseline Selection

50< m_{Z1} < 120 GeV

12< m_{Z2} < 120 GeV

m_{4l} >100 GeV/c²

Observed events: 72

Expected events: 67.1 ± 6.0

Baseline	4e	4μ	2e2μ
ZZ	12.27 ± 1.16	19.11 ± 1.75	30.25 ± 2.78
Z+X	1.67 ± 0.55	1.13 ± 0.55	2.71 ± 0.96
All background	13.94 ± 1.28	20.24 ± 1.83	32.96 ± 2.94
m_H = 120 GeV/c²	0.25	0.62	0.68
m_H = 140 GeV/c²	1.32	2.48	3.37
m_H = 350 GeV/c²	1.95	2.61	4.64
Observed	12	23	37

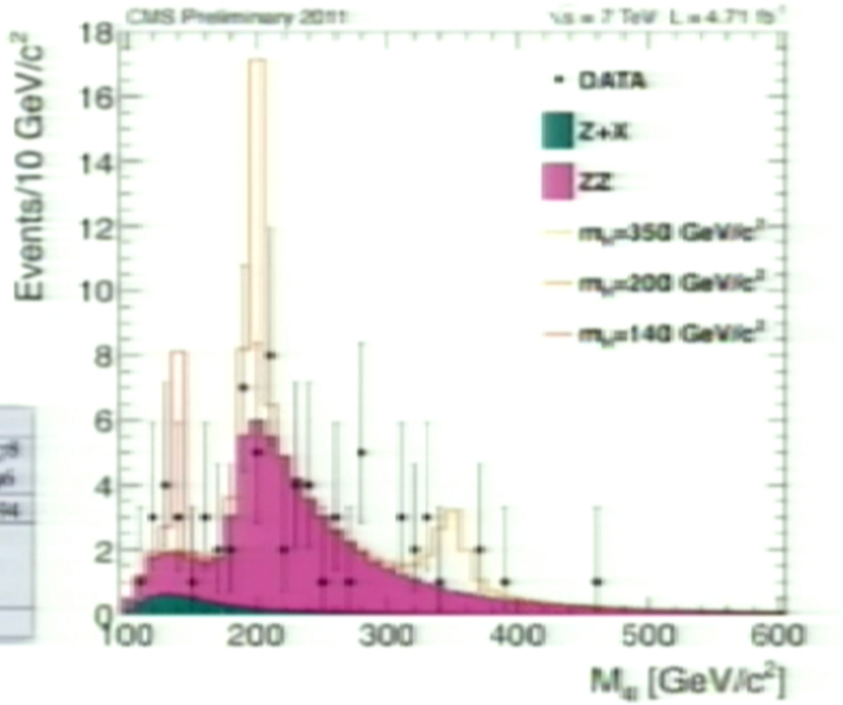

Zoom in the low mass

$50 < m_{Z1} < 120$ GeV
$12 < m_{Z2} < 120$ GeV

$100 < m_{4l} < 160$ GeV/c²
Observed events: 13
Expected events: 9.5 ± 1.3

Final state:	4e	4μ	2e2μ
Obs. events:	3	5	5
Exp. events:	1.7	3.3	4.5

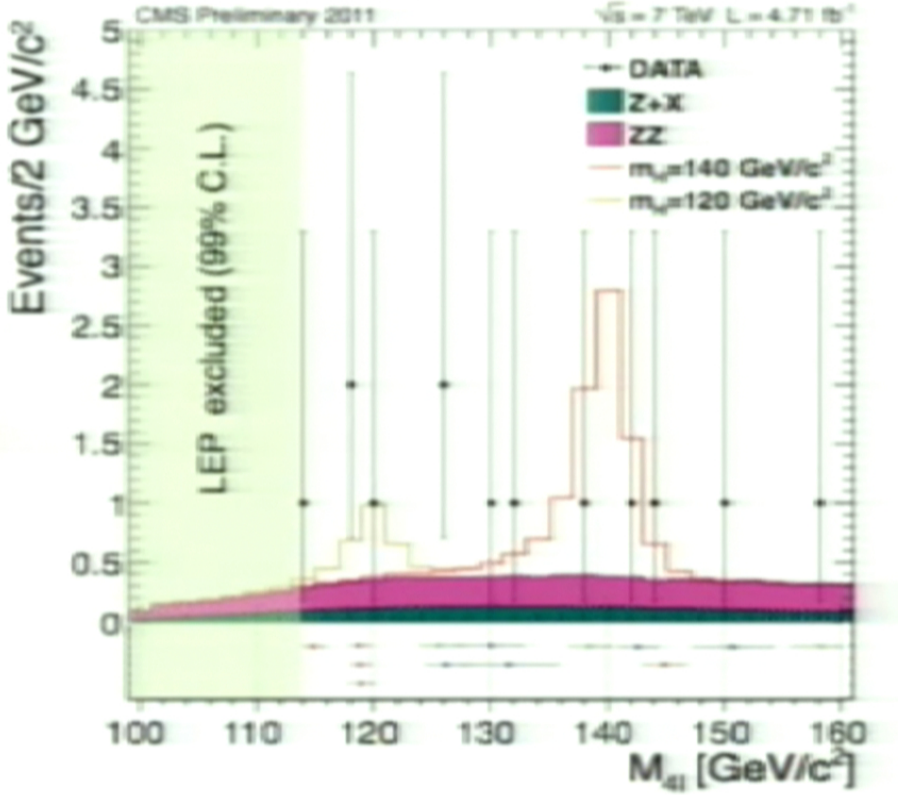

H→ZZ→4l: 95%CL Excl. Limits

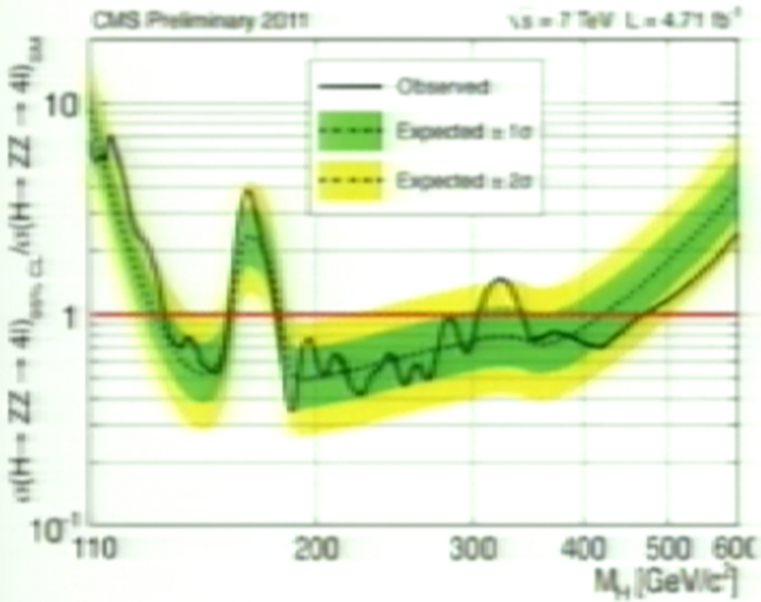

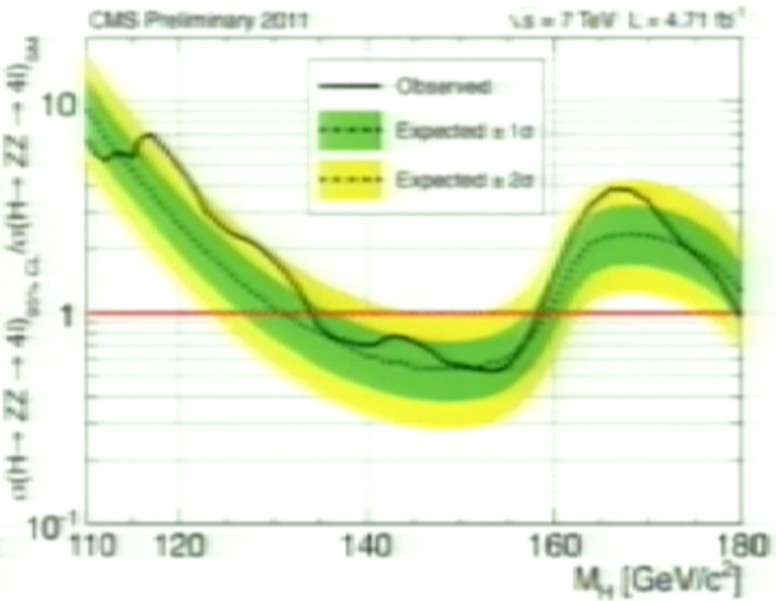

Expected range: $130 < M_H < 160$ GeV; $182 < M_H < 420$ GeV
Observed range: $134 < M_H < 158$ GeV; $180 < M_H < 305$ GeV; $340 < M_H < 460$ GeV

H→ZZ→4l: 95%CL Excl. Limits

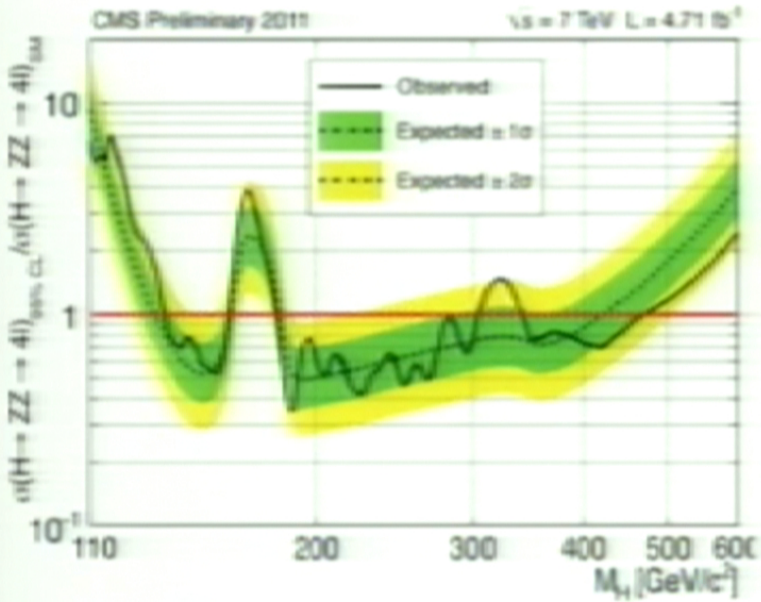

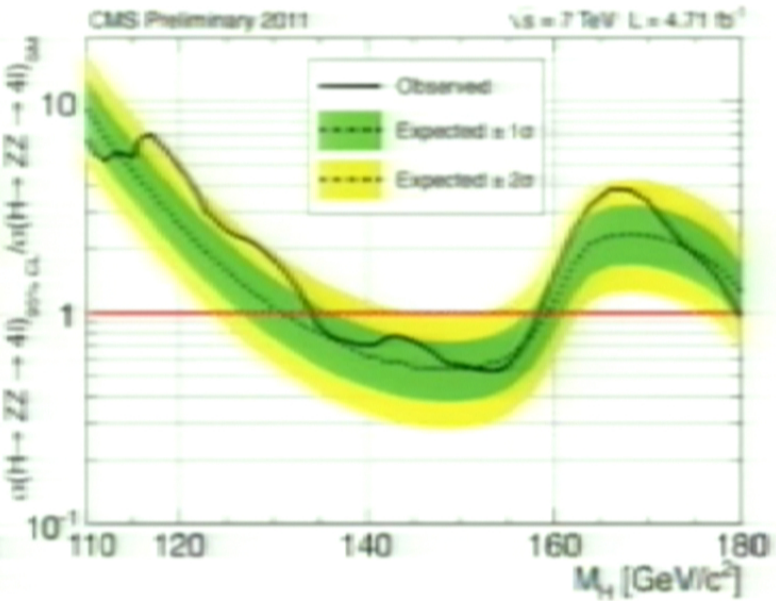

Expected range: $130 < M_H < 160$ GeV; $182 < M_H < 420$ GeV
Observed range: $134 < M_H < 158$ GeV; $180 < M_H < 305$ GeV; $340 < M_H < 460$ GeV

Low Mass Higgs Search : H→ γγ

Signal: 2 energetic, isolated γ.
Search for a narrow mass excess over a smoothly falling background.

Challenges: vertexing with PU, calibrations and transparency corrections for the crystals.

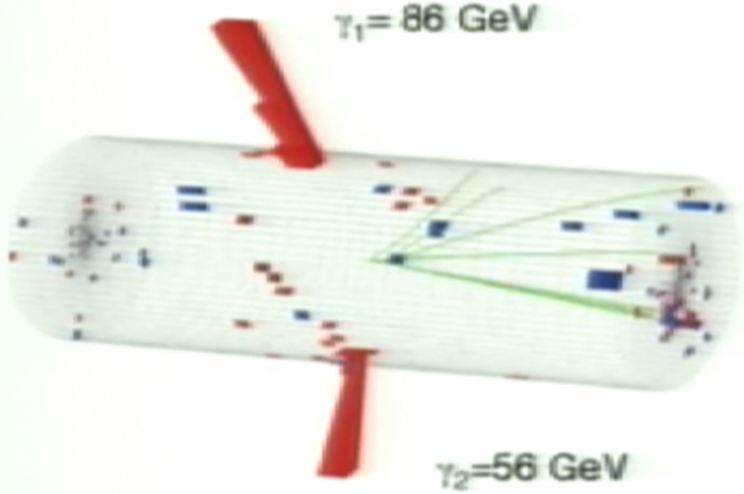

Calibration constants derived from Z→ee data

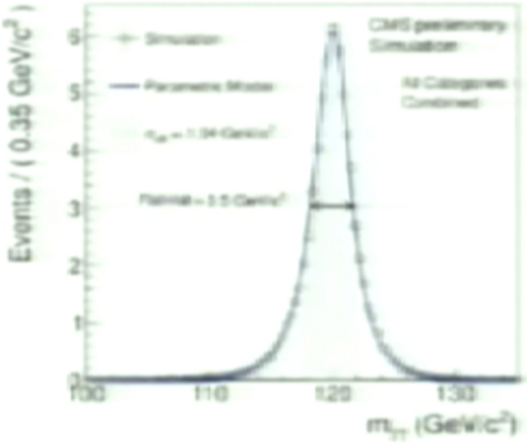

Background: Large and mostly irreducible QCD di-photons. Measured from $M_{\gamma\gamma}$ sidebands in data

Improvements in the H→ γγ analysis

- Vertex ID uses BDT
  - Improved vertex identification (gain → 3%)
- Progressive ("sliding") cuts on photon p_T
  - $p_T^1 > m_{\gamma\gamma}/3$, $p_T^2 > m_{\gamma\gamma}/4$
- Cluster energy corrections + new intercalibrations+new transparency corrections
- using the lasers.
  - Improved energy resolution
- $p_T^{\gamma\gamma}$ event classification dropped for SM analysis
  - Remove threshold shaping of mass spectrum

- In order to take advantage of
  - The better signal over background ratio in the central part of the detector
  - The better resolution for central/unconverted photons
- The analysis is performed simultaneously in 4 categories (R9 is a metric of the shower transverse size: $R9 = E_{3x3\ array} / E_{super\text{-}cluster}$. It discriminates unconverted from converted photons)
  - Both photons in the Barrel, min(R9) > 0.94
  - Both photons in the Barrel, min(R9) < 0.94
  - At least one photon in Endcap, min(R9) > 0.94
  - At least one photon in Endcap, min(R9) < 0.94
- Better parameterization of background shape.

Improvements in Vertex finding Efficiency

- Training BDT using input variables computed from
  - Track momenta
  - Photon kinematics
- BDT improves correct vertex selection efficiency by 3% with respect to ranking algorithm used in EPS/LP analyses.
- 'Correct vertex' is defined as being within 10mm of true vertex z position
- Vertex finding efficiency
  - From Z →μμ and γ+ jets
  - Photon Selection efficiency
  - From Z → ee

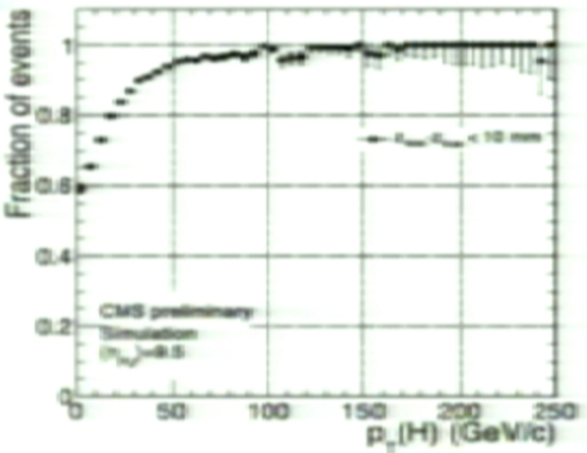

2011A	2011B	2011
86.3% ± 0.2% ± 0.4%	79.8% ± 0.2% ± 0.5%	83.0% ± 0.2% ± 0.4%

Improvemens in Photon Energy Resolution

- **Comprehensive energy resolution studies made with Z →ee, W →eν and E/p, π^0 intercalibrations and laser signals for transparency corrections**

Effect of new laser corrections and intercalibration on barrel-barrel Z→ee
Resolution in data improves typically by 10%, EB, |η|>1, R9>0.94
Instrumental contribution to the mass resolution in the best EB category is 0.99 ±0.01 GeV

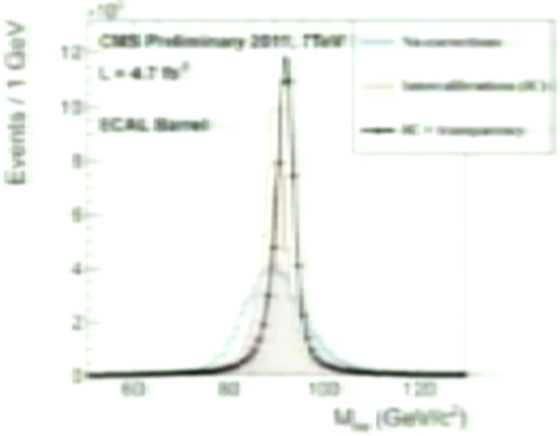

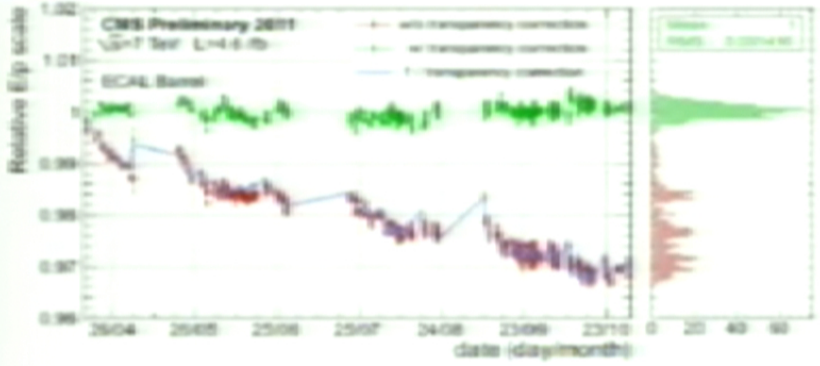

Energy scale for W→eν and Z→ee stable throughout 2011 at the level of 0.1 GeV.

EB inter-calibration and transparency correction fully understood for EB for the entire 2011 data set.

H→ γγ: data and exclusion limits

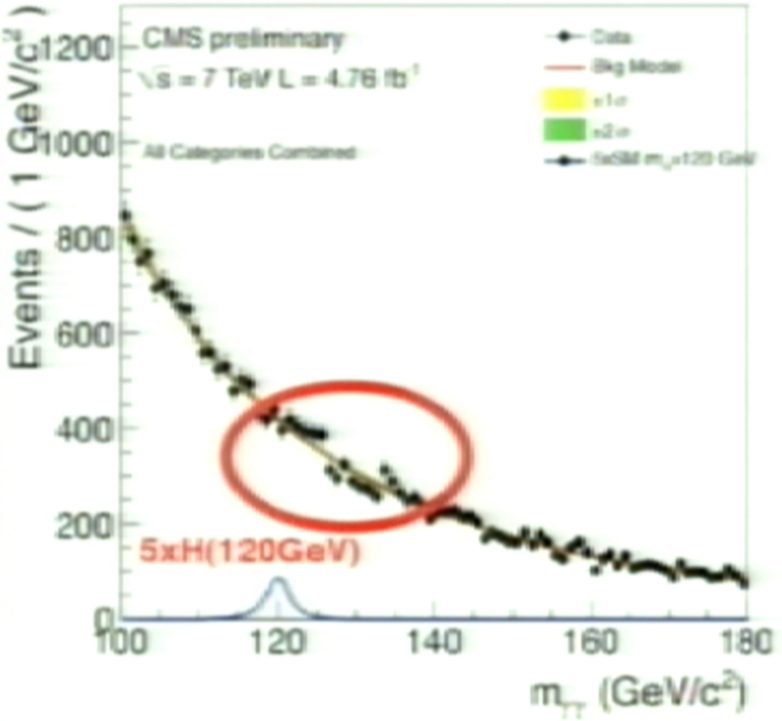

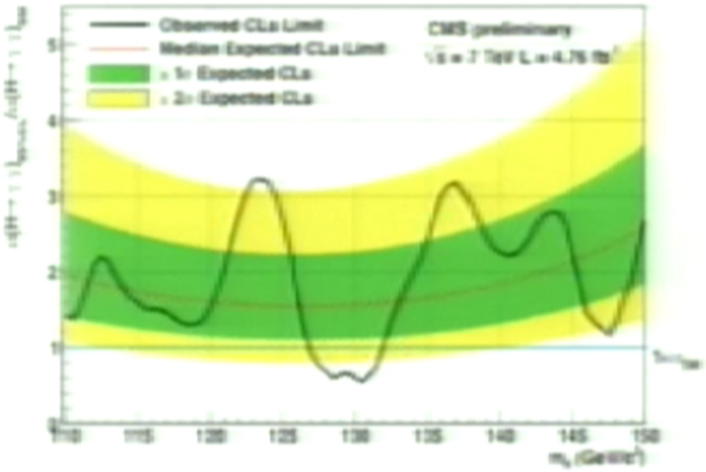

A lot of studies on the background fit model. Is the structure/shape of the observed limit due to the chosen background model? No – this has been shown to not be the case.

Using 5th order polynomial fit to background: some loss in sensitivity but negligible bias.

CMS expected sensitivity @4.7fb^{-1}

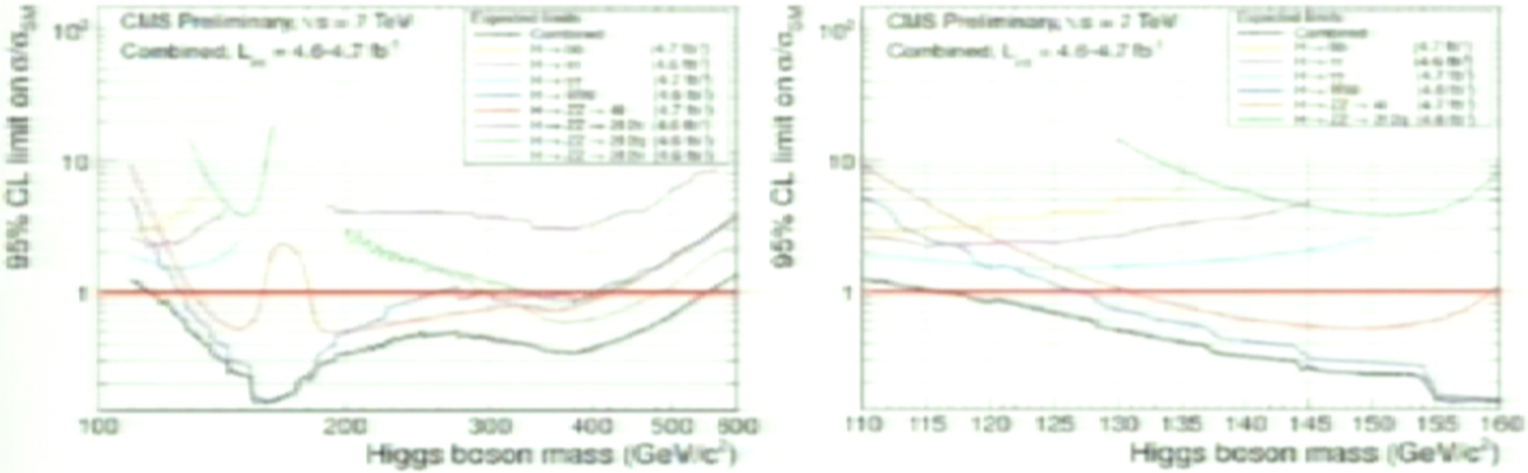

Very close or better than 1xSM in the full mass range.
Optimization of some analyses still ongoing.
Additional sub-channels under study.

Met the expectations set at the end of 2010.

CLs for SM Higgs

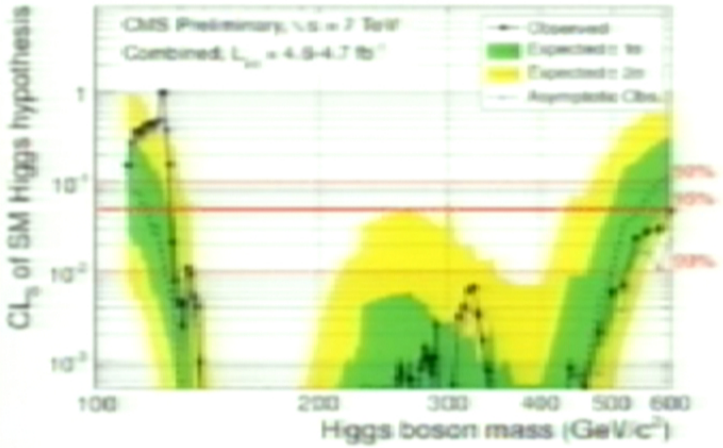

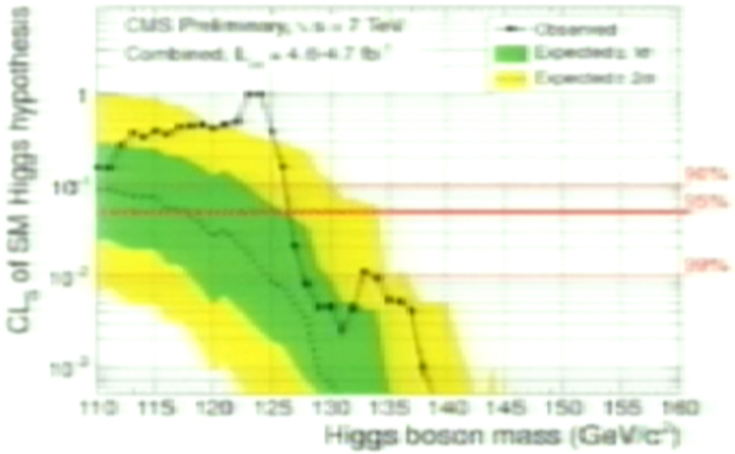

Preliminary 95 and 99%CL exclusion limits

95% CL:	obs 127-600,	exp:117-543
99% CL:	obs 128-525,	exp:125-500

Limits on σ/σ_{sm} (CLs method)

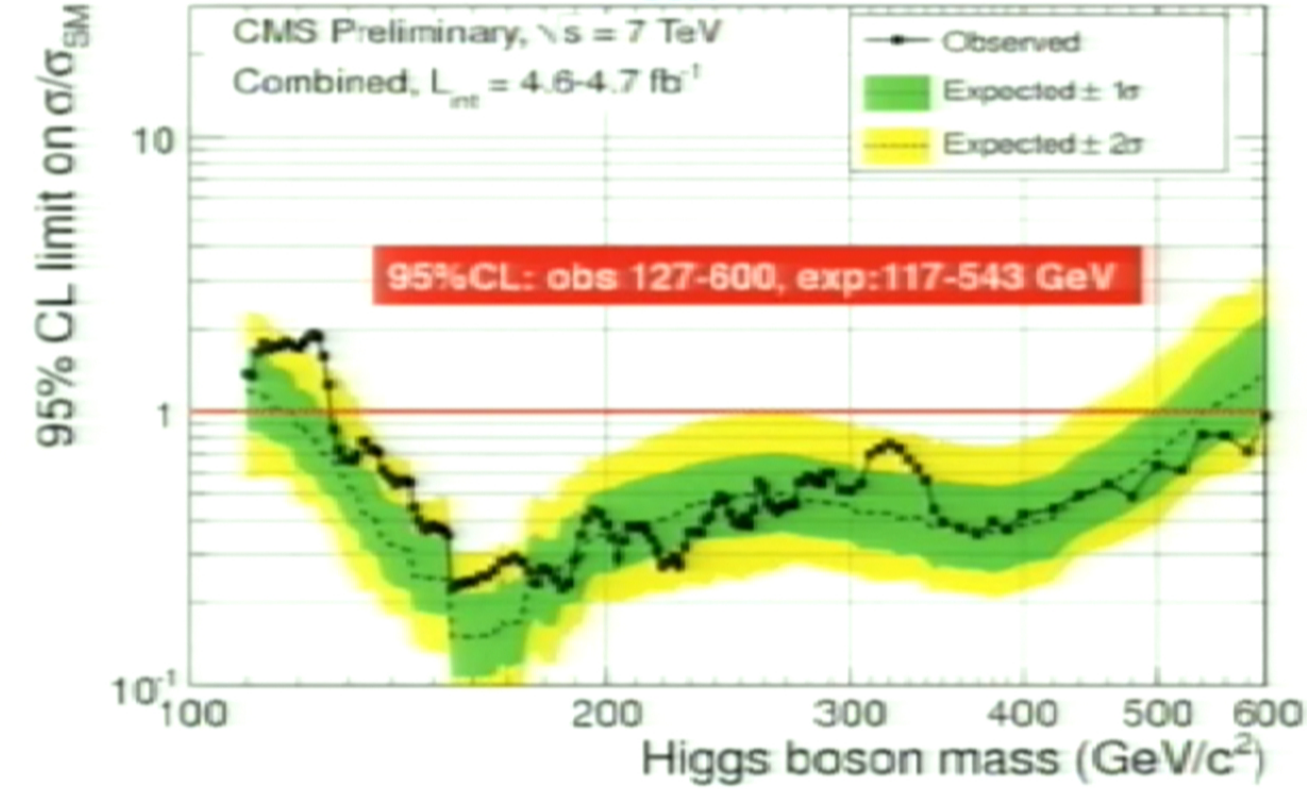

Freshly squeezed EWK plots

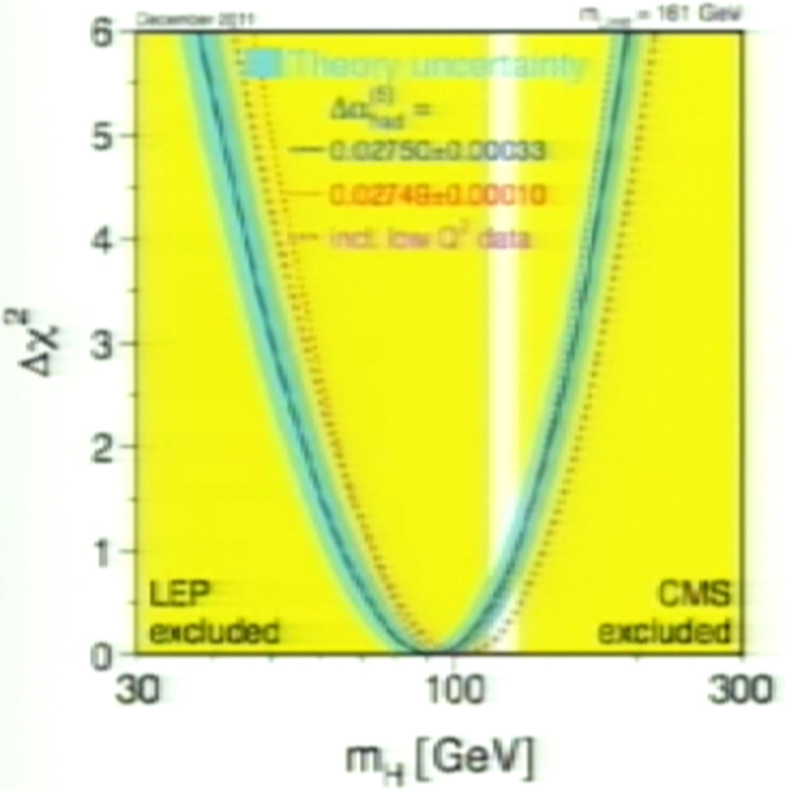

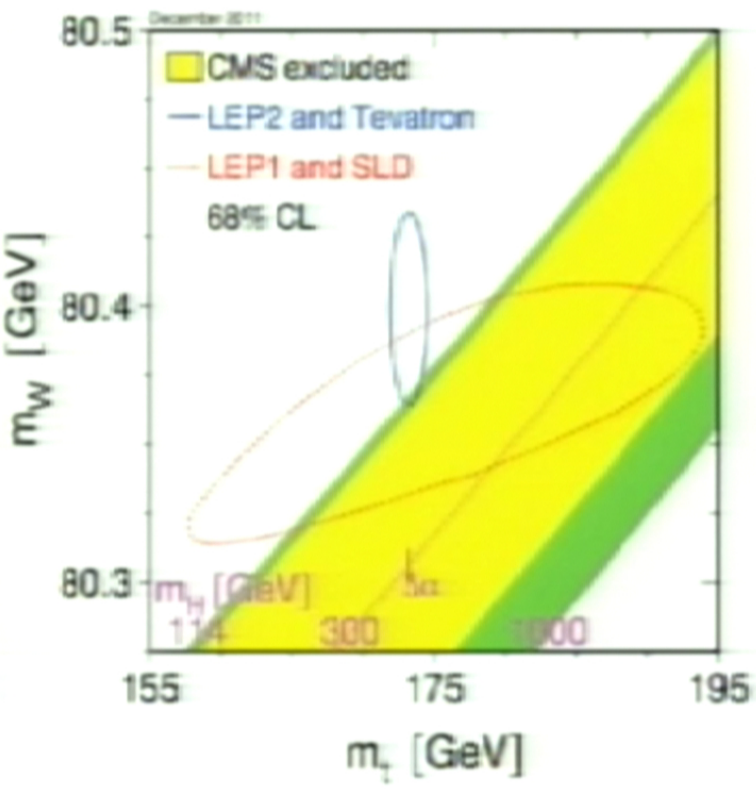

Limits by channel

Solid line = Observed limit ; Dashed line = Median Expected

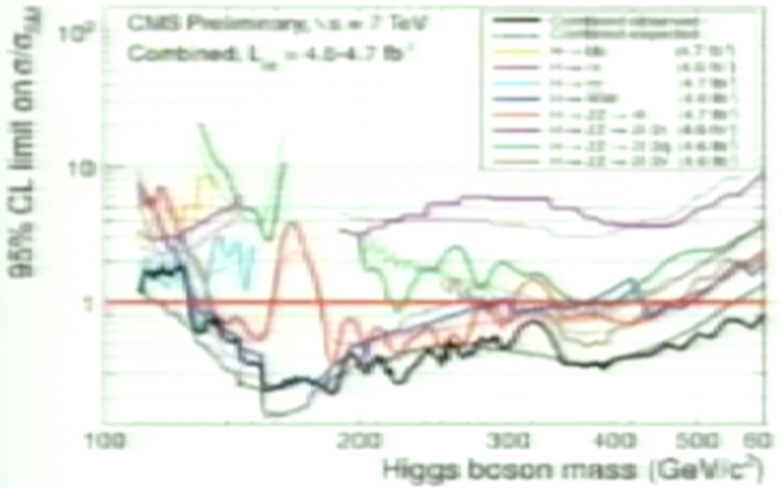

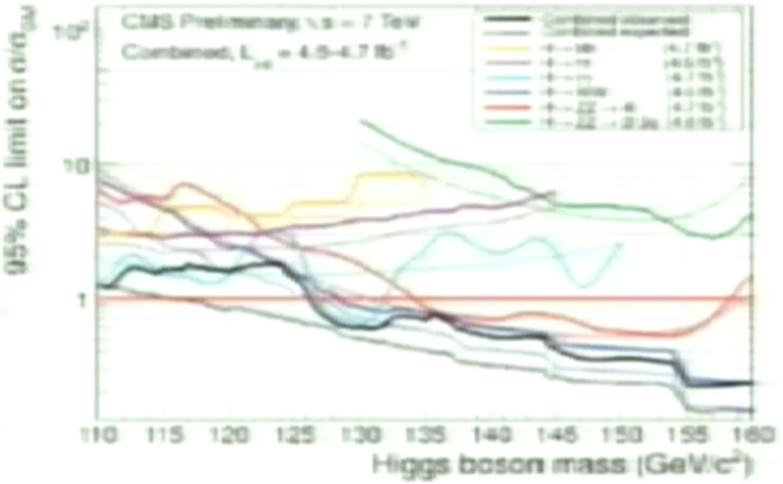

(Asymptotic CLs only)

Zoom in the low mass region

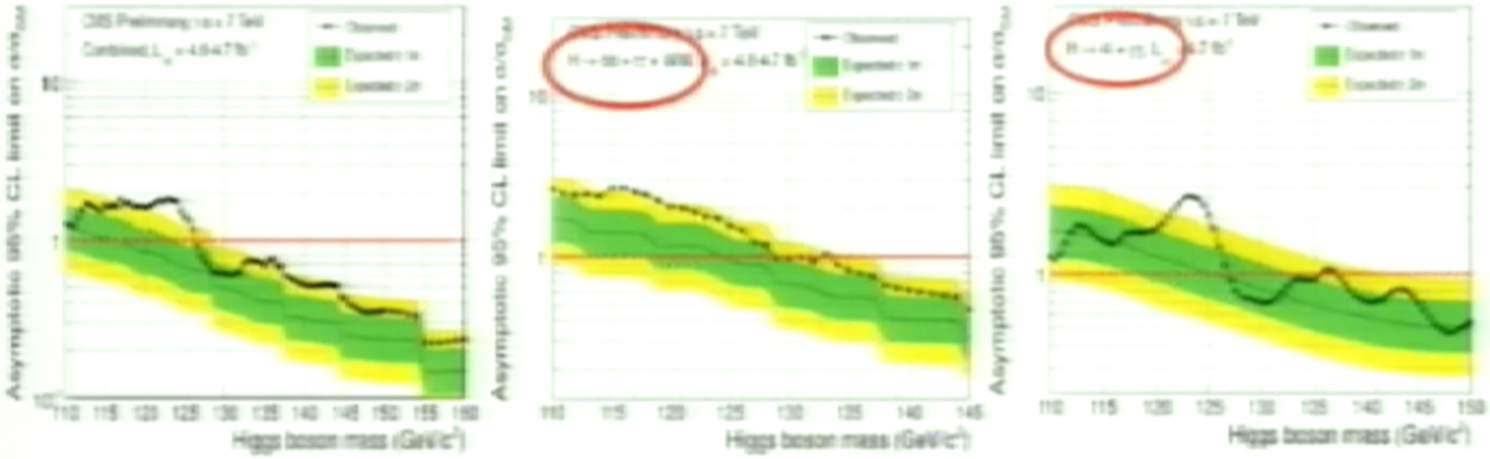

We cannot exclude the presence of the SM Higgs boson below 127GeV because of a modest excess of events in the region between 115 and 127GeV.

The excess at low mass is produced by a broad excess driven by the low resolution channels (H2TT, H2WW, H2BB, center), modulated by the localized excesses seen by the high resolution channels (H2GG and H2ZZ, right).

Anatomy of an excess: local and global p-values

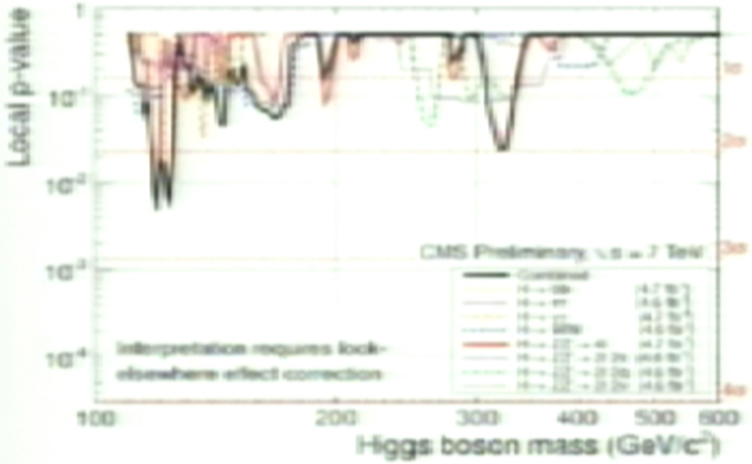

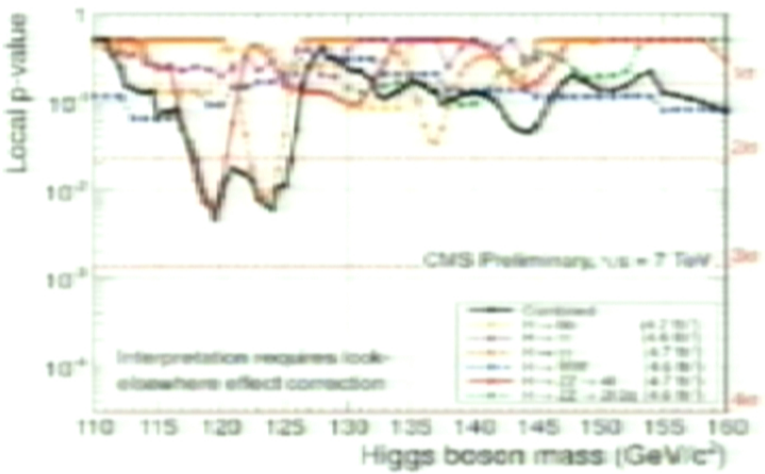

Maximum local significance 2.6σ.

LEE-corrected significance (full mass range: 110-600GeV)= 0.6σ

LEE-corrected significance (low mass range: 110-145GeV)= 1.9σ

The excess we see in the low mass region has a modest statistical significance and could be reasonably a fluctuation of the background.

Anatomy of an excess: Observed and Expected

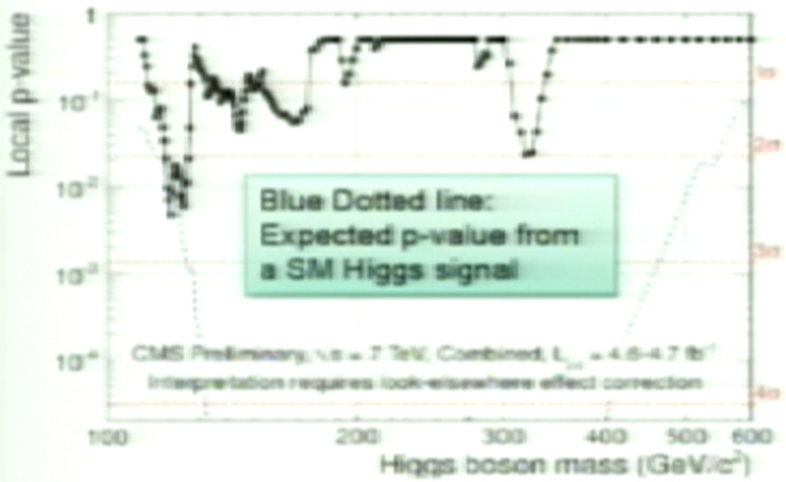

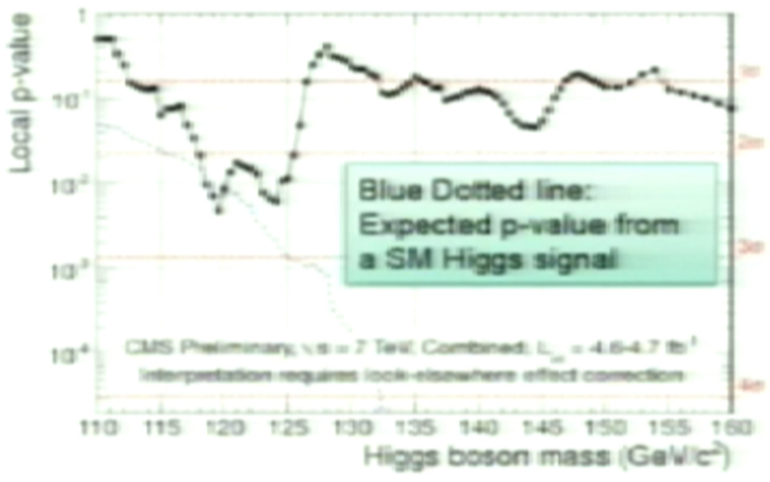

The only region where the observed p-value seems to be compatible with the expected p-value from a SM Higgs is the low mass region.

In this region a SM Higgs boson is expected to yield a modest p-value
(2-3σ median value in the range 115-127GeV)

Anatomy of an excess: best fit σ/σ_{sm}

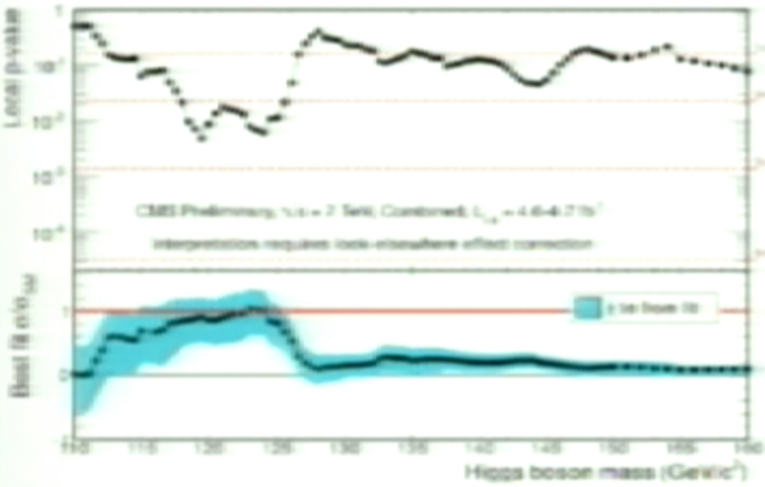

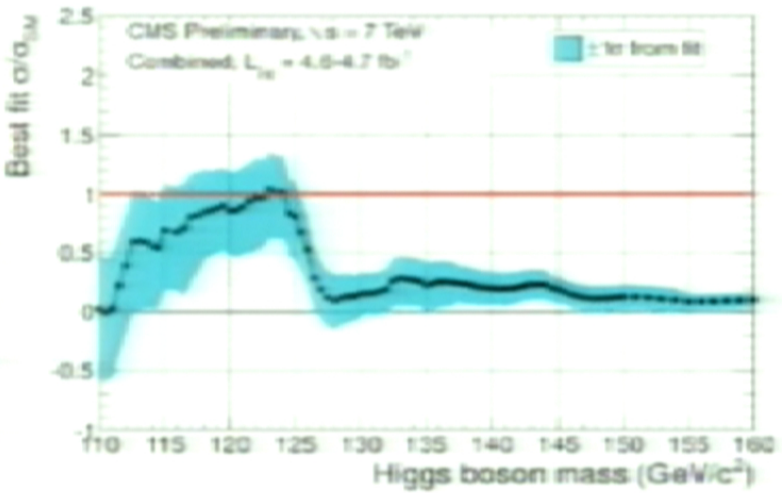

Fitted σ/σ_{SM} compatible with 1 in the full low mass range.
Median value touching 1 at a mass of 124 GeV and below.

Anatomy of an excess: the high resolution channels

$H \rightarrow \gamma\gamma$

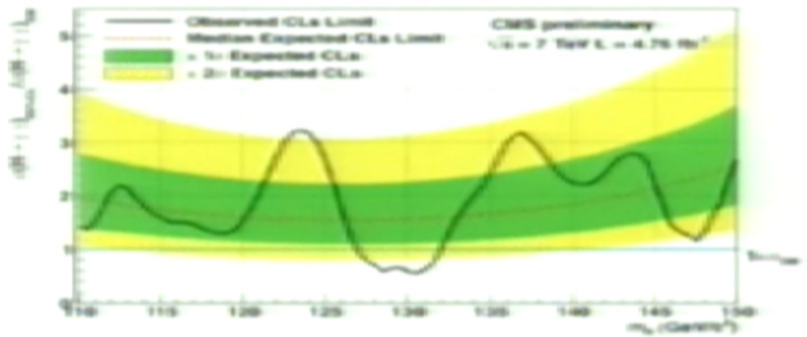

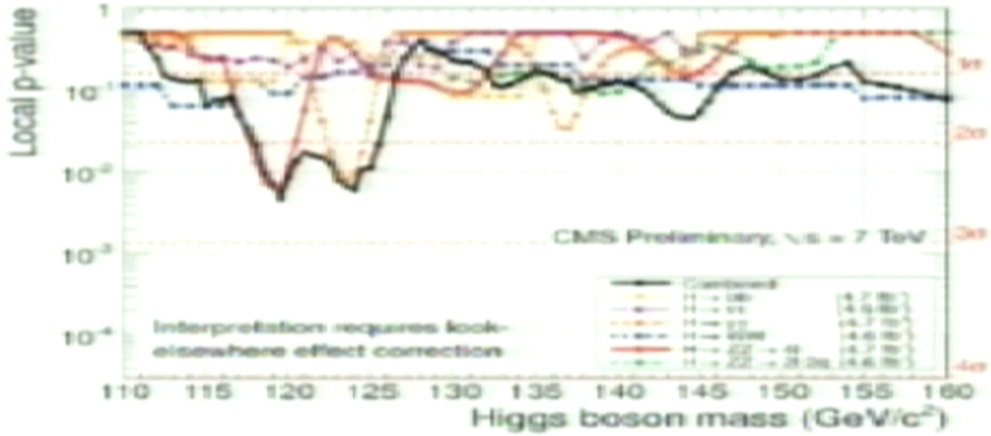

Anatomy of an excess: the high resolution channels

$H \rightarrow \gamma\gamma$

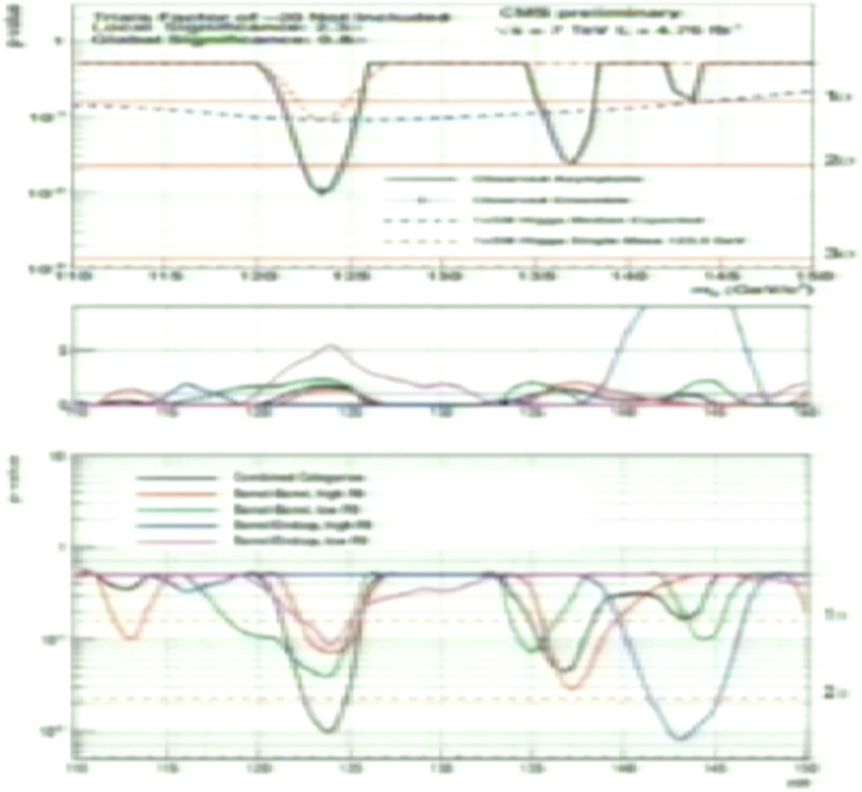

Anatomy of an excess: the high resolution channels

H → ZZ→ 4l: 4e, 4μ, 2e2μ

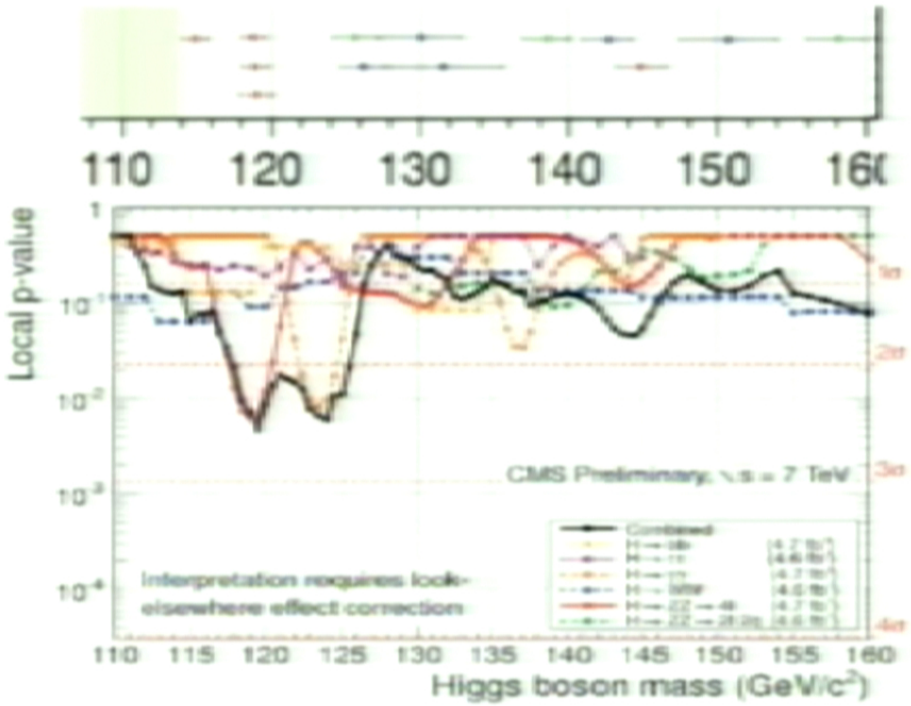

Anatomy of an excess: the high resolution channels

H → ZZ→ 4l: 4e, 4μ, 2e2μ

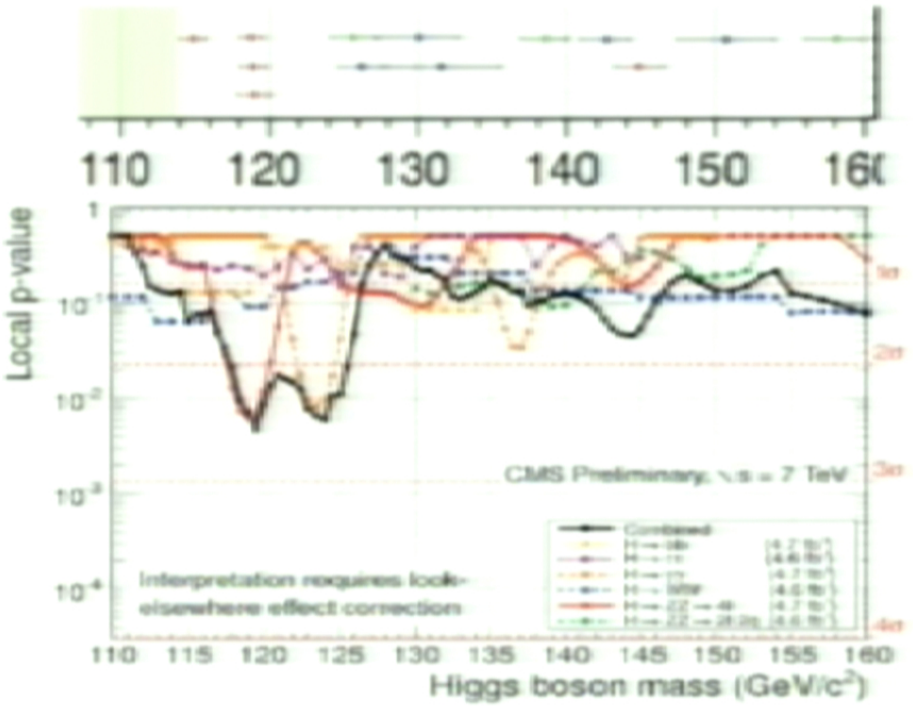

Limits on σ/σ_{sm} (CLs method)

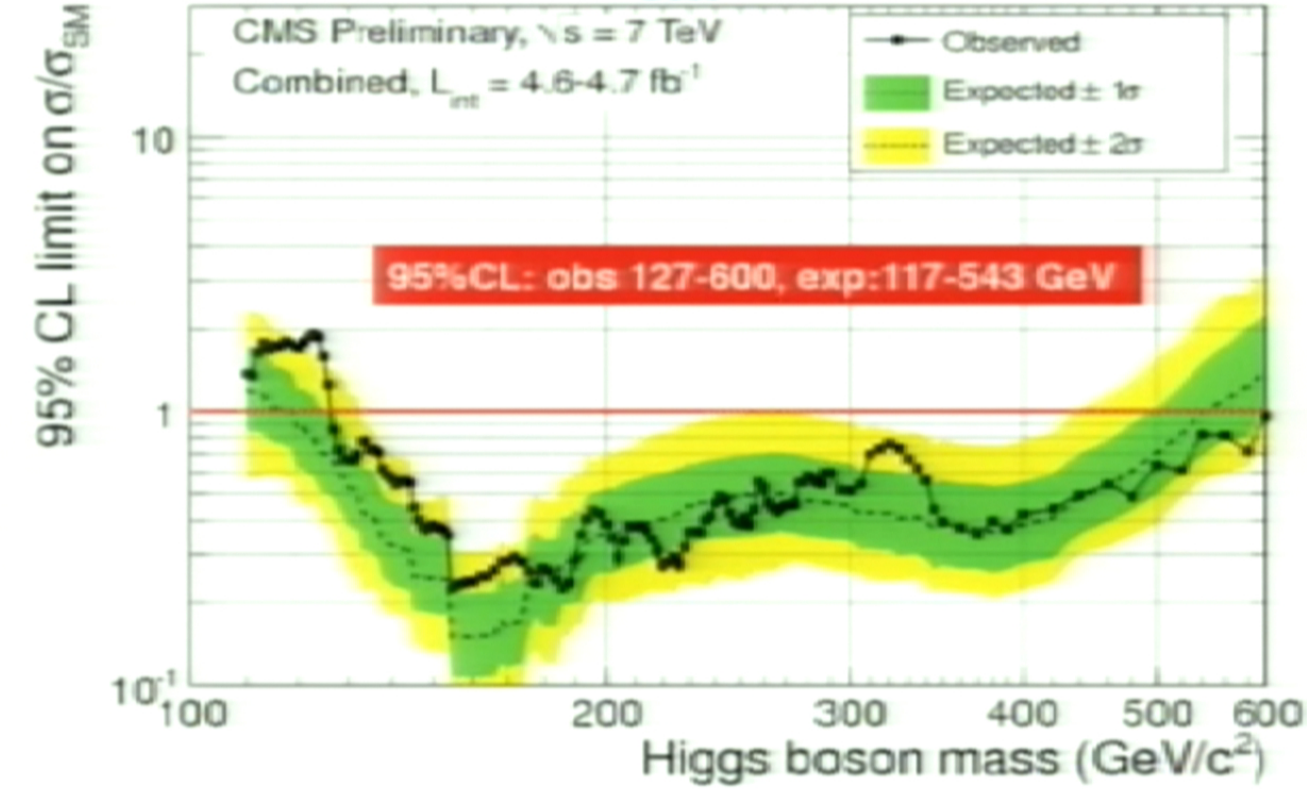

Summary.

- We have been able to analyse very quickly the full data set collected in 2011 and to present here a comprehensive set of preliminary results.
- Final results and submission of papers are expected around the end of January (new additional channels, refined analyses).
- **We have reached the expected sensitivity (around or better than 1xSM) in the full mass range of our current exploration (115GeV-600 GeV).**
- We have established **new 95% CL exclusion limits: 127GeV-600GeV.**
- We are not able to exclude the presence of the SM Higgs below 127GeV since we observe in our data **a modest excess of events between 115 and 127GeV that appears, quite consistenly, in five independent channels.**
- **The excess is most compatible with a SM Higgs hypothesis in the vicinity of 124 GeV and below, but the statistical significance (2.6σ local and 1.9σ global after correcting for the LEE in the low mass region) is not large enough to say anything conclusive.**
- As of today what we see is consistent either with a background fluctuation or with the presence of the SM Higgs boson.
- Refined analyses and additional data in 2012 will definitely give an answer.

Conclusion

- **Many thanks** to the thousand of people that contributed to the success of the CMS experiment, from the conceptual design throughout the construction, commissioning and operation of our magnificent detector.

- **Many thanks** to the hundreds of analysers, software and computing experts that worked so hard to produce these complete set of results just a few weeks after the end of 2011 data taking.

- **Many thanks** to Steve Myers and the whole LHC team for having delivered to the experiments an integrated luminosity exceeding our most optimistic expectations.